POLITECNICO DI TORINO

Corso di Laurea Magistrale
In Ingegneria Biomedica

Tesi di Laurea Magistrale

"Development and clinical validation of radiological" evaluation method for osteointegration of xeno-hybrid bone substitute

Relatore: Prof. Cristina Bignardi
Co-relatore: Prof. Giuseppe Perale
Co-relatore: Ing. Carlo Grottoli

Candidato: Laila Pantaloni

ANNO ACCADEMICO 2017/2018

INDEX

PREFACE

This master thesis in bioengineering by Ms. Laila Pantaloni is part of a wider multidisciplinary research project coordinated by Industrie Biomediche Insubri SA, *a.k.a.* IBI, the Swiss med-tech company manufacturing the bone substitute SmartBone®.

IBI is continuously running marketing surveillance activities, as a due normative prescription, and in parallel conducting clinical research activities to consolidate scientific basis of its products. Moreover, in line with its attention to research and education, IBI continuously hosts students from all over the world, involved in its research projects, in agreement with their academic tutors. Most commonly, several of them are taken from different curricula and teamed together on the same research: this is a good chance to allow multidisciplinary interaction, favoring knowledge and expertise exchange, while offering them the chance to experience a real applied research challenge.

Indeed, this thesis entitled "Development and clinical validation of radiological" evaluation method for osteointegration of xeno-hybrid bone substitute" is part of a wider study aiming at quantitatively assessing the remodeling timing and performances of SmartBone®, once grafted into patients who had suffered traumatic bone losses. This study has been started back in 2016 and has seen the involvement of tens of people, from surgeons to radiologists, from biophysicists to bioengineers, and of course master students from different academies. Within the framework of this retrospective observational clinical study, approved by local Ethical Committee, following good clinical practice and adhering to the principles of the Helsinki declaration, anonymized data from patients who underwent reconstructive surgeries with SmartBone® were retrieved for this work. Informed consents were duly recorded too.

Here, Laila followed the preliminary work by Lucrezia Pilone, master student from Politecnico di Torino, and was confronted with the development of a radiological protocol to assess the recovery-time related variation of SmartBone® density as a reliable measure of integration and hence remodeling of the graft.
Laila was teamed with a biomedicine student, Riccardo Garibaldi, from the University of Genova and a MD specializing radiologist Vanessa Furfaro, from the CTO Torino.

The supervision and guidance was provided by the team from CTO Torino, namely Dr. Alda Borrè, Dr. Alessandro Bistolfi, Dr. Alessandro Tombolesi, Dr. Osvaldo Rampado, by IBI team, Ing. Carlo Grottoli and Dr. Bettina Overgaard, all being scientifically coordinated by Prof. Dr. Riccardo Ferracini from University of Genova and finally myself.

Giuseppe Perale

Prof. Dr. Giuseppe Perale, PhD
Exec. VicePresidente
Industrie Biomediche Insubri SA
Switzerland

RIASSUNTO

L’obiettivo principale di questo lavoro è stato quello di andare a costruire un Protocollo di acquisizione TC, includendo i parametri tecnici, per valutare dal punto di vista radiologico il sostitutivo osseo SmartBone® dopo la fase di innesto ed ottenere immagini tomografiche utili per la valutazione quantitativa densitometrica del processo di osteointegrazione nel tempo.

Per valutare la risposta radiologica dello SmartBone® sono stati eseguiti dei test di acquisizione in cui sono stati cambiati i parametri tecnici. Nel test sono stati inseriti 4 campioni di SmartBone® due compatti di differenti dimensioni: campione #1 di dimensioni 10x20x20 mm and campione #2 di dimensioni 10x10x10 mm; e due granulati con differente granulometria: campione #3 con granulometria di 2-4 mm e campione #4 con granulometria di 0.25 mm. Inoltre, sono stati inseriti due campioni cilindrici di densità omogenea: uno di osso compatto e l'altro di acrilico ed è stato inserito nella prova anche un pezzo di osso bovino preso da un macellaio.

Successivamente sono stati inseriti degli elementi metallici in differenti posizioni con l'obiettivo di andare a simulare il comportamento del sostitutivo osseo in presenza di protesi metalliche. Questi materiali metallici erano: uno stelo di protesi inversa di spalla e una vita e una placca.

La peggior condizione è stata considerata quella in cui lo stelo di protesi inversa di spalla è stato posizionato vicino al sostitutivo SmartBone®. Tutti i test sono stati eseguiti in presenza di un phantom di calibrazione (QRM-BDC-6 / Phantom) costituito da 6 inserti omogenei, ognuno avente una quantità di Idrossiapatite nota; precisamente le sei differenti densità sono: *i.e. 0, 100, 200, 400, 600, 800 mg HA / cm^3*.

I test sono stati eseguiti presso il C.T.O di Torino con lo scanner Optima CT660 della GE Healthcare. Le acquisizioni sono state eseguite in modalità elicoidale con un ASIR al 30% e con un kernel di ricostruzione standard.

I parametri tecnici che sono stati variati per sviluppare un protocollo di acquisizione affidabili sono: il voltaggio, la centratura, il MAR (Metal Artifact Reduction) e la presenza e l'assenza di elementi metallici. L'analisi radiologica dello SmartBone® è stata eseguita con il software Image j il quale applica un'analisi basata sulla scala di grigi. Questo programma permette di calcolare il valor medio di unità hounsfield (HU) su un volume, la deviazione standard e di calcolare il valore massimo di HU e il valore minimo di HU su un volume in studio.

Questo software permette quindi di svolgere una caratterizzazione densitometrica di un volume.

Il software Image j è stato validato con l'utilizzo del software Mimics Innovation Suite di Materialise: infatti con il software Image j sono stati calcolati i range di unità hounsfield per tutti gli elementi presenti nella prova e con il secondo software è stata verificata la correttezza di tali range di HU. Questo metodo quindi ha permesso di calcolare i range di HU per il materiale SmartBone®.
Dopo aver validato il software Image j, è stata valutato come la variazione dei parametri tecnici di acquisizione influenzi le unità hounsfield durante l'acquisizione del materiale SmartBone® e degli altri elementi presenti nella prova. Grazie ai risultati ottenuti è stato possibile definire un protocollo di acquisizione TC per una corretta acquisizione dello SmartBone® e per una valutazione densitometrica quantitativa della rigenerazione ossea.

Successivamente è stata definita la relazione tra la quantità di Idrossiapatite dei sei inserti del phantom di calibrazione, fornita dall'azienda produttrice, e la media di HU calcolata sul volume di ognuno dei sei inserti: è stata ottenuta una relazione di tipo lineare.
A partire dal valore medio di HU per i campioni di SmartBone® e usando la relazione lineare ottenuta è stato possibile calcolare la mineralizzazione del materiale in termini di mg HA/cm^3.
Dopo l'impianto di un sostitutivo osseo è importane valutare la rimodellazione ossea. I metodi principali sono: analisi istologica, analisi volumetrica e analisi densitometrica. La TC è una tecnica di Imaging diagnostica ed è il punto d partenza per condurre un'analisi della rigenerazione ossea.

In questo lavoro di tesi è stato proposto un metodo per valutare la rigenerazione ossea dopo l'operazione chirurgica, basato su un'analisi in scala di grigi da eseguire sulla TC post-operatoria.
La scala di grigi della regione dell'impianto osseo è stata confrontata con i range di HU determinati al fine di identificare le zone appartenenti all'osso corticale, quelle dell'osso spongioso e infine quelle dello SmartBone®.
La metodologia sviluppata è stata validata attraverso due casi clinici: il paziente 1 del quale erano disponibili una TC pre-operatoria ed una TC post-operatoria eseguita dopo 9 mesi; il paziente 2 del quale erano disponibili una TC pre-operatoria ed una TC post-operatoria eseguita 17 mesi dopo l'intervento chirurgico. L'analisi densitometrica è stata quindi eseguita sulla TC post-operatoria di entrambi i casi ed è stata valutata anche la mineralizzazione. Inoltre, è stato possibile eseguire una valutazione volumetrica, attraverso la sovrapposizione di due modelli 3D ed il calcolo del volume dell'osso rigenerato.

ABSTRACT

The goal of this work is to define a CT-Scan Protocol, including all technical acquisition parameters, to assess the radiologic characterization of SmartBone® after grafting, in order to evaluate the osteointegration over time.

In order to evaluate the SmartBone®'s radiological response, acquisition tests were carried out in which technical parameters were changed; tests included four samples of SmartBone®, two compacts of different shapes: sample #1 of size 10x20x20 mm and sample #2 of size 10x10x10 mm; and two different granulates: sample #3 with granulometry of 2-4 mm and sample #4 with granulometry of 0.25 mm.

Furthermore, two cylindrical samples of homogeneous density were used: one of compact bone and an acrylic one, and a piece of bovine crude bone taken directly from a butcher.

Subsequently, metallic elements were inserted in different positions in order to simulate the behaviour of the bone substitute in the presence of metal prosthesis. These metallic materials were: a reverse shoulder prosthesis stem, a screw and an elbow plaque. The worst condition is the one in which a shoulder prosthesis stem has been placed closed to SmartBone®. All tests were performed in the presence of a calibration phantom (QRM-BDC-6 / Phantom) consisting of six homogeneous inserts, each having a known amount of Hydroxyapatite and hence six precisely different densities (*i.e. 0, 100, 200, 400, 600, 800 mg HA / cm^3*).

The tests were carried out at the C.T.O in Turin, Italy, with a GE Healthcare - Optima CT660 scan.

The acquisitions have been performed in helical mode and with ASIR-30%, with a standard reconstruction kernel.

The technical parameters that have been varied to develop a suitable acquisition protocol were: Voltage, Centering, MAR (Metal Artifact Reduction), presence and absence of metallic elements.

Radiological analysis of SmartBone® was carried out with Image j software, which applies a greyscale analysis (applying Hounsfield scaling system). This program permits to calculate the average HU value on a volume, the Standard Deviation and calculate the value of Maximum HU and the Minimum HU value of the study volume.

This allowed to always perform a densitometric characterization of the volume.

Image j software was validated with Mimics Innovation Suite by Materialise Software: indeed, the HU ranges for all elements in the test were calculated with Image j software and the correctness of

these values was verified with the second software. This method allowed calculating HU ranges for SmartBone®.

After validating the Image J software, the influence of the variation of the acquisition parameters on the Hounsfield units was allowed during the acquisition on SmartBone® and on the other homogeneous elements. From the results obtained it was possible to define a TC protocol for a correct acquisition of SmartBone® and a quantitative evaluation of bone regeneration.

Successively, the relationship between the hydroxyapatite quantity of six inserts of calibration Phantom, supplied from producer company, and the mean HU values calculated on volumes of six inserts was evaluated: a linear correlation was recorded.

Starting from the average HU value of SmartBone® and using the obtained linear correlation, the Mineralization of material in term of mg HA/cm^3 has been calculated.

After bone substitute's implant, bone remodelling has to be evaluated. Main methods are: histologic, volumetric and densitometric analysis. TC is an imaging diagnostic technique and it is the starting point to conduct the bone regeneration analysis.

A method to evaluate bone regeneration after surgery was proposed, it is based on a grayscale analysis on the post-operatory CT.

The grayscale on bone graft region was compared with HU ranges determined, to identify cortical bone, cancellous bone and SmartBone®.

For clinical validation of developed methodology, clinical data has been used: a pre-operatory TC and a post-operatory TC, after 9 months, of patient 1 and a pre-operatory TC and a post-operatory TC, after 17 months, of patient 2 were available. Densitometric analysis was hence performed on post-operative TC with evaluation of mineralization too. Moreover, it was possible to execute a volumetric evaluation, basing on overlapping of 3D models to calculate the volume of bone regeneration.

1. INTRODUCTION

1.1. NATURAL BONE

The bone tissue is a mineralized and highly specialized connective tissue with important structural and metabolic functions. The bone tissue is the main component of the skeleton and it provide a scaffold for the body. The structural functions are to supply support, rigidity and hardness in order to endure physiological and accidental loads that act on the body, supporting the soft tissue and protecting the organism. Instead, the metabolic function is that of store the minerals. Indeed, it acts like a major deposit of calcium ions and it is important for preserve a proper homeostatic equilibrium of mineral within a body, moreover, the metabolic function has an important role in the phenomenon of haematopoiesis. [1]

Bone tissue is made of cells, fibers, and ground substance. [2] Bone is a heterogeneous and anisotropic composite biomaterial and it has a hierarchical structure. In bone tissue, the extracellular matrix is the 90% of the weight and it is mineralized, while the remaining part is made of water (10%). The matrix is made of inorganic components, especially calcium phosphate in the form of hydroxyapatite microcrystals. The organic component is type I collagen, organized in fibres in which hydroxyapatite mineral crystal are immersed. [3] [4]

Bone tissue is different from other connective tissues, because it has good mechanical properties of stiffness and compression strength and torsion. This is due to the particular structure of bone tissue, it is formed by deposition of minerals, apatite or hydroxyapatite, in a frame of collagen and this tissue is characterized by the abundant presence of the organic components of the intercellular substance. [1]

The bone is called “living tissue”. This is because, In the mineralized collagen fibrils there are several cells, in particular osteocytes and osteoblasts, which allow the continuous reconstruction of tissues.[5]

The osteoclasts produce acids that dissolve the bone matrix, releasing mineral salts contained within. The osteoblasts are responsible for osteogenesis, in fact, they synthesize organic components of the bone matrix, producing the osteoid that is a mixture of collagen fibres, proteoglycans, and glycoproteins.

Origin	Water H_2O [%]	Hydroxyapatite $Ca_5(PO_4)_3(OH)$ [%]	Collagen [%]	GAG [%]
Human	9,1	76,4	21,5	
Bovine	7,3	67,2	21,2	0,34

Table 1.1 - Volumetric composition of cortical human bovine tissue (Herring 1997, Pellegrino and Blitz, 1965; Vejlens, 1971

The most of components of bone tissue depends of different elements, for example: species, the anatomical place, age, sex and type of bone tissue.

Table 1.1 shows some literature data regarding the composition of human and bovine cortical bone. The mineralized extracellular matrix is composed of osteoblasts, which look like thin laminae resting one on top of the other, forming lamellas of variable thickness (4-11µm) in which the mineralized collagen fibrils are organized parallel to each other.

Accordingly, the bone tissue has a major capacity of accepting loads. Usually, these fibrils are arranged in bundles or aligned in groups that can be organized differently according to the type of tissue and anatomical site. [6] [7]

Lastly, Bone consist of two types of tissue: lamellar tissue and not lamellar tissue (fibrous bone tissue). The fibrous bone tissue or interwoven fibre tissue is an immature bone normally found in the embryo, in infants, in metaphysical sites and during healing of bone fracture. When this type of tissue is deposited, the fibrous tissue is reabsorbed and replaced by lamellar bone. By looking at fibrous bone tissue in the microscope, it looks like a series of braided fibers randomly organized in a three-dimensional space. The meshes of this '3D web' are composed of large collagen fibers of important thickness (5-10 µm in diameter). Non-lamellar bone is more elastic and less compact than lamellar bone, due to the lesser quantity of minerals and the absence of favoured orientation of the collagen fibers. The lamellar bone tissue builds the mature bone deriving from the remodelling of the fibrous bone or existing bone. The lamellar tissue is more organized than the non-lamellar tissue; indeed, it has a well-organized orientation of collagen fibers, which are put in overlapping layers, called 'bone lamellae'.

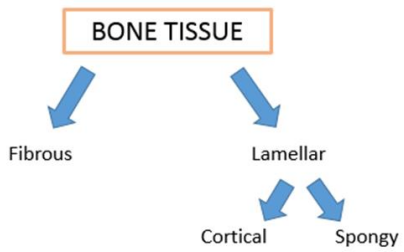

Figure 1.1 - Description of different parts of bone tissue

Lamellas are separated by small intercommunicating spaces. Within these gaps there are cells that obtain nutrients through a system of canals.

Almost all the bone tissue of adult body is of the lamellar kind and it composes almost all of the compact bone and a large part of spongy bone. [8]

The lamellar bone tissue is divided into spongy bone and compact or cortical bone. The basic composition is the same, but their three-dimensional arrangement is different. This difference allows optimizing the weight and size of the bones depending on the different stresses that they undergo. [9]

1.1.1. SPONGY OR TRABECULAR BONE

The spongy bone, as its name says, seems a 'sponge' under the microscope [10]; indeed, it may be observed a large amount of spaces between the trabeculae.

The cancellous bone mainly forms the innermost layer of bones. It is found in short bones, flat bones and in epiphyses of long bones.

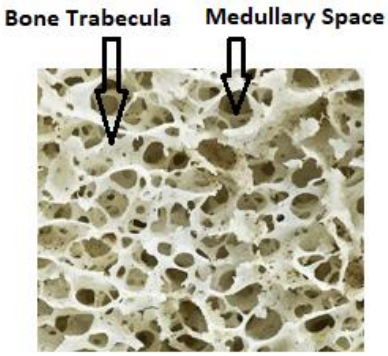

Figure 1.2 - Sponge Bone extracted by microscopy https://askabiologist.asu.edu/bone-anatomy

Osteons are not present in spongy bone, differently from compact bone.

Instead, cancellous bone consists of trabeculae, which are well-organized lamellae.

The trabeculae are diversely oriented and intersect between them; also, they define cavities known as ‘medullary cavities’. These contain the red (hematopoietic) and yellow (fat) marrow.

Inside of this tissue there are Blood vessels, which carry nutrients to osteocytes and remove waste. [8] [11] The sponge tissue has an alveolar structure, which decrease density of bone. Moreover, this structure gives lightness to bone and it allows muscles to move the bones easily.

The distribution of trabeculae depends on the load lines and this allows to the sponge tissue of resist stresses, as long as they are not too strong; it is also resistant to loads that come from various directions. This type of bone is more present in the spine, ribs, jaw, and wrists. It represents only 20% of the skeletal mass, but it is the most active metabolic component.

1.1.2. COMPACT BONE

The compact bone forms the external layer of short bones, flat bones and long bones as well as the diaphysis of the latter; moreover, it encloses the bone marrow. Compact bone is hard and dense, because it has not macroscopically visible cavities and it supplies protection and strength to bones. Compact bone composes 80% of the skeletal mass. The structural units of cortical bone are called Osteons or Haversian systems. Compact bone consists from cells called Osteocytes and these cells are aligned in circles around the canals. Inside the osteon, bone cells (osteocytes) are distributed in biconvex cavities called bone lacunae. The most obvious feature of osteons is the presence of concentric strips (from 4 to 20) enclosing a central canal known as Haversian canal, which contains nerves as well as blood and lymph vessels.

These small canals, called Haversian canals, reserved for blood vessels, cells, nerve fibers and the processes that are necessary to keep the bone alive. [8]

Together, the lamellas and canal the Haversian system (also known as osteon). The different systems communicate with the medullary cavities and with the free bone surface through canals arranged transversely and obliquely, called Volkmann canals.

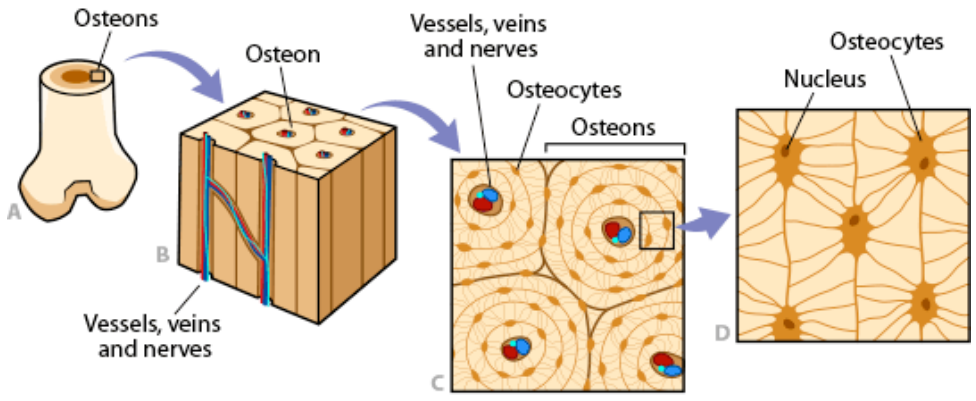

Figure 1.3 - Looking at the osteons in bone (A) under a microscope reveals tube-like osteons (B) made up of osteocytes (C). These bone cells have long branching arms (D) which lets them communicate with other cells. https://askabiologist.asu.edu/bone-anatomy

In the cortical bone, we can identify two types of canals: longitudinal canals (known as Haversian canals) in which blood flows and transversal canals (or Volkmann's canals) that start from the periosteum and endosteum and lead to longitudinal canals. [12]

The compact bone gives rigidity, toughness, and resistance to mechanical stress. Most of the cortical bone is to be found in the long bones which are in the lower and upper limbs, for example, femur, radius, and humerus.

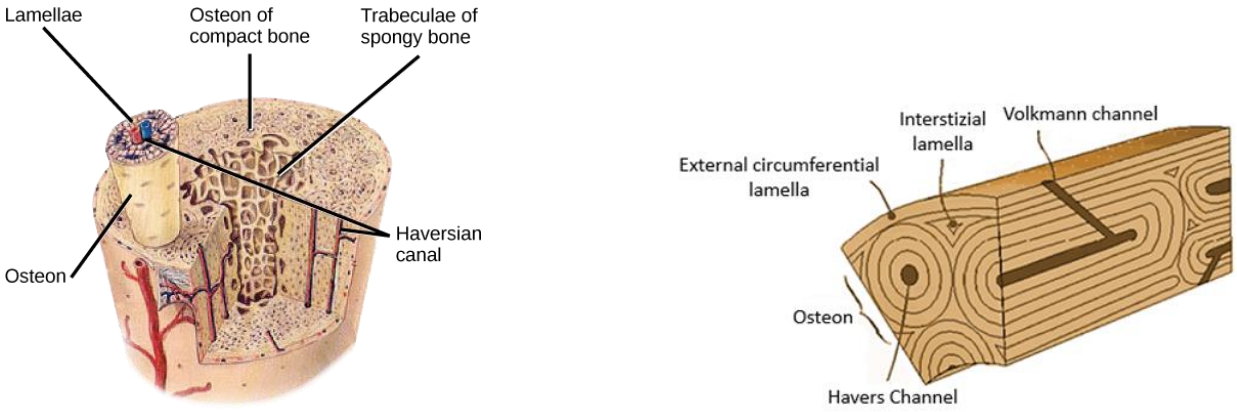

Figure 1.4 - – (A) Compact bone tissue is made up from: osteons and Haversian canal. Osteons are aligned parallel to the long axis of the bone. Haversian canal contains the bone's blood vessels and nerve fibers. The living osteocytes are small dark ovals. https://

1.1.3. BONE REMODELLING

The bone tissue is metabolically active; indeed, this tissue has continuous bone resorption and deposition processes, that allow the bone structure to adjust to various mechanical physiological stresses. This process is relevant also because it contributes to regulating the quantity of calcium present in the body. [13] At a microscopic level the result of bone remodeling is the morpho-functional bone modification. This process does not entail macroscopic modifications, indeed the shape of the bone segment remains the same. [14] This means that, bone remodelling is used by the bone to optimize its shape according to the load it has to support. Therefore the bone suits the mechanical strains acting on it. [15] Moreover, remodeling is the replacement of old tissue by new bone tissue. This mainly occurs in the adult skeleton to maintain bone mass.

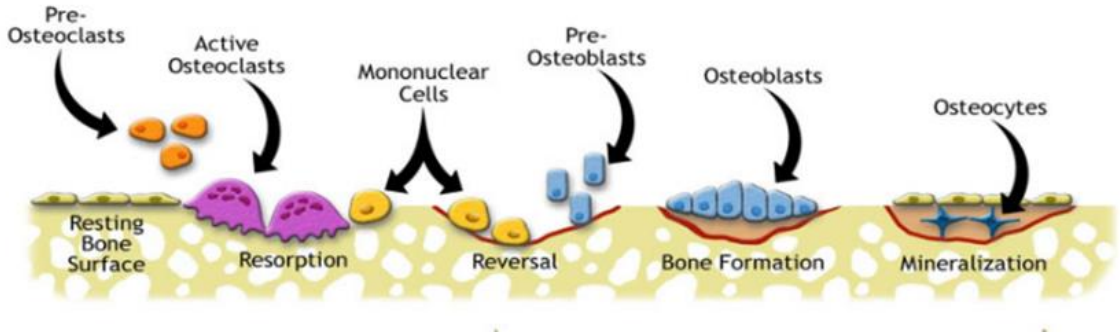

Figure 1.5 - Resorption of bone remodelling process. From: http://www.orthopaedicsone.com/display/Clerkship/Describe+the+process+of+bone+remodeling

Bone remodeling is operated by different cells, present in the tissue, that carry out different functions. The process starts with the recruitment of pre-osteoclasts, that are dragged into the circulatory system and are induced to grow into osteoclasts when they arrive at the site of active bone resorption.

Osteoclasts are large multinucleated cells, like macrophages, derived from the hematopoietic lineage. They destroy and reabsorb existing bone material. [16] [17]

Osteoclasts have the ability to consume bone tissue slowly, because they secrete lactic acid that dissolves calcium and magnesium minerals in the bone and because these cells release a special proteolytic enzyme that breaks and digests the organic substance of the tissue (bone matrix). [18]

Simultaneously , other progenitor cells form new cells: the osteoblasts. Osteoblasts derive from mesenchymal stem cells. Osteoblast synthesize new bone, when the body grows and also after bones are broken. [16] [17]

These cells adhere to the cavities formed by osteoclasts during the reabsorption phase and they produce new bone layers to form concentric lamellae. progressively minerals are added, giving it strength and hardness. This process results in the creation of flexible structures called osteons.

When osteoblasts have completed their task, they become osteocytes or lining cells. These cells form a part of deposited bone layers and they have to maintain the mature bone in good condition. Actually, the osteocytes are osteoblasts that have completed their task but are ready to turn back into osteoblasts in case of necessity. Moreover, osteocytes have prolongations that create a branched system of communication where metabolic and gaseous exchanges occur. [19]

This balance mechanism between reabsorbed bone and new bone is a lifelong process, although there is a progressive loss of total bone mass with advancing age. [20]

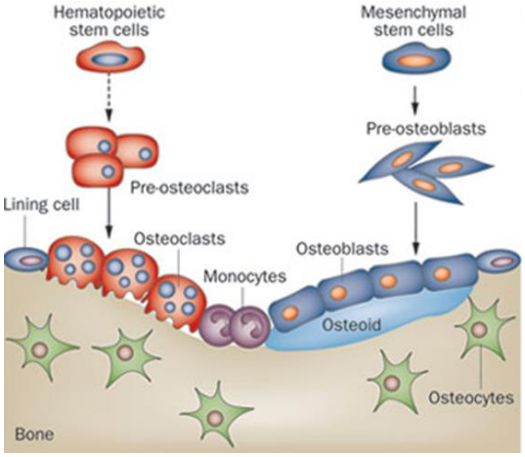

Figure 1.6 - All phases of bone remodelling process. From: https://www.researchgate.net/figure/221791788_fig4_Figure-1-The-bone-remodeling-cycle-and-regulation-of-bone-tissue-homeostasisa

Many studies have been made to define the origin of such phenomena. In the nineteenth century, surgeon Julius Wolff stated that: "the shape of the bone follows the function", namely bone architecture is influenced by the mechanical stresses associated with its normal functioning. [21]

In fact, the activation mechanism of osteoclasts and osteoblasts is triggered by the presence of stresses, while a bone resorption phenomenon occurs when stress is not applied. [22]

It is possible to sum up the Wolff laws in three qualitative laws:

1. bone remodelling is governed by flexural stresses and not by major stresses;
2. Bone remodelling is stimulated by cyclic dynamic loads and not by static loads;
3. The dynamic flexion produces bone growth where the bending is concave.

These laws explain that new bone formation prevails on reabsorption when there is an optimal load, on the other hand, the reabsorption mechanism prevails on bone deposition when the load is either too small or excessively high. [23]

Bone remodeling takes place in all the bones of our body.

1.2. BONE SUBSTITUTES

Millions of people all over the world are affected by bone and articular problems, which can generate degeneration or inflammation of tissues. The damage of bone and joint tissues may also occur following trauma, due to a violent event. These problems often require surgery, to improve the patient's life, with application of permanent, temporary or biodegradable devices.

Bone substitutes are used always more frequently in: traumatology, oncologic surgery, spine surgery and revision prosthetic surgery.[24]

Bone grafting is one of the most commonly used surgical procedure to augment bone regeneration in orthopaedic field.[25]

Bone grafts are composed of biomaterials that are implanted in a specific anatomical site. Bone substitutes can be used in different anatomical district.

Bone graft is colonized by the cells of the tissue of implant and integrated, in order to perform the biological functions of bone tissue. [23] Therefore, bone substitute is incorporated through a sequence steps: the implant causes an inflammatory response with the heap of cells; later mesenchymal cells, that are into the graft site, undergo the chemotaxis. The primitive cells then differentiate into chondroblasts and osteoblasts, thanks to presence of osteoinductive factors. Bone implant revascularization and necrotic graft resorption happen simultaneously. At the end, bone generation from osteoblasts and bone remodeling, in reply to mechanical stress, happen. [24]

Bone substitutes should meet certain requirements to perform their function.

- These materials must be biocompatible, and they must not evoke any adverse inflammatory response.
- The bone grafts primarily should provide mechanical or biologic support.
  They should have mechanical properties similar to those of native bone, indeed they should be able to sustain and absorb loads. The biological properties are also influenced by porosity, surface geometry and surface chemistry. Pores need to be interconnected and with adequate pores size distribution to facilitate cell migration, proliferation and also the revascularization.[26] They also should possess a mechanism to allow diffusion and/or transport of ions and nutrient.
- These materials should be easy to model in the graft site with a functional time to set and they should be Radiographically visible to perform an evaluation.

- The ideal bone substitute should also be thermally non-conductive, sterilisable without suffering degradation of characteristics and performances, and readily available at a reasonable cost. [24][27][28]

The desired biological properties for bone graft materials are the following:

- Osteoconduction is the ability to support the attachment, the migration and the ingrowth of osteoblast and osteo-progenitor cells into three-dimensional structure of the graft. This is an ordered process that promote the formation of blood vessels and new Haversian system. An osteoconductive biomaterial supply a three-dimensional interconnected scaffold where local bone tissue may regenerate new living bone. However, osteoconductive biomaterials are unable to form bone or to induce its formation.
- Osteoinduction is capability to induce differentiation of primitive, undifferentiated and pluripotent cells to develop into the bone-forming cell lineage, by which osteogenesis is induced. An osteoinductive material supplies biologic signals able to induce the local cells differentiation leading to mature osteoblasts. This material stimulates the generation of new bone tissue by activating the mesenchymal cells through the presence of bioactive proteins and growth factor, like Bone Morphogenetic Proteins (BMPs), which take part to bone metabolism.
- Osteogenesis means the new bone formation through progenitor cells, derived from either the host or grafts, which proliferate and differentiate to osteoblasts.
- Osteointegration is the ability of the host and the graft material to create a bond. This phenomenon is fundamental to graft survival. the formation of new bone at the bone-implant interface should be exist without the formation of fibrous tissue.

The only graft material that contains all four qualities is autologous bone. [24] [25] [28] [29]

The bone substitutes for repairing bone defects can have a natural or synthetic origin.
The natural bone devices mainly used are autologous, homologous and heterologous substitutes.

1.2.1. AUTOGRAFT

The best natural bone substitute is **autologous bone**, indeed is considered the "gold standard" to repair bone defect. Autogenous bone is used both for cortical area and for spongy area of the bone. This bone grafting is collected from the same patient receiving the implant. Autologous bone has fundamental properties for bone regeneration: osteoinductive, osteoconductive and it is osteogenic. Moreover, it holds growth factors and cells without immune or infective risks.

Autologous bone can be picked up from non-essential bones, like: iliac crest, fibula, ribs, chin, mandible and parts of the skull too. New regenerated bone slowly replaces autogenous bone implant. However, this bone grafting has some disadvantages: a donor site is necessary, surgical procedure is longer and more complex, post-operative can be painful. Other possible complications can be: blood loss, infection, hematomas , fracture, neurovascular injury and aesthetic disadvantage. [24] [30]

If cells do not survive, this clinical method can cause the implant failure. Moreover, this approach cannot be used in patients too younger, too older or affected by cancer.

1.2.2. ALLOGRAFT AND XENOGRAFT

Other natural bone substitute are Allografts and Xenografts bone.

Allograft bone consists of homologous bone and it is a good alternative to autogenous bone. Allograft bone is collected from other humans, which can be living donors or non-living donors and this substitute has to be prepared inside a bone tissue bank.

Allograft bone substitute is osteoconductive and not much osteoinductive, this feature depends on the presence of growth factors, following the processing. This substitute has the same disadvantage as the autologous bone. Moreover, Allografts require sterilization and it has to be processed to prevent the immune response of recipient organism. This causes a reduction of mechanical properties of bone and the deactivation of proteins present in healthy bone. mineralized component is removed to increase osteoinductive potential and the release of BMPs (Bone Morphogenic Proteins) induces mesenchymal cell differentiation in osteoblasts. [31]

The amounts of available natural bone grafts traditionally used are still far from meeting the clinical demands. [25]

In conclusion, the limits of allografts are costs, difficult procedure, mechanical resistance, limited osteoinduction and risk of infection. [24]

Xenograft bone consists of heterologous bone, taken from animals.

Xenograft bone consists of heterologous bone, taken from animals. Xenograft bone substitutes most commonly used come from bovine bone or porcine bone, which can be freeze dried or demineralized and deproteinized. The organic component is taken off by thermal or chemical treatments to avoid immunological reactions and the transmission of diseases. However, these production methods might alter the morphology of the bone structure, like reducing the micro-roughness and the porosity of materials.

Nevertheless, the DBBMs (Deprotenized Bovine Bone Minerals) are biocompatible and osteoconductive, although the methods by which they are produced, have a strong impact on their biological behaviour. Indeed, depending on the production technique used, it is possible to notice the differences in osteoconduction properties. [32] The advantages are the easy availability, the osteoconductivity, the good mechanical properties and low costs.

Xenografts have given good results in dentistry, but scarce validation in orthopaedics. [24]

1.2.3. SYNTHETIC BONE SUBSTITUTES

Synthetic bone substitutes are also called **Alloplastic biomaterials**. These materials, being completely of synthetic origin, have no risk of transmitting diseases. Therefore, they do not provoke immune or extraneous reactions to the body. These materials are generally only osteoconductive and can be: absorbable, non-absorbable or partially resorbable.

The synthetic bony substitutes, during creation in the laboratory, have a composition controlled at both macroscopic and microscopic level, in fact they are indicated for each type of graft. Each characteristic of the material is defined for its specific clinical use, such as the size of the macropores, the interconnections to favour the revascularization and the morphology in blocks or granulated of different sizes.

In addition, these bone substitutes have short healing times, are free from systemic or local toxicity, are easily sterilizable and commercially available. But the ideal material has not yet been found, because there are limits to the interaction between biological tissue and these materials.

Calcium phosphates (Ca3(PO4)2, in particular Hydroxyapatite-HA and Beta-Tricalcium-Phosphate-TCP are the most widely used, due to their composition similar to the inorganic phase of bone. Synthetic bone substitutes are widely used either alone or also combined with biological factors, like recombinant human bone morphological proteins (rhBMPs, e.g. rhBMP-2 and rhBMP-7). [25] [32][33]

Tricalcium phosphate (TCP) consists of calcium and phosphorus in relation to 3:2. This material has a high biocompatibility, is biodegradable (it rapidly absorbs in about 6 weeks) and has osteoconductive properties.

These properties are based on porous micromorphology, the interconnected structure of pores and its total resorbibility. The latter is due to the chemical solubility of the material, but it does not cause any PH changes. During the degradation of TCP, the calcium and phosphate ions are released and are used for the formation of new bone tissue, in this way the resorption of the TCP leaves place gradually to the formation of new bone. For this reason, TCP has a more rapid bone healing than the HA-based compounds. However, the reabsorption of this material makes it unsuitable for critical situations like lateral and vertical ridge rises and also has scarce mechanical properties.

Hydroxyapatite-HA is a hydrated calcium phosphate and is considered to be osteoconductive and non-absorbable. Therefore, the HA is the crystalline form of Tricalcium phosphate (TCP). HA is a relatively inert substance that is retained ‘‘in vivo’’ for prolonged periods of time. It is the primary mineral component of bone tissue and of hard tissues of teeth. For this reason, HA has a very high mechanical strength. It can be of natural and synthetic origin. In fact, it can be derived from natural substances such as the skeleton of the coral or extracted from bovine bone or obtained through a process of synthesis starting from calcium phosphate salts. HA has become popular in orthopaedic, craniofacial and orthognathic surgery, filling bony defects and smoothing contour irregularities.

The various forms of the commercially available hydroxyapatite differ in form, Solid or granular, for the size of the granules and the volume of porosity present.

HA and TCP (Hydroxyapatite and tricalcium phosphate) ceramics are manufactured in a variety of forms including granules and porous blocks. There is a controlled resorbibility biphasic hydroxyapatite, consisting of the combination of HA and TCP (biphasic calcium phosphates) in different proportions in order to yield a more physiological balance between mechanical support and bone resorption. In this way we exploit the capacity of the hydroxyapatite to maintain the space and the property of TCP resorbibility. As the tricalcium phosphate is reabsorbed, the hydroxyapatite becomes more porous and an ever-greater proportion enters into contact with the host tissues, favouring a slow substitution process. [24] [32] [33]

Another type of bone substitutes are the **bioglasses** that are made up of silica (SiO_2) (45%), calcium oxide (CaO) (for 24.5%), sodium oxide (Na_2O) (24.5%) and phosphorus oxide (P_2O_5) (6%).

The bioglasses are biocompatible and osteoconductive and establish a chemical-physical bond with the bone, exchanging ions or molecular groups with it. They are not absorbable, as osteoclasts are not able to eliminate silicates-based materials and remain in the form of vitreous solid matter.
They are used when good structural stability and integration with the receiving site are required.[33]
Due to their granular and non-porous nature they do not have the same performance of reliability in revascularization maintaining space compared to other materials. [32]

Polymer substitutes have physical, mechanical, and chemical properties different from other material. The polymers can be divided into natural polymers and synthetic polymers. A very important natural polymer in bone is collagen.
Two types of synthetic polymers are: Poly(methyl-methacrylate) (PMMA) and Poly(hydroxyethyl methacrylate) (pHEMA) and those consisting of polylactic and polyglycolic acid copolymers.
The first polymers are nondegradable. Polymethylmethacrylate confers the mechanical characteristics, while Poly(hydroxyethyl methacrylate) gives the characteristics of haemostasis and adhesion.
Degradable synthetic polymers are polylactic acid and poly(lactic-co-glycolic acid) because they can be resorbed by the body. Polylactic acid and polyglycolic acid constitute many commercially available products, which are used as medical devices in the surgical, dental, maxillofacial and orthopaedic fields. They can be used as standalone devices and as extenders of autografts and allografts. Polylactic and polyglycolic acid copolymers are synthetic products. These polymers are biocompatible, do not induce immunological or inflammatory reactions, are osteoconductive and are completely replaced by trabecular bone. In fact, their degradation time is between 4 and 8 months. The material comes in the form of block, granules and gels.
Currently, the use of these polymers in the form of polylactic and polyglycolic acid gels is implemented in association with other heterologous materials that become more easily treatable.[32] [33]
Another polymers type is the aliphatic polyesters such as polye-caprolactone (PCL).
PCL is semi crystalline polyester and it is biocompatible and biodegradable polymer. This material is highly processable with a wide range of organic solvents. This also has a high thermal stability.
In bone engineering, PCL is being used to enhance bone ingrowth and regeneration in the treatment of bone defects but it has a slow degradation time. [24]

In this thesis work has been focused attention on SmartBone®, which is an xeno-hybrid bone substitute. It is created from a demineralized bovine matrix and has a good integration and features of osteogenesis.

1.3. SMARTBONE®

Figure 1.7 - SmartBone® sizes available in the company.

SmartBone® is bone substitute produced by Biomedical Industries Insubri S.A. (IBI-SA, Mezzovico, Switzerland). This company fosters research and development technologies and medical devices for tissue engineering. SmartBone® was put on the international market as a Class III medical device in 2012 by IBI-SA, after obtaining the CE mark.

SmartBone® is a composite material constitutes of bovine matrix reinforced by absorbable bioactive polymers and it is used as a substitute bone to support the cell colonization and promote regeneration of bone. Through *in vivo* e *in vitro* tests, it has been shown that this bone substitute has a satisfactory biological behaviour, a morphology similar to human cortical bone and mechanical properties that endow it with good resistance. For these reason SmartBone® is widely used in oral and maxillofacial surgery and in orthopaedic surgery. Moreover, SmartBone® has a good workability; in fact, it is possible to obtain different specific shapes and sizes for each patient (see figure) [34]

1.3.1. FORMULATION

SmartBone® is produced by combining decellularized bovine spongy bone matrix with a copolymer of polylactic acid (PLA) and polycaprolactone (PCL); and moreover, with the addition of polysaccharides.

The bovine bone is a mineral matrix that is made of calcium, hydroxyapatite (HA, Ca5(PO4)3OH) and collagen residues. This mineral matrix has a chemical composition and morphology similar to humane bone. [35]

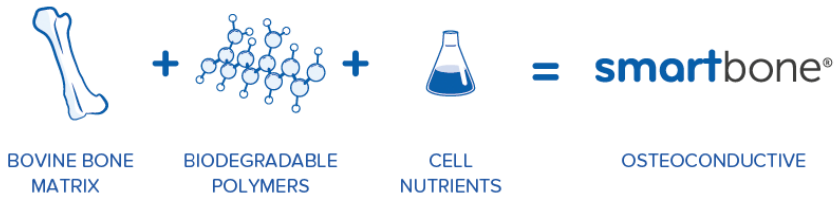

Figure 1.8 - Materials that composed the SmartBone®. From: https://www.ibi-sa.com/products/SmartBone® /

Follow Figure shows the images that are obtained through scanning electron microscopy (SEM) of bovine bone and decellularized human bone.

It is noted that the bovine matrix has a 3D structure made up of interconnected pores and that its morphological features are comparable to the cadaveric human bone. [34]

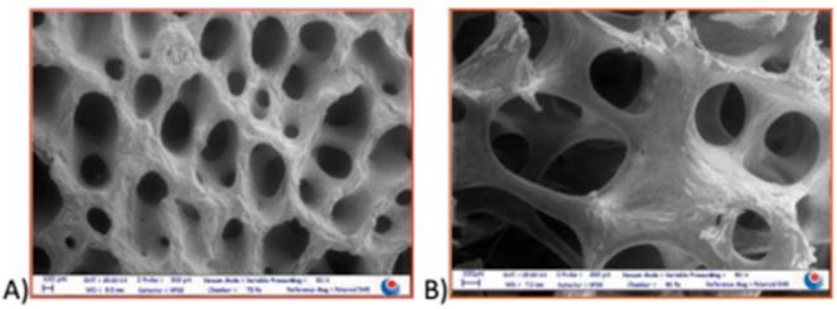

Figure 1.9 - - Images were obteined by SEM at the same magnification A) bovine bone B) cadaveric human bone.

The disvantage is that the bovine matrix alone is rigid, not elastic and too frail. Furthermore, decellularization and sterilization treatments destroy the biochemical structure, and this prevents cellular adhesion. The IBI-S.A researchers worked with the objective to reinforce the matrix structure with an elastic component, this has been achieved with a polymeric coating. This proved that PLA and PCL coatings, which are bio-absorbable polymers already used in medical applications,

give resistance to the structure. The addition of small doses of polysaccharides makes the bone substitute more hydrophilic, thereby increasing blood affinity and promoting cell adhesion.

Figure 9 shows the SEM image of the bovine bone matrix before and after the polymeric treatment and the EDS spectrum. [35]

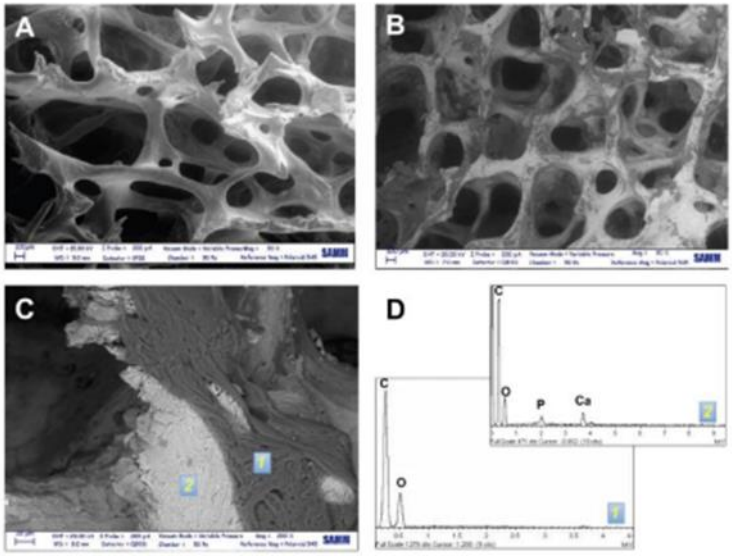

Figure 1.10 - images were obtained by SEM at the same magnification : A) bovine bone matrix; B) SmartBone® graft; C) SmartBone® graft at a larger magnification; D) energy-dispersed spectrum (EDS).

In image C there are two different areas: the first area corresponds to the polymeric coating, in fact only carbon and hydrogen appear in the spectrum (EDS). In the second area, we can see the bovine bone; in fact, calcium and phosphorus also are shown in the spectrum, because these elements are typical of a mineral matrix.

1.3.2. MORPHOLOGY

The manufacturers, through scanning electron microscope, have analyzed the morphological structure of SmartBone® samples and they have compared them with human bones.

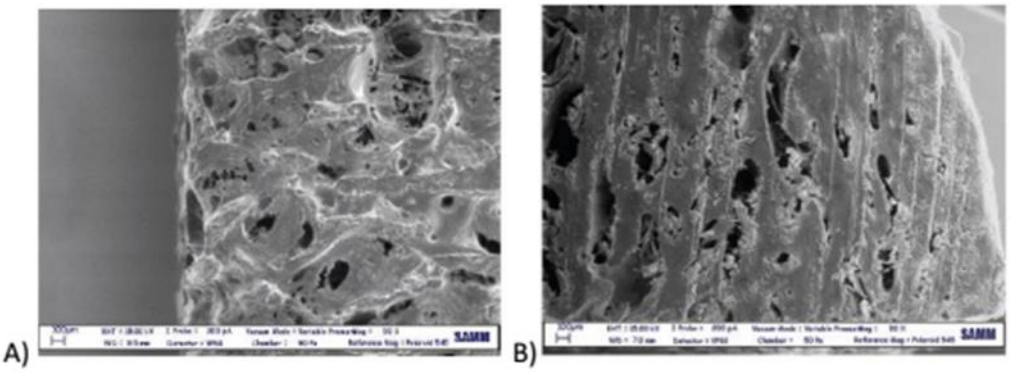

Figure 1.11 - ESEM images at the same magnification A) SmartBone® graft B) human iliac crest.

Figure 10 shows that bone graft is very close to human iliac crest sample, which is commonly used like autograph implant. [36]

In particular, porousness and pore size of these two samples seem to be comparable and therefore the graft is a favourable environment for cell migration.

A micro computed tomography (micro-tc) was also performed on a SmartBone® cube to calculate the volumetric parameters on the 3D image (see figure 11). [35]

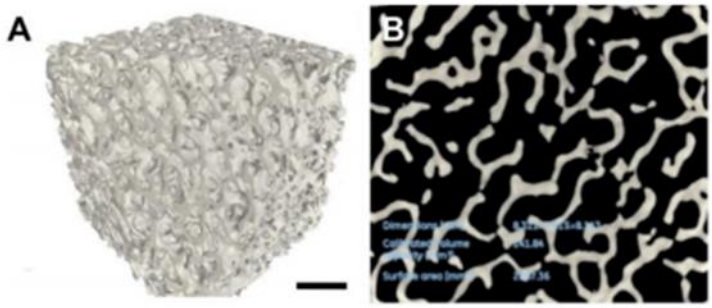

Figure 1.12 - 3D interpretation of a cubic sample of SmartBone® (A) and its 2D with volumetric data (B).

The porosity is homogenous in the sample. It has pores interconnected throughout the thickness. The free volume is approximately 27% and the surface/volume ratio is 4.46 mm-1.

1.3.3. HYDROPHILICITY AND POLYMER DEGRADATION

An important clinical property is the hydrophilicity of the scaffold. A number of experiments demonstrate that when blood is absorbed into the graft it releases growth factors and it generates biochemical signals that can promote the integration of host tissue. The SmartBone® microstructure allows an elevated hydrophilicity with an absorption of 38% w/w in less than 60 minutes (this test was performed in PBS using the Mettler-Toledo calibrated scale).

Degradation time of polymeric coating is another substantial parameter. A differential equation model is used to study this parameter because it simulates the degradation of the polymeric coating. The SmartBone® sample is represented as a cube with spherical pores, whose number and size were determined by micro-TC. The chart (see figure 12) shows the theoretical trend of polymer layer with four different thicknesses. It is noted that each polymeric coating completely dissolves within 5-6 months from implant, which corresponds to the time of bone integration. [35]

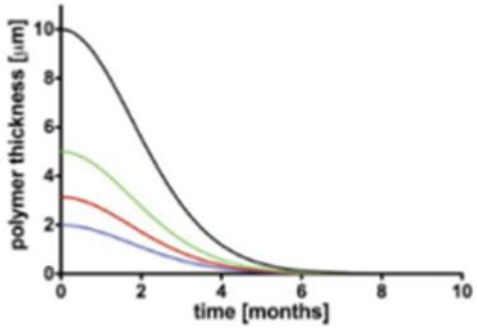

Figure 1.13 - The thickness of polymer film in relation to degradation time

1.3.4. MECHANICAL PROPERTIES

The IBI-S.A. researchers performed some tests to evaluate mechanical behaviour of SmartBone®. the results showed that SmartBone® is able to withstand the required loads, therefore this material yields an efficient response to body loads. The researchers carried out a uniaxial compression test, which allowed to calculate the maximum strength and elastic modulus of material. The tests were carried out with a hydraulic machine MTS 858 Mini Bionix on cubes of material with 10 mmx10 mm faces and a deformation velocity of 1mm/min.

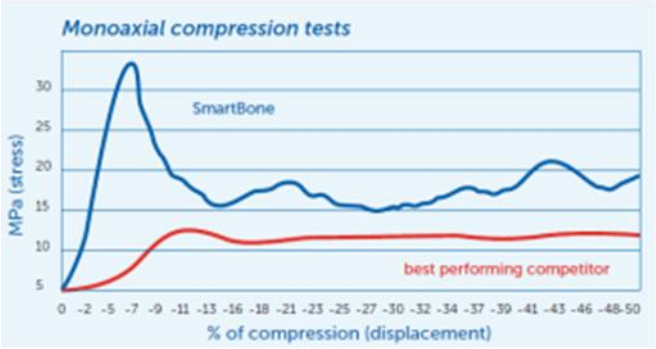

Figure 1.14 - stress-strain graph for SmartBone® (blue line) and for bone substitute produced by Starling (red line).

The figure 1.15 shows the SmartBone® stress-strain curve in comparison to that of another bone substitute.

From the graph it is noted that SmartBone® has the typical trend of a porous matrix under increasing load; indeed, it shows a first linear trait due to mechanical resistance followed by an oscillating trait due to the progressive breakage of the structure and the matrix compacting.

It has been shown that the sample of SmartBone® has a maximum load resistance three times higher than Starling, which is the best competitor on the market; moreover, SmartBone® presents an elastic modulus four times higher than that of the other bone substitute.

1.3.5. MECHANISM OF ACTION

The figure 1.24 shows a histological image of the implanted SmartBone® and the tissue around it. In figure A, the growth of new bone tissue within the graft (black arrows) appears to be supported by the presence of osteocytes in the gap (yellow arrow). It is noted the formations of mature lamellar bone and osteoblasts that create the new bone tissue (green arrows).

The figure B shows an enlargement of the figure B, where it can possible observe the lines of bone regrowth shown by violet colour. The SmartBone® graft (black arrows) is progressively replaced by new bone tissue (green arrows). The osteoblasts are present both in the active and in the quiescent states; once they have formed mature bone (yellow arrows) they become osteocytes.

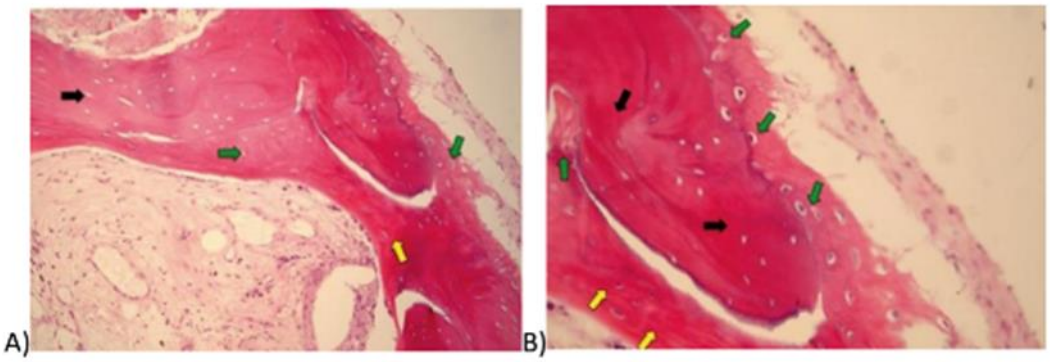

Figure 1.15 - Histological images of the SmartBone® implant

In conclusion, SmartBone® is an innovative ideal material to be used as a bone substitute. in fact, it has mechanical and physical properties that make it suitable for the purpose and it has also proved to be biocompatible and osteogenic. [34]

1.4. CLINICAL EVALUATION METHODS OF BONE SUBSTITUTES

Many treatments for bone substitution exist nowadays; as previously discussed, different materials can be employed according to the type of problem. These materials, scientifically well researched, have to support bone regeneration through osteoinduction and osteoconduction processes. [37]

In time, the use of these materials is become increasingly frequent in clinical practice and for different anatomic districts. For this reason, **bone substitute evaluation methods** are become essential to appraise if the product yields optimal results. The post-operatory analyses are both qualitative and quantitative, beside the quality of the regenerated bone and how much bone formation is present are important to study.

In this way it is possible evaluate whether bone graft was able to repair the initial defect and if the quality of regenerate bone it's like that of healthy bone.

There are different methods to evaluate a bone substitute, which are based on three types of analyses: **histologic, densitometric and volumetric**.

The histologic and densitometric analyses are used to observe bone quality, while the volumetric method aims at determining the amount of new bone produced in or near the bone substitute.

1.4.1. HISTOLOGIC METHOD

Histology is a scientific methodology that analyze microscopic tissue at morphological and functional level. Histologic method is applied to bone substitutes few months after the implant and as far as possible, to assess how the bone substitute is integrated and replaced by new bone. [38]

The specific tissue features are examined to evaluate the validity of the graft. These characteristics are: the formation of the lamellae to make up the osteon and the cemented lines around it. Furthermore, researchers inspect if there is a good angiogenesis for the nourishment of the new formed bone. (see figure 1.13). [39]

The cells are also studied, indeed the presence of osteoblasts in active and in quiescent states is evaluated, because these cells are essential to allow the formation of new bone. Furthermore, the presence of osteocytes is also investigated, because their existence implies a mature bone together with the presence of lamellae. [40]

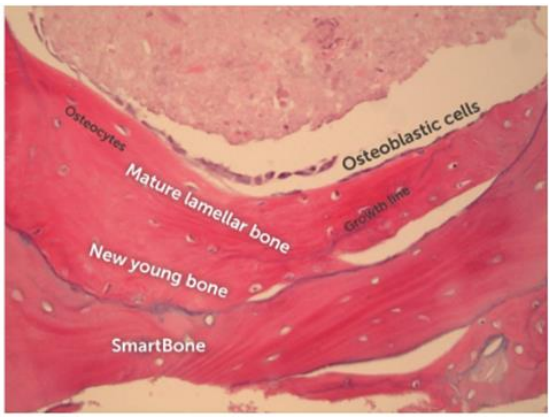

Figure 1.16 - SmartBone® Histology post-intervention. From: histology IBI S.A

After histology, histomorphometry is performed, which is considered as quantitative histology. The histomorphometric analysis is carry out on two-dimensional histological sections and is based on the evaluation of 3 types of measurements: length, perimeters and areas. These parameters are expressed to represent the three-dimensional bone structure in terms of areas, distances and volumes. The extrapolation from 2D to 3D is a limit of this approach. Nowadays there is a standardization of the main histomorphometric measurements. [41] [42]

These parameters are divided into the following macro groups:

- Bone structure parameters;
- Parameters of bone microarchitecture;
- Static parameters of bone reformation;
- Dynamic parameters of bone reformation;
- Derivative parameters.

These techniques are used mainly in the clinical practice. However, these methods are invasive; indeed, it is essential to perform a biopsy on the grafting site to carry out the investigations. Moreover, the difficulty of biopsy depends on the body district involved.

Micro-TC is another qualitative test and this technique is performed by a biopsy. A sample of tissue is collected and scanned with suitable instruments. [33]

This method is appropriate to study of bone tissue and to study of bone substitute implant, because modern devices offers spatial resolutions below 10 µm.

The most widely used imaging technique to analyse bone microstructure is the micro-TC. This allows to define the histomorphometric measurements that are calculated during histomorphometry, directly in three dimensions, thus overcoming the limitations of histomorphometry. But the micro

TC image can show artefacts that has to be eliminated or reduced as much as possible, and this image modification may attenuate important bone tissue features. [43]

1.4.2. VOLUMETRIC METHOD

Volumetric investigation methods permit to assess quantitatively a bone substitute.

These techniques are not much applied a clinical level, but they are much used in industrial sector, to perform a post-marketing surveys by companies which produce bone substitutes.

In clinical practice doctors carry out a qualitative analysis, indeed they observe a CT exam to evaluate if the implant fulfilling well its role. Instead, at industrial level, a quantitative analysis is important to define in engineering way the regenerate bone within or near a bone substitute.

For this reason, there are few studies in literature on volumetric growth.

CT scan is the starting point to perform the volumetric analysis of regenerated bone, because this exam permits to reconstruct the 3D matrix, and successively the overlapping and the subsequent volumetric subtraction of these rebuilt matrices. [44]

Indeed, on a previously thesis work, a method that permit the calculation of volumetric growth, namely the volume of new generation bone, was found. This method is not based on three-dimensional matrices in Hounsfield units, but it creates 3D volumetric models that permit a more accurate computation to overlap and subtract volumes. [27]

1.4.3. DENSITOMETRIC METHOD

Densitometry is a technique to evaluate a bone substitute, which permits to assess the mineral density of bones. This method allows to study the initial bone density of the bone graft and to understand how this varies over time. If after a few months, the mineral density is equal or similar to that of the healthy bone, it means that osteogenesis is happening properly.

The most of densitometric techniques use X-ray attenuation which is obtained when the radiations cross the skeletal region to be examined. [45]

Two Transmission ways are available: the SXA (single energy X-ray absorptiometry) and the DXA (dual energy X-ray absorptiometry). The basic principles are the absorption and the interaction

between bone tissue and photons produced by X-ray source. The densitometry scanners differ in calibration, generation, energy spectra and voltage used. These two techniques are based on the two-dimensional representation of the examined bone structure, like the imaging in traditional radiology. This is a flaw of this technique, because the different anatomic regions are represented on a plane. [46]

That means the integrated measure comprising all parts of the tissue that the radiant beam meets. This is unsatisfactory because it does not permit to investigate a single part of tissue.

Bone densitometry allows to define the property of the bone tissue or the graft, the main ones are:

- Measurements of cortical thickness;
- Measurements of bone mass;
- Measurements of bone mineral density in a given area (BMD)

The bone mineral density ("Bone mineral density", BMD) is the amount of minerals contained in a bone volume unit.

Quantitative Computed Tomography (QCT) is another method applied to evaluate bone mineral density.

Quantitative computed tomography is an imaging modality, used in the research field, for the study and evaluation of quantitative parameters, the most frequent of which are skeletal system evaluation parameters. [47]

Before to talk about the QCT analysis, the basic aspects of computed tomography are shown in brief.

1.4.3.1. COMPUTERIZED TOMOGRAPHY – BASIC ASPECTS

Computed tomography (CT), which uses X-rays to produce three-dimensional images, is particularly useful for imaging skeletal structure. [48]

CT images are created by shooting a series of X-rays through an object of interest onto a detector.

The main components of a CT scanner are the **gantry** and the **table** on which the patient is placed, shown in Figure 1.18.

Figure 1.17 - Diagnostic room for a TCMS scanner (Lightspeed VCT; General Electric), where the gantry and the patient table are visible

The Gantry is the main structure of a CT scanner and contains: the X-ray tube, the detectors, the high voltage generator, energy transmission devices, collimators and the DAS (Data Acquisition System). Usually, the gantry has a ring opening with a diameter of about 70cm, through this gap the patient table flows during the scan. In Modern multi-layer CT systems (MSCT) (third generation CT), an arch constituted by more rows of detectors rotates around the patient together with the X-ray tube, which is opposed of 180 °.

The X-ray tube represents the core of CT system and must own a high thermal dissipation capacity. Whereas detectors make up the detection system of computerized tomograph.

The X-ray tube produces the photons which irradiate the anatomical site. These photons are then collected by detectors. In this way the energy of the photons, that emerge from the patient, is transformed into electrical signals to form the CT image.

The X-ray beam and detector rotate around the object so as to obtain many different projections.

The CT images are reconstructed images, which are obtained with the reconstruction of Raw data using a back-projection technique, to deduce features of the object in question. [49]

Each reconstructed image is a 3D matrix of volume pixels, or “voxels”. These voxels have typical sizes between 0.5 to 1.5mm per side. Each voxel has a gray value that is related to X-ray attenuation and is usually expressed in Hounsfield Units (HU; [50]) named after the inventor, Sir Godfrey Hounsfield. Hounsfield Units are normalized units, such that values of −1000 and 0 correspond to air and water at STP, respectively, with positive values being associated with tissues that attenuate X-rays more, such as muscle and bone. [48]

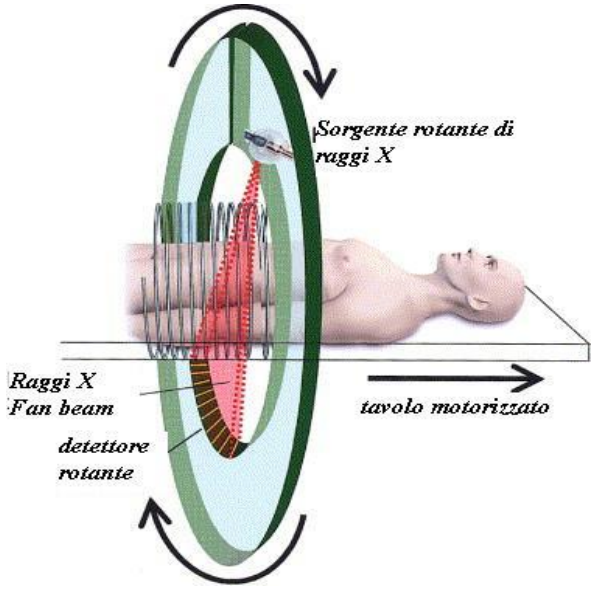

Figure 1.18 - - Computerized Tomography operation [58]

Multislice computerized tomographs (MSCT), are an evolution of spiral computerized tomographs. They carry out a simultaneous acquisition of multiple layers of the patient; the MSCT can be used both in axial and spiral mode. The advantages of these systems are: shorter acquisition time, scan of larger volumes in the same time intervals, reduction of artefacts caused by movement of the patient, acquisition of thin layers, improvement of spatial resolution. For this reason, the reconstructed images have a better quality. MSCT devices have a cone-shaped X-ray beam and the detection system is a matrix of symmetrical detectors. Scanning method is roto-translational (helical) continuous. MSCT systems are also able to rebuild layer thicknesses different from those acquired by combining data from multiple detectors. [49]

1.4.3.2. QCT

The QCT analysis is a non-invasive method and entails the calculation of certain parameters like volume and density through CT image data and therefore can be a powerful means for evaluating bone quality and quantity. [48]

This technique surveys the real density of bone tissue in a specific volume (mg/cm3) without influence of other bone structures or tissues that may alter the result. In this way, this technique exceeds the limits of projective techniques (SXA and DXA).

The Bone densitometry (DEXA) calculates the density value of a defined area and this measure is conditioned by all components of the bone tissue. Instead, the innovation of QCT is the distinction and calculation of bone density separately in the trabecular and cortical components or soft tissue.[51]

In order to carry out a Quantitative TC analysis it is possible to use a normal multilayer tomograph with a resolution of the order of millimetre and modern image processing and reconstruction software. In fact, these instruments need a dedicated software for bone densitometry.

The anatomical district in study is scanned from the scanner, which divide the anatomical part into 'slices' that have a specific thickness based on the examined body area. Successively in the scanned anatomical site is defined a region of interest (ROI) and inside this selection it is analyzed the BMD of the graft or bone part with a calibration phantom of reference.

The use of calibration phantom in the QCT analysis is very important.

The values of Hounsfield (HU) are based on linear regression of TC numbers derived from calibration phantom; and a calculate on voxels within the ROI is performed. Indeed, an intensity matrix is built, namely a voxel array, and for each voxel is associated a defined density value. To achieve the conversion from Hounsfield unit (HU) to density units (mg/cm3) is used a sample nomogram transformation, namely an empirical linear relationship (calibration line) between density and HU.

After the mean density of anatomical district has been calculated, this value is compared with reference parameters, for instance in literature.

To limit the errors due to the operator's manual setting of parameters, the scanner should have a specific software for automatic setting of parameters.

With this method if features of calibration phantom are known, it is possible achieve properties relating to anatomical district on study. [52][53][54]

QTC is also used because it combines bone mineral density and bone structure, for example microarchitecture and trabecular orientation, that permit to establish bone quality**.**

1.4.3.3. DESCRIPTION OF THE TECHNICAL PARAMETERS OF ACQUISITION IN CT QUANTITATIVE

To conduct a quantitative analysis, it is necessary to set the correct parameters to the computerized Tomograph console. It is important to achieve the compromise between image quality for adequate quantitative assessments and patient radio exposure, in accordance with the **ALARA** (as Low as Reasonably achievable) principle. [49]

Properly studied protocols are pre-set in the TC, in order to respond correctly to the questions of tomographic examination at any time, both in emergency situations and during normal work.

The parameters of scanning the protocols can be modified by the operator in moderation and only if strictly necessary, evaluating the consequences.

The main objective is therefore to obtain the desired information while keeping to a minimum the dose dispensed to the patient.

Among the main parameters assessed in this thesis work are: [49]

- **VOLTAGE -** The value of this parameter represents the potential difference (expressed in KV), between anode and cathode of the X-ray tube, which accelerates the electrons produced by the heated wire of the cathode to the anode. The interaction between electrons and anode produces the X-ray beam, which has a changeable energy with continuity between zero and the peak voltage of the X-ray tube (KVP) and according to the difference in potential will be more or less penetrating. The voltage used in a CT scanner typically varies between 80 and 140 KV.

  Usually the choice of the KV value to be used is based on the patient's size: greater is the patient's diameter, higher is the voltage required to ensure adequate penetration by the X-rays. The variation of KV influences image quality, indeed, greater is the voltage and greater is the average energy of photons, therefore a greater number of photons will cross the human body. This means an increase of the number of photons detected, therefore higher image quality.

  But, the variations of this parameter can also bring significant differences in the dispensed dose as well as in the Hounsfield numbers and therefore in the quantitative evaluations.

- **CURRENT** - The current of the Tube regulates the amount of photons that pass through the patient in the unit of time, is measured in mA. The mA influences both the image quality and the radiation dose that the patient receives. Between the mA and the delivered dose there is a linear relationship, so if you increase the mA you have a dose increase and a noise reduction.

In tomography machine of the last generation, the delivery of mA is controlled by automatic modulation systems that act on the three X, Y and Z axes, adapting the delivery of the mA to varying the attenuation of the tissues examined. To ensure that the modulation is correct it is necessary that the patient is centered correctly or the system compensates by increasing the mA and increasing the dispensed dose. The variations of the mA have a little influence on Hounsfield units always if they do not change so much noise.

- **FIELD OF VIEW** - In TC, there are two types of field of view (Field of View; FOV); the Scan Field of View (SFOV) and the Display Field of View (DFOV). The SFOV is the circular region of the XY plane that originates at the isocentre of the gantry that is acquired by the scanner. The Scan FOV must always be larger than the patient's circumference. All that is not included during the acquisition by the Scan FOV cannot be rebuilt later, so it is important to center the patient well. The Display FOV is the circular region of the XY plane, which includes the part of the image that will be rebuilt with the appropriate reconstruction algorithm.

- **RECONSTRUCTION ALGORITHM - STANDARD E BONE** - STANDARD and BONE are two reconstruction algorithms. The reconstruction algorithms are convolution filters and differ in relation to spatial resolution and the contrast characteristics of the images they determine. These two aspects concerning the quality of the images are, in general, in opposition to each other: if one wants to enhance the contrast resolution one has a loss of the spatial one, and vice versa. Therefore, the reconstruction algorithms can be classified into two main families:
  - Smoothing algorithms, which improve contrast resolution and reduce image noise;
  - Edge/enhancement algorithms, which improve spatial resolution by highlighting the details, have a sharpening function.

  The choice of the algorithm to be used depends on which type of visualization is most suitable for the interpretation of the images. It is important to rebuild the same TC scan with different kernels in order to get a full view of all the details of the image.

  Usually the first reconstruction is always the one with the "standard" filter that allows to obtain an image with a right compromise between spatial resolution and background noise. The Subsequent reconstructions will be chosen according to the type of district that it is wanted to analyse and what it is wished to privilege eg. In the study of bone structures, it is necessary to

have also a reconstruction with "bone" filter aimed at increasing the sharpness of the smallest details. [49]

- **ASIR** - ASiR™ (Adaptive Statistical Iterative Reconstruction) is a system patented by GE (General Electric) to reconstruct the raw data of images using iterative algorithms based on statistical models. These algorithms, usable by the first reconstruction or subsequent rework of images, allow to obtain examinations with a high diagnostic value interacting with the modulation capacities of the current of the tube and exceeding the limits of Filtered back projection.
  The great advantage of a correct use of the ASiR ™ software is to allow a more accurate reconstruction of the raw data acquired by the scanner, allowing an important reduction of noise and dose delivered to the patient and maintaining the diagnostic value of the images.
  ASiR ™ image reconstruction involves defining the desired noise reduction level (Noise Index. More precisely, 10 levels of balance are available (ASiR ™ percentages) that simply correspond to the amount of noise reduction based on a maximum of 100% of the image reconstructed with the original image data. Image reconstruction is a fusion of the original image and a percentage of a reconstructed image. [55] [56]

- **MAR** - Metal artefact reduction (MAR) algorithms were developed to combat the problem, like streak artefacts, caused by the presence of metallic elements. Metals produce a number of non-physical artefacts in CT scans including beam hardening and photon starvation, resulting in poor image quality. These artefacts lead to less accurate contouring of bone and organs at risk and inaccurate HU values throughout the patient. To remove unwanted artefacts, a metal artefact reduction (MAR) algorithm is implemented during CT reconstruction. General Electric Healthcare is the company producing GE-Optima CT660, CT scanner used in this study. In 2013, this company released “Smart Metal Artifact Reduction (MAR)”, which is an algorithm to reduce metal artefacts in projection space using a method known as projection inpainting. The principle of projection inpainting is to replace corrupted projections with synthesised projection data. These data are created using interpolation of neighbouring projections or with a prior image. The disadvantages of using projection inpainting consist of resolution decrease and shortage of consistency between synthesised and real projections.
  The GE-MAR algorithm has three different steps to remove these drawbacks.

- The first step of the algorithm identifies corrupted samples, that coincide to metallic elements. Successively, synthesized projections are produced through “higher order interpolation”. After this operation, these projections are back-projected, creating the first step MAR image.
- The second step entails the realization of an advanced prior image using an “innovative signal processing technique”. This image is segmented and the tissue classified image is created. Successively the tissue classified image is forward projected to create the synthetic data in projection space. Through an “advanced technique”, the synthetic data substitute the corrupted projections to produce the inpainted data. this step must be correct to avoid the production of additional unwanted artefacts.
- The third step finish in projection space, showing anatomical parts that are hidden by metal artefacts in image space. The original projection data, inpainted projection data and a metal mask are combined to produce the final corrected projection data. The low contrast resolution is superior than the original projection data and artefacts are also reduced from the inpainted projection data. Finally, the corrected projection data is back-projected to produce the MAR corrected image. [57]

- **CTDIvol** - Computed Tomography Dose Index Volume. CTDIvol is a dose descriptor that treats the absorbed dose for non-contiguous scans. It calculates the absorbed dose from the entire scan volume for a given Protocol. The CTDIvol is usually supplied by the scanning equipment.

Quantitative CT (QCT) analysis calculate specific parameters from CT image data. To obtain a correct data, it is necessary give attention at all steps of the acquisition.

The quality of the CT images is influence by many factors, these accordingly also affect the quality and the precision of QCT data. Some of these factors can be: CT acquisition parameters, reconstruction algorithms, patient positioning, artifacts, and the presence or absence of a calibration phantom. To carry out Quantitative CT analysis in specific anatomic districts, like bone, it is essential use a calibration phantom. Therefore, for bone analyse, the calibration phantom is included in the CT image. The calibration phantom, usually, includes a known equivalent density of potassium phosphate or calcium hydroxyapatite in order that to define an empirical linear relationship between density (ρ) and HU, like $HU=m * \rho+b$ where ‘m’ is the slope and ‘b’ is the intercept. Parameters such as bone mineral content (BMC; g) can be calculated by multiplying the

ρHA, or vBMD (g/cm3), of a single voxel by its volume (cm3). the same regions must be exactly identified for each analysis to can do comparisons.

To conduct a correct QCT analysis it is important define a consistent protocol that standardizes as many parameters; in order to minimize the influence of non-anatomic factors on image acquisition for QCT analysis. Practices for bone densitometry , Standard Operating Procedures (SOPs) should be established for QCT scans to define and standardize data acquisition. [48]

1.5. EXSISTING DENSITOMETRIC EVALUATION OF SMARTBONE®

On previous thesis work, a first densitometric analysis of bone substitute SmartBone® has been carried out, in collaboration with the CTO of Turin.

Through preliminary evaluations, it has been defined that density of SmartBone® is lower than that of the compact bone, so often it is not clearly defined within radiographs or TCs.

Therefore, it is essential analyze the QTC parameters to be set to obtain a better image of the SmartBone® in the TC exam and a more suitable evaluation of osteointegration and osteogenesis.

Some aspects of Qualitative radiologic evaluation vary based on type of osteointegration that will be assessed with SmartBone® (cortical, spongy or different behaviour). Indeed, HU values have a different distribution and the parameters to be extracted from the selected volume have to be selected appropriately.

Previously, the ROI (region of interest) has been selected in bone district to assess and the mean value of Hounsfield units within the ROI has been defined to determinate of BMD.

It was observed that the average of Hounsfield units varies depending on the ROI selected and with the variance of following parameters of scanner: the kernel which is a reconstructive algorithm that processes raw data in order to get better results, the ASIR that reduces radiation doses and the MAR that allows the reduction of metal artefacts.

Moreover, other tests have been conducted to permit a better SmartBone® recognition during image analysis. Qualitative evaluations on SmartBone® were carried out on phantom in the ankle district.

The goal of these tests has been that to assess the influence of exposure parameters on the image. The exposure parameters determine the mode of photon emission by the X-ray tube and are kilovolt (kV), milliAmpere (mA), scan time and the collimation beam.

An example of these tests is shown in the image (see figure 1.15), where four different ROIs (represented by the circles) as follows: spongy bone, compact bone, tissue around the bone and the SmartBone® block attached to the puppet's ankle are visible. For each of these ROIs, the HU average and the HU standard deviation were obtained.

It was observed that: HU varies strongly depending on the selected kV parameter; instead, HU does not vary significantly depending on the selected mA parameter and with the change of beam collimation.

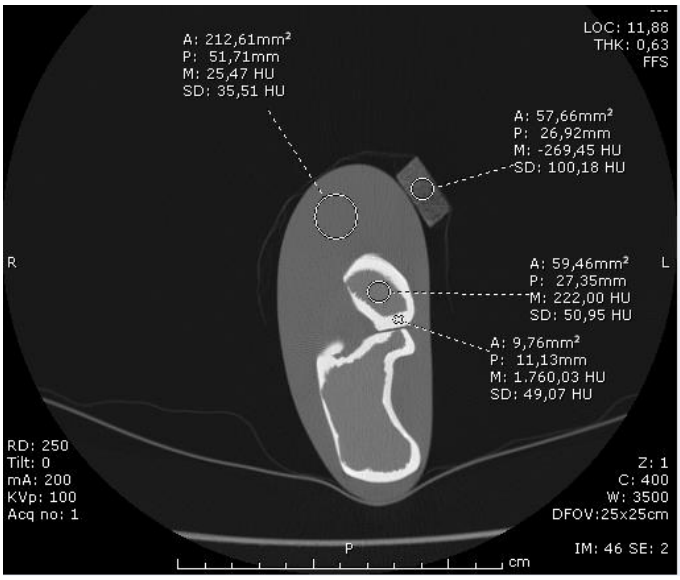

Figure 1.19 - Different ROIs in the test

In this way, it was possible to establish that kV is a key parameter, to improve the image quality of SmartBone®. But the choice of kV is not easy, because it is also necessary to consider the filters applied by the machine and in particular the MAR filter.

1.6. AIM OF THIS WORK

The aim of this study is to perform a radiologic characterization of the SmartBone®, defining the technical parameters of CT acquisition in order to build an acquisition Protocol TC-Scan for a correct evaluation of the SmartBone®.

Chapter 2 shows how the TC acquisition test it has been carried out, in which the main technical parameters have been changed, in order to evaluate the effects on the materials present in the test, in particular for the SmartBone® samples and for the calibration Phantom known values of density. In order to do a quantitative evaluation, Image J software was used, which allowed to evaluate the HU trends within a specific volume. For the Calibration phantom, the manufacturer has supplied the density values of six inserts on phantom, but the HU values are not known. For this reason, it was appropriate validate Image software with the use of Mimics software. The validation was performed going to calculate the HU ranges for all elements present in the test with the Image j software and later the correctness of these HU ranges was verified with Mimics software. Because with both software the results are the same, so the quantitative analyse will be reliable. Chapter 3 shows the results obtained from the acquisition test with the variation of technical parameters and the following chapter evaluates these effects in order to construct a TC protocol.

Moreover, in Chapter 2, the mg HA/cm3 values of the calibration phantom, supplied by the company, are also related to the average HU values calculated and a linear relationship is obtained. Going to replace the average HU values on the volumes of SmartBone® previously calculated, in the linear model obtained, it was possible to obtain the mineralization of the SmartBone® in terms of mg HA/cm3. After the TC pre and TC post of a patient in which SmartBone® was implanted, it was possible to evaluate bone regrowth after the SmartBone® implant. In Chapter 2 the methods used are shown: a densitometric analysis and a volumetric one. Chapter 3 shows the results obtained from the application of this method. In chapter 4, the results obtained from the Densitometric analysis and the quantification of the volume of regenerated bone are discussed. In chapter 5 of conclusion a CT scan protocol are presented, a developed methodology for evaluation of bone regrown are shown and finally mineralization of SmartBone® obtained with a relation between HU values and amount of hydroxyapatite is proposed.

2. MATERIALS AND METHODS

2.1. ACQUISITION PROCEDURE

Acquisition tests were carried out at the Radiology Department of the Orthopaedic Traumatology Center (CTO) in Turin with several samples of SmartBone®.

The experiment was made up of the following elements:

- a QRM-BDC / 6 calibration phantom with six inserts of different homogeneous density,
- a basin of water containing the following elements:
    - four SmartBone® samples in different formats:
        - a compact sample of SmartBone®, rectangular-shaped and measuring 20x10x10mm,
        - a compact sample of SmartBone®, cubic-shaped and measuring 10x10x10 mm,
        - a test tube containing a granular sample of SmartBone®, of 2-4mm granulometry,
        - test tube containing a granular sample of SmartBone®, of very fine-sized like a powder, with a 0.25mm granulometry;
    - two cylinders of known homogeneous density: one of compact bone and one of acrylic (similar to water) of dimensions: diameter 28mm and length 90mm;
    - a sample of bovine bone. It is not a SmartBone®, but a sample of bovine bone taken from a butcher. It has been covered with latex gloves to reproduce the effect of vacuum and avoid areas with air. It has been placed inside the container with the other components to have an element that was as close as possible to a human bone sample.

The study was conducted with **64-slices GE Healthcare - Optima CT660.**

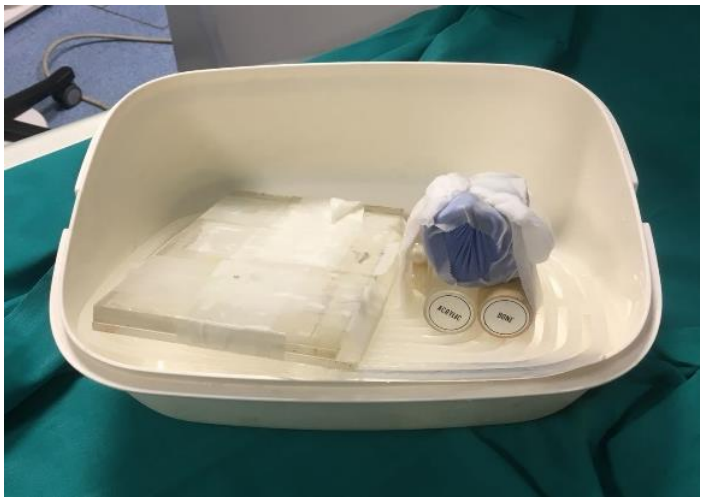

Figure 2.1 - Image of the test: the two homogeneous cylinders and the bovine bone covered by blue glove are visible

Figure 2.2 - Image of the test: The Calibration phantom is located under the basin, but above the basin are the other elements in the studio

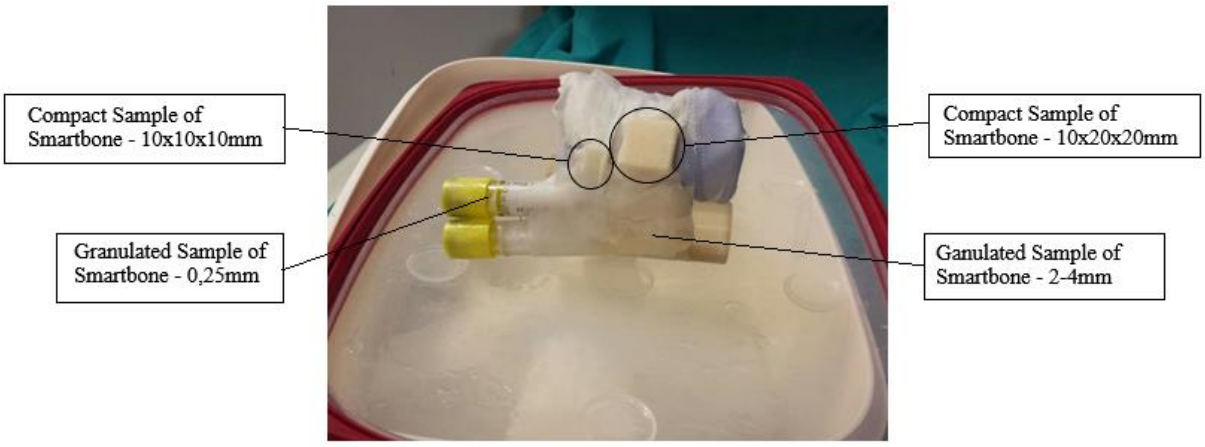

Figure 2.3 - This image shows the four samples of SmartBone®

2.1.1. GE HEALTHCARE - OPTIMA CT660

The equipment used is a third-generation CT scanner belongs to MSCT: GE Optima ™ CT660 with 64 banks; it is able to collect 64 scan data files at the same time. This data collection is obtained through a 64-file detector associated with a DAS (Data Acquisition System) also equipped with 64 files. The 64-file detector and the 64-DAS offer the greatest advantages when used in helical mode, as the data of the 64 detector files are selectively combined and weighed during reconstruction in order to achieve the optimal balance between axis resolution Z of the image, noise and helical artefacts. [58][59][60]

Figure 2.4 - – Two views of GE HEALTHCARE - Optima ™ CT660 [60]

Technical Specifications	
X-Ray Generator	
Generator type	PERFORMIXTM 40
Generator power (KW)	72 KW for a heat content of the anode of 383 KJ
Selectable KV values	80, 100, 120 ,140
Values mA selectable	range values: 10 - 600 mA, in increments of 5 m
X-Ray Tube	
Radiogenic Source Thermal Capacity (Mhu)	7.0 Mhu
Anode rotation	8400 rpm
Detectors	
Type of detectors	Ceramic scintillators
Maximum number of data series simultaneously acquirable (N ° Slices)	64
Number of detectors per row	776
Number of elements along the z-axis	64
Axial and Helicoidal scans	
Rotational times for axial scans (s)	0.4, 0.5, 0.6, 0.7, 0.8, 0.9, 1 or 2 seconds (p408)
Rotational times for helical scans (s)	0.4, 0.5, 0.6, 0.7, 0.8, 0.9, 1 second
Nominal beam thicknesses along the z-axis for axial scans (mm)	0.625, 1.25, 2.5, 5, 10, 20, 40 mm
Nominal beam thicknesses along the z-axis for helical scans (mm)	0.625, 1.25, 2.5, 3.75, 5, 7.5 and 10mm

Table 2.1 - System Features [59]

The acquisitions have been performed **helical mode** and with ASIR **30%** with a **standard reconstruction kernel.**

During the acquisition tests the following technical parameters have been modified, so that they can be evaluated:

- **Patient Centring**, which has been changed by -5cm and +5cm;
- the **voltage,** which was been set at 120KV and 140KV
- the **MAR,** Metal Artifact reduction, its presence and absence have been evaluated;
- the **FOV,** that is Field of view. A **FULL FOV (FOV40)** and a **REDUCED FOV (FOV20)** have been set. The REDUCED FOV is utilized to improve the spatial resolution transversal; [49]
- the use of the **STANDARD** or **BONE** algorithm;
- The **Presence of Metallic Material** like: a reverse shoulder prosthesis, a screw and an elbow plaque
- The different position of metallic material;
- The different orientation of calibration phantom;
- The different position of calibration phantom QRM-BDC/6;

2.1.2. QRM-BDC/6 - CALIBRATION PHANTOM

The QRM-BDC-Phantom allows a direct HU vs. HA calibration with respect to a bone mineral density evaluation by quantitative computed tomography. The QRM-BDC/6 Phantom houses six 18 mm diameter cylindrical inserts each providing 0, 100, 200, 400, 600 and 800 mg HA / cm^3 (specified BMD), respectively.

Known diameter has been possible to determine the area of the six cylindrical inserts that is equal to 254.34 mm2. The calibration phantom has a standard length of 700 mm.

The Phantom can be directly placed under an object to evaluate the bone mineral content of the object by quantitative CT. As base material of the six inserts CTWater® is used. CTWater® is a solid water equivalent plastic offering the same X-ray attenuation properties as real water. The shape of the phantom is slightly bended for an adequate fit under the object of interest. [61]

Phantom material:	resin (soft tissue equivalent)
Overall dimensions:	
Width x Height	225 mmx 25 mm
Length:	up to 700 mm
Inserts Ø:	Ø 18 mm
Inserts L:	up to 700 mm
BMD:	0, 100, 200, 400, 600 & 800 mg HA/cm^3

Table 2.2 - Datasheet of QRM-BDC/6 [61]

Figure 2.5 - QRM-BDC/6 Phantom

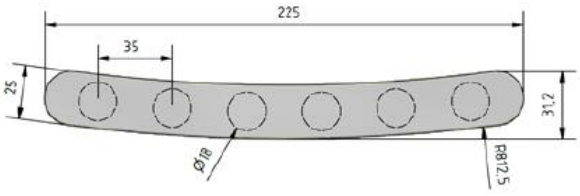

Figure 2.6 - schematic drawing of the panthom

2.2. CLASSIFICATION OF CT IMAGES

After the Acquisition Test all the images related to the test were present inside ST0 folder. Subsequently, the classification of the images within the ST0 folder was performed.

Inside the folder ST0 there were 84 subfolders corresponding to the series (SE) of acquisition tests executed. These subfolders have been divided into 13 folders related at the tests done:

- 11 folders correspond to the acquisitions to be taken into consideration,
- a folder contains the SE 82 and SE 83 relative to DOSE REPORTS,
- and finally, there is a last folder containing the series from SE 24 to SE 43 corresponding to the acquisitions carried out in axial mode with which it isn't possible to obtain the MAR and therefore have been excluded.

The 11 folders correspond to 11 acquisition tests performed:

1. In the absence of Metallic Material
2. Patient Centring +5cm
3. Patient Centring -5cm
4. In the presence of metallic material: screw and plaque
5. In the presence of metallic material: stem close
6. In the presence of metallic material: far stem
7. In the absence of Metallic Material
8. In the absence of calibration phantom QRM-BDC / 6
9. Placing the calibration phantom QRM-BDC / 6 sideways
10. Rotating the system
11. Placing the calibration phantom QRM-BDC / 6 sideways

Within the 11 folders the different series have been inserted. For each test there are always 5 folders related to the different setting of some parameters and sometimes there is an additional folder containing the SCOUT of the test.

The 5 folders correspond to:

- ACQUISITION - STANDARD - FULL FOV
- RECONSTRUCTION – STANDARD WITH MAR– FULL FOV
- RECONSTRUCTION - STANDARD – FOV 20
- RECONSTRUCTION - BONE – FOV 20
- RECONSTRUCTION – STANDARD WITH MAR – FOV 20

Each folder inside has 202 images divided into two subfolders containing 101 images each, related to the test carried out with 120KV and the test performed with 140 KV.

The exception is the folder '10. Rotating system' that contains 380 images.

For this study the first 7 acquisitions were considered:

1. In the absence of Metallic Material
2. Patient Centring +5cm
3. Patient Centring -5cm
4. In the presence of metallic material: screw and plaque
5. In the presence of metallic material: stem close
6. In the presence of metallic material: far stem
7. In the absence of Metallic Material

The acquisitions carried out in axial mode have been excluded, because it is not possible to obtain the reconstruction with MAR and therefore to evaluate its efficacy. The last four acquisitions are also excluded:

8. In the absence of calibration phantom QRM-BDC / 6
9. Placing the calibration phantom QRM-BDC / 6 sideways
10. Rotating the system
11. Placing the calibration phantom QRM-BDC / 6 sideways

The acquisition in the absence of calibration phantom has been excluded because the phantom is essential for the study.

The acquisitions with the calibration phantom placed sideways have not taken into consideration because during the test it was observed that there were obvious artifacts with the phantom placed laterally.

Finally, the acquisition with the rotated system was not taken into consideration because it was not comparable with other acquisitions.

Furthermore, for each acquisition the following two tests has been considered:

- **ACQUISITION - STANDARD - FULL FOV**
- **RECONSTRUCTION – STANDARD WITH MAR– FULL FOV**

In fact, in the other three tests a REDUCED FOV (FOV 20) is used while in this case it is necessary that the vision of the calibration phantom and of all the elements present in the test is complete.

The goal is to calculate the average values of HU on a volume, which was possible using the Image J analysis software.

2.3. IMAGE J SOFTWARE

ImageJ is an open source software, programmed in JAVA, born with the aim to emulate the functionality of the most common commercial software for image processing and that allows to visualize, modify, analyze, process, save and print 8-bit images, 16 - bit, 32 - bit. It supports TIFF, GIF, JPEG, BMP, DICOM, FITS and "raw" formats.

This software allows to perform operations in parallel, to measure distances, angles, and plot graphs. It supports "stacks", that is the series of images that share the same window and offers the possibility to calculate the area and statistics on pixel values relative to the regions (ROI, Region Of Interest) selected by the user.[56]

This software associates the x and y axes to each 2D image; along the z-direction, instead, it has all the slices that have been acquired through the TC.

By selecting a point in the 2D image, the program returns all the HU values corresponding to the selected point for all the slices that make up the TC image.

In the case where a region of interest (ROI) is selected in the 2D image, Image J allows to obtain the average HU value of the selected region. Furthermore, for all slices of the TC image, the software is able to return the average HU values of the selected region.

Therefore, for all the slices of the TC image, it is obtained the average HU value within the region of interest.

Then going to mediate the series of values obtained for the number of slices you get the average HU value on the volume considered.

2.3.1. TRACK THE ROI

Regions of Interest (ROI) were drawn on the elements under study, to calculate the values of the HU on a volume. The ROIs were plotted on the 4 samples of SmartBone®, on the 6 inserts of the calibration phantom, which have a known amount of Hydroxyapatite, and on the two homogeneous samples, one of bone and one of acrylic.

2.3.2. TRACKING A ROI WITH IMAGE J

Once you have opened Image j (Fig.), To select the TC you select *'File'- 'Import'- 'Image sequence'*

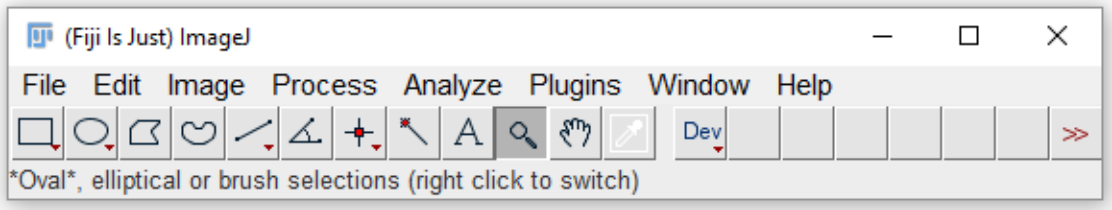

Figure 2.7 - Software ImageJ Interface

At this point, the software opens a new window *'open image sequence'* where it is possible select the folder containing the CT to be imported. Furthermore, it is also advisable to check that the slices are all in sequence because in this way the software can correctly reconstruct the 3D image.

Once the folder is selected and the option *'open'* is pressed, the software opens a *'sequence options'* window with the options on the sequence of images to be selected. In this case, the default options were left. It was then checked that the CT was the right one and that it correctly represents the object under study.

One of the selection options is used to trace the ROIs.

On the six inserts of the calibration Phantom, on the two homogeneous cylindrical samples and on the two samples of granulated SmartBone® s, the *'oval selections' + shift* option was used to select the regions of interest. Instead, on the two SmartBone® blocks, the *'Polygon selections'* option was selected to trace the ROIs.

After tracing the regions of interest, select *'Analyze' - 'Tools' - 'ROI Manager'*, then it is opened the *'ROI Manager'* window whereby selecting 'Add [t]' the traced region is added as ROI. Going to select *'more' - 'save'* it was possible to save all the ROI defined as '.roi' files

2.3.3. ROI ON SMARTBONE® SAMPLES

To obtain the HU values on the volume of the 4 SmartBone® samples, a ROI was traced for each sample of the SmartBone® on the 2D image and the mean HU values of the ROI were obtained for each slice of the TC image.

In this case, however, to obtain the average HU value on the volume of the SmartBone® sample, all slices of the CT image were not taken into consideration. For each sample of SmartBone® the slices were taken into consideration that highlight the presence of the element in question.

To obtain the average HU value on the volume considered:

the values corresponding to the mean of the values of HU within the same ROI for all the images of the considered element have been obtained.

To do this, select the ROI of interest from the *'Roi Manager'* window. Then from the main window of Image j select *'Image'* - *'Stacks'* - *'Plot z-axis profile'* and you get a graph that represents the trend of the mean value of HU within the ROI for all slices. To obtain these values just select *'list'* and the software opens a *'Plot values'* window that shows the average value of HU within the selected ROI for all the slices that make up the CT image.

These values have been reported on an Excel sheet and **then going to mediate the series of values obtained for the number of slices considered we obtain the average HU value on the volume considered.**

This procedure was repeated for all four SmartBone® samples. For each test the values were obtained for the following four cases:

- 120KV ACQUISITION - STANDARD-FULL FOV
- 140KV ACQUISITION - STANDARD- FULL FOV
- 120KV RECONSTRUCTION - STANDARD MAR- FULL FOV
- 140KV RECONSTRUCTION - STANDARD MAR- FULL FOV

Moreover, given that these samples are not completely homogeneous and sometimes areas of presence of air are highlighted, a reference slice has also been considered, showing the average HU value of the selected region and the standard deviation.

The four SmartBone® samples are shown below:

- **Sample 1**: is a sample of a compact, rectangular-shaped SmartBone® with dimensions of 10x20x20 mm. This sample is present from the slice 23.75 to slice 42.5. Observing all the slices, however, it is observed that in some areas there are black spots that correspond to the presence of air due to intrinsic porosity. This material is not homogeneous, and it has porosity. This SmartBone® sample has also a defect in a block edge, which is like a larger black spot. The reference slice was considered: 38.75, of which the average value and the standard deviation are reported.

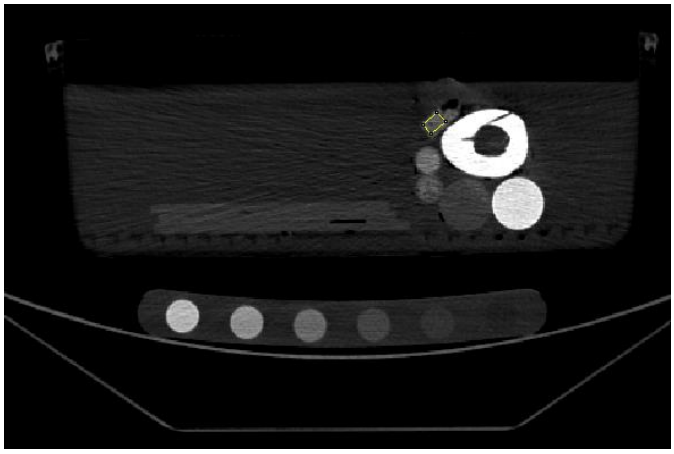

Figure 2.8 - ROI on SmartBone® Sample 1 (10x20x20 mm)

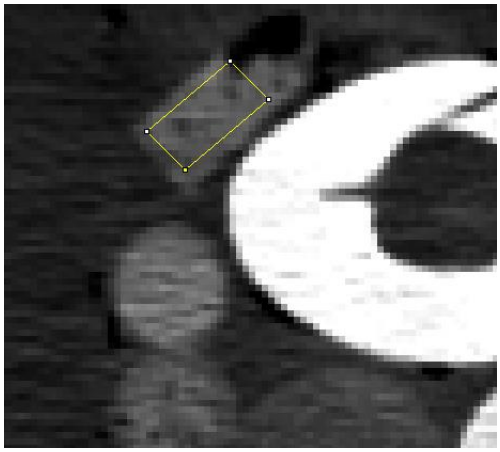

Figure 2.9 - ROI on SmartBone® Sample 1 (10x20x20 mm) - Zoom view

- **Sample 2**: it is a sample of a compact, cubic-shaped SmartBone® with a size of 10x10x10 mm. This sample is present from 8.125 to 14.375. As a reference point was taken: 38.75

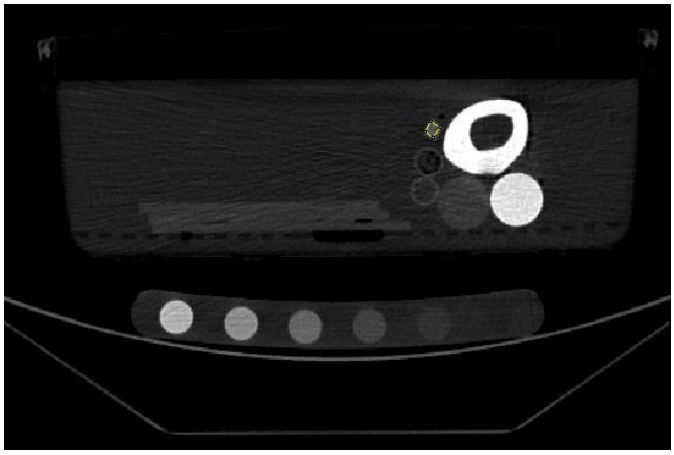

Figure 2.10 - ROI on SmartBone® Sample 2 (10x10x10 mm)

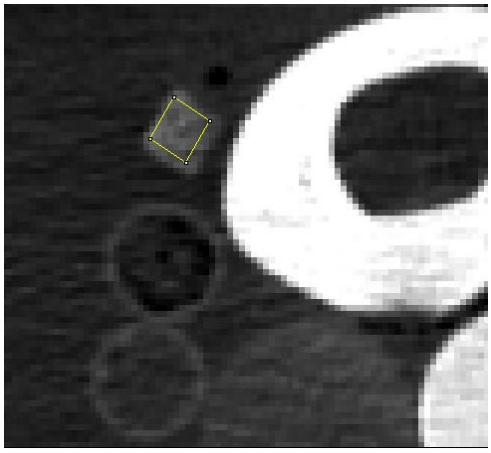

Figure 2.11 - ROI on SmartBone® Sample 2 (10x10x10 mm) – Zoom view

- **Sample 3**: it is a test tube containing a granulated SmartBone® sample with 2-4 mm granulometry. This sample is present from the slice 17.5 to 47.5. As a reference slice we considered: 32.5

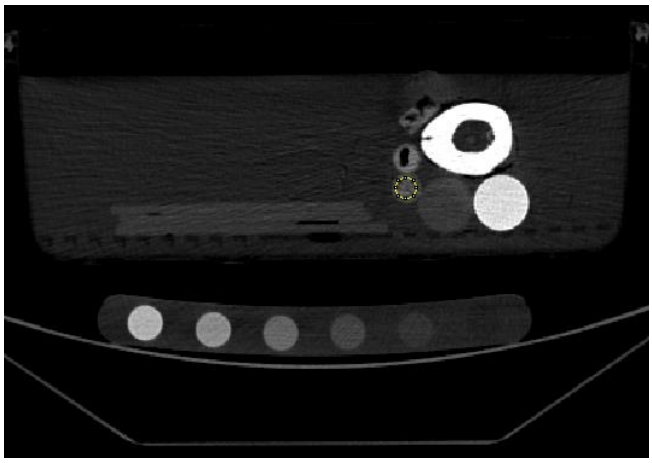

Figure 2.12 - ROI on Granulated SmartBone® Sample 3 (2-4 mm)

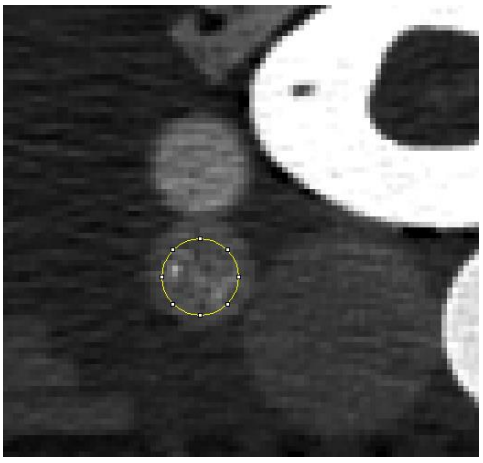

Figure 2.13 - ROI on Granulated SmartBone® Sample 3 (2-4 mm) - Zoom View

- **Sample 4**: it is a tube containing a sample of very fine-sized SmartBone® similar to a powder, with a 0.25mm particle size. This sample is present in the slice interval between 23.125 and 47.5. Observing all the slices, however, it is observed that in some areas there are black spots that correspond to the presence of air. This is due to the fact that the water inserted into the tube containing the granulate did not fill all the spaces. So, it is not a defect due to the material. As a consequence, a series of slices of the CT was considered, from 34.375 to 40.625, which are more homogeneous in which there are no black zones due to the presence of air. As a reference slice was considered: 38.75.

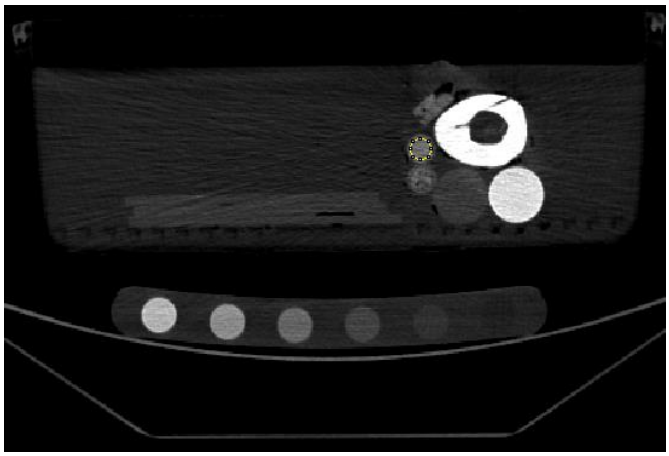

Figure 2.14 - ROI on Granulated SmartBone® Sample 4 (0.25 mm)

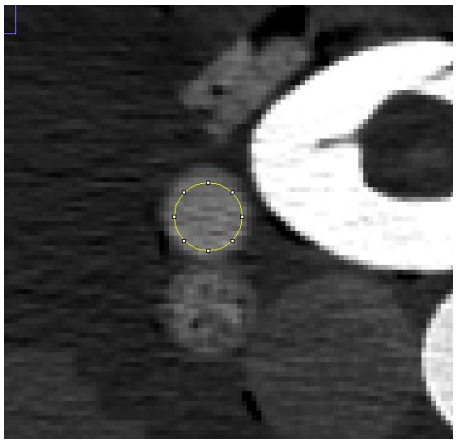

Figure 2.15 - ROI on Granulated SmartBone® Sample 3 (0.25 mm) - Zoom View

2.3.4. ROI ON THE PHANTOM AND ON THE CYLINDRICAL SAMPLES

The ROI (Regions of Interest) were plotted on the 6 inserts of the calibration phantom, which have a known amount of Hydroxyapatite, and on the two homogeneous samples, one of bone and one of acrylic.

The ROI that have been drawn are all circular in shape. On the inserts of the phantom we tried to trace the ROI that had dimensions very close to those of the six inserts provided by the company producing the phantom QRM-BDC / 6.

These ROI have an area equal to 256.598mm^2, a value very close to the area obtained from the data supplied by the manufacturing company (area = 254.34mm^2).

On the two cylindrical elements, two circular ROI were drawn, with an area equal to 593,872mm^2.

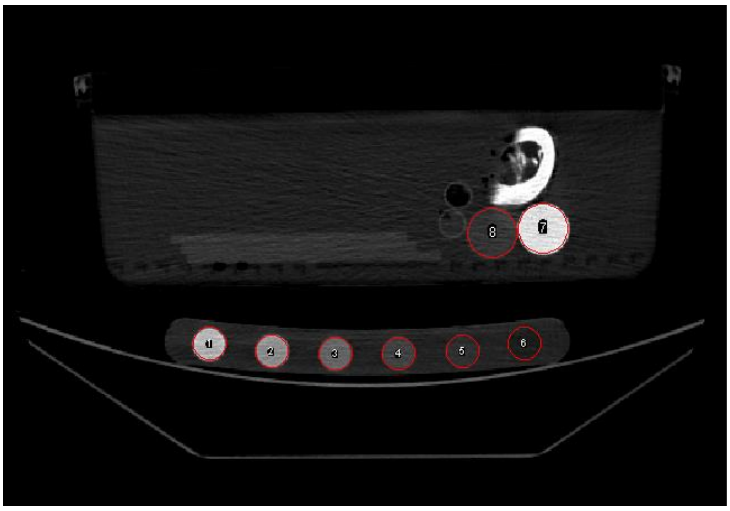

Figure 2.16 - - ROI on the phantom and on the cylindrical samples

Subsequently, the values corresponding to the average of the values of HU within a ROI for the whole series of images were obtained; this was repeated for all eight Regions of interest drawn. These values have been reported on 8 Excel sheets, each corresponding to a ROI.

Then going to mediate the series of values obtained for the number of slices you get the average HU value on the volume considered. This procedure was repeated for all seven tests and for each test the values were obtained for the following four cases:

- ACQUISITION 120KV- STANDARD-FULL FOV
- ACQUISITION 140KV - STANDARD- FULL FOV
- RECONSTRUCTION 120KV - STANDARD MAR- FULL FOV
- RECONSTRUCTION 140KV - STANDARD MAR- FULL FOV

2.4. PATIENT CENTERING EVALUATION

The first evaluation is related to the centering.

The first three tests were considered in the absence of metal elements and where the centering has been changed by + 5cm and 5cm:

1. In the absence of metal,
2. Centering + 5cm,
3. Centering -5cm.

The goal is to evaluate how the Centering (raising and lowering the bed) can influence the CT acquisition. To do this, we focused on the behaviour of the SmartBone® and then on the reference phantom and on the two cylindrical samples of known and homogeneous density.

The ROI were tracked on the various elements of interest and for all slices. After, the trend of the HU, within the ROI e for all the slices, was traced and it was evaluated.

To compare the results and perform reliable evaluations, HU trends was traced for all three tests both in the case of 120 KV and in the 140KV one.

The reconstructions with the MAR were not considered because this algorithm, as mentioned above, reduces the metallic artefacts, but in this case the acquisitions in the presence of metal elements were not considered. Moreover, for the granulated SmartBone® samples, the HU trend was not evaluated as a function of centering to avoid incorrect evaluations due to an inhomogeneous distribution of the material inside the test tube.

In the event that the HU trend is homogeneous, the variation of the centering does not influence the acquisition. If the HU trend is fluctuating and cyclical, then the centering influences the quality of the acquisition.

Furthermore, for SmartBone® samples, since all slices are not taken into consideration, the difference between the average ROIs values obtained from the metalless acquisition and the average values of the ROIs obtained from the acquisitions in which the centering was changed has been also calculated (Centering +5 and Centering -5).

It was observed in which conditions a minor difference is obtained, in order to highlight the parameters which permit to obtain the best acquisition.

2.5. VOLTAGE AND MAR PRESENCE EVALUATION

Acquisitions in the presence of metal elements and an acquisition, without metal objects, were taken into consideration to assess which is the best voltage and if the activation of MAR is effective:

1. In the presence of metal: screw and plate
4. In the presence of metal: close stem
5. In the presence of metal: far stem
6. In the absence of metal

The attention was paid to the acquisition in the absence of metal elements and the acquisition that has as its metallic element: the close stem, which is the worst condition. Indeed, the metal element (stem) is more significant in size than the other elements and is closer to the SmartBone® samples.
The difference between the HU average values within the ROIs obtained from the acquisition without metal elements and the HU average values within the ROIs obtained from the acquisitions in the presence of metal (screw and plate, close stem and distant stem) was calculated, to perform this analysis.
Calculating this difference between the acquisition in the presence of metal and the one without metal, it is assessed whether the acquisition in the presence of metal is influenced by metallic artefacts. The calculated average HU values of the volumes of the elements present in the test were considered to carry out this analysis. Reference slices were also considered to have more reliable results and to avoid problems of irregular homogeneity. The best acquisition is one in which a lower difference value was obtained and the best combination of acquisition parameters was highlighted.

2.6. DOSE EVALUATION

The parameters to be chosen, in particular the voltage, to define the protocol must also take the dose to the Patient. For this reason, the CTDIvol values supplied by the scanner were recorded during the acquisition Test.

2.7. CROSS-VALIDATION OF IMAGE J SOFTWARE WITH MIMICS SOFTWARE

The radiological study was carried out with the ImageJ software. The HU values were not given as a reference, but they were calculated, so another software: Mimics Innovation Suite by Materialise was used to validate the work done. In particular, the HU ranges of the elements present in the test were found with Image J and then the correctness of found HU ranges was verified through the Mimics Innovation Suite software.

The test, carried out in the absence of metal and without changes in the centring, has been chosen in order to validate the use of both software.

The following tests were assessed, to have a more correct analysis of the calculated HU range and the use of the MAR algorithm:

- The acquisition at 140KV in STANDARD mode, with a FULL FOV without the MAR
- The reconstruction at 140KV in STANDARD mode, with a FULL FOV and with the presence of the MAR.

2.7.1. USING IMAGE J SOFTWARE

With the software Image J were obtained the intervals of HU for each element. The first step was to import the TC of the acquisition to 140KV in STANDARD mode, with a FULL FOV.

To select each item in the test, the previously created ROI was used. To import ROI, you select ' *Analyze ' – ' Tools ' – ' ROI Manager '*, then the *' ROI Manager '* window opens, where selecting *' More ' – ' open '* allows you to select the. roi files containing interest ROI.

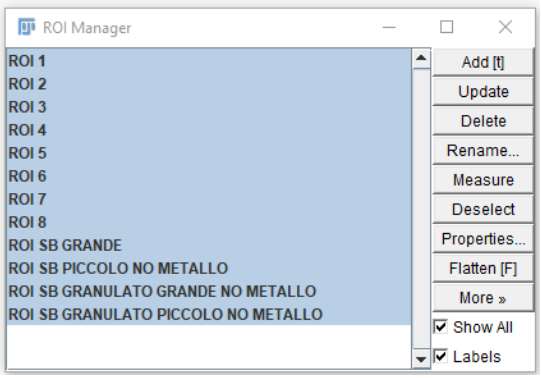

Figure 2.17 - ' Roi Manager ' window, where imported ROIs are visible

On each ROI and for all the slices constituting the CT image were derived the following parameters of interest, to determine the HU ranges for each element:

- Average HU Value,
- HU Standard Deviation,
- Minimum HU value,
- Maximum value of HU.

A ROI has been highlighted and then *' more '* – *' Multi measure '* has been selected to obtain these values; this procedure has been repeated for each region of interest. These values have been reported on an Excel spreadsheet. These parameters on the volume considered were obtained going to mediate the set of values obtained by the number of slices.
For each average value has been added and subtracted the standard deviation, for example going to consider the ROI 1, the following parameters have been obtained:

ROI 1			
AVERAGE	STD	MIN	MAX
884	127	218	1104

AVERAGE + STD	AVERAGE - STD
1011	757

Table 2.3 - the obtained parameters on the volume of ROI1 are shown in blue row of 'ROI 1' table. The green table shows the obtained values adding e subtracting the Standard deviation to average value

These values were rounded up in the following manner, to define the bounds of the HU range for an element, and taking care not to exceed the limits defined by the minimum value and the maximum value:

RANGE	750-1050 HU

Table 2.4 - HU range determinated for ROI 1

This procedure was repeated for all ROI to define the HU ranges for all elements:

	1 - ACQUISITION NO METAL - 140 KV - STANDARD FULL FOV							
	ROI 1				ROI 2			
	AVERAGE	STD	MIN	MAX	AVERAGE	STD	MIN	MAX
	884	127	218	1104	648	102	129	836
	AVERAGE + STD		AVERAGE - STD		AVERAGE + STD		AVERAGE - STD	
	1011		757		750		547	
RANGE	750-1050				550-750/800			
	ROI 3				ROI 4			
	AVERAGE	STD	MIN	MAX	AVERAGE	STD	MIN	MAX
	410	61	139	544	202	40	57	301
	AVERAGE + STD		AVERAGE - STD		AVERAGE + STD		AVERAGE - STD	
	471		349		241		162	
RANGE	300-500/550				150-300			
	ROI 5				ROI 6			
	AVERAGE	STD	MIN	MAX	AVERAGE	STD	MIN	MAX
	98	25	14	167	-7	26	-86	65
	AVERAGE + STD		AVERAGE - STD		AVERAGE + STD		AVERAGE - STD	
	123		73		19		-33	
RANGE	50-150				(-50) - 50			

Table 2.5 - Calculated HU range for the Phantom ROIs

	ROI 7 - HOMOGENEOUS BONE SAMPLE				ROI 8 - HOMOGENEOUS SAMPLE OF ACRYLIC			
	AVERAGE	STD	MIN	MAX	AVERAGE	STD	MIN	MAX
	1184	71	939	1414	165	82	1	878
	AVERAGE + STD		AVERAGE - STD		AVERAGE + STD		AVERAGE - STD	
	1255		1113		247		84	
RANGE	1050-1400				50-400			

Table 2.6 - Calculated HU range for the cylindrical samples ROI

	SMARTBONE 20x10x10 mm				SMARTBONE 10x10x10 mm			
	AVERAGE	STD	MIN	MAX	AVERAGE	STD	MIN	MAX
	205	142	-167	453	325	75	119	473
	AVERAGE + STD		AVERAGE - STD		AVERAGE + STD		AVERAGE - STD	
	347		63		400		250	
RANGE	100-400				200-400			
	GRANULATED SMARTBONE 2-4 mm				GRANULATED SMARTBONE 0,25 mm			
	AVERAGE	STD	MIN	MAX	AVERAGE	STD	MIN	MAX
	287	92	22	560	478	82	274	702
	AVERAGE + STD		AVERAGE - STD		AVERAGE + STD		AVERAGE - STD	
	379		195		560		396	
RANGE	150-400				250/300-600			

Table 2.7 - Calculated HU range for the Smartbone samples ROI

For the samples of SmartBone® a reference slice was also considered. Unlike the other samples, these elements are not totally homogeneous but have an intrinsic characteristic porosity of the material. Also, for the granules there are black zones corresponding to the presence of air due to the fact that the water inserted in the tube containing the granulated did not fill all the spaces.
As a result, the procedure was repeated for a reference slice on each SmartBone®-sample:

	REFERENCE SLICE 38,75				REFERENCE SLICE 11,25			
	ROI SMARTBONE 20x10x10 mm				ROI SMARTBONE 10x10x10 mm			
	AVERAGE	STD	MIN	MAX	AVERAGE	STD	MIN	MAX
	341	84	101	547	334	79	142	509
	AVERAGE + STD		AVERAGE - STD		AVERAGE + STD		AVERAGE - STD	
	425		256		414		255	
RANGE	100-400				200-500			

Table 2.8 - Calculated HU range for the Reference slice of compact Smartbone® samples

	REFERENCE SLICE 32,5				REFERENCE SLICE 38,12			
	ROI GRANULATED SMARTBONE				ROI GRANULATED SMARTBONE			
	AVERAGE	STD	MIN	MAX	AVERAGE	STD	MIN	MAX
	278	82	38	573	482	69	287	699
	AVERAGE + STD		AVERAGE - STD		AVERAGE + STD		AVERAGE - STD	
	361		196		551		412	
RANGE	100-400				250-600			

Table 2.9 - Calculated HU range for the Reference slice of granulated Smartbone® sample

This whole procedure was also carried out for the acquisition at 140KV in STANDARD mode, with a FULL FOV and with the MAR.

Analysing the results obtained it was observed that in the absence and in the presence of the MAR the intervals of HU for each element are the same.

This also allows to assess the correctness of the MAR algorithm in relation to the initial acquisition because it does not introduce any major distortion of HU.

The HU ranges determined for all the elements present in the test are as follows:

SAMPLES OF SMARTBONE	HU RANGES
SAMPLE 1: Smartbone 10x20x20 mm	100-400
SAMPLE 2: Smartbone 10x10x10 mm	200-500
SAMPLE 3: Smartbone granulated 2-4mm	100-400
SAMPLE 4: Granulated Smartbone 0, 25mm	250 - 600
CYLINDRICAL SAMPLES	
Homogeneous Bone Sample -ROI 7	1050-1400
Homogeneous Acrylic sample -ROI 8	50-400
ROI PHANTOM	
ROI 1	750-1050
ROI 2	550-750
ROI 3	300-550
ROI 4	150-300
ROI 5	50-150
ROI 6	(-50) - +50

Table 2.10 - HU ranges for all elements in the test

2.7.2. USING THE MIMICS INNOVATION SUITE SOFTWARE

It was possible to identify whether the HU ranges of the various elements present in the test obtained with the software Image J were correct, with the Mimics Innovation Suite software by Materialise through segmentation and thresholding, in order to validate the results obtained previously. Later it has been possible to rebuild a 3D model.

The first step is to import the TC of the test performed. The acquisition was imported to 140KV in **STANDARD mode, with a FULL FOV**.

The CT-scan was imported, selecting *' File '-' New Project Wizard '*. Moreover, it is also advisable to check that the slices are all sequentially because in this way the software can correctly reconstruct the 3D image.

After selecting the folder and pressing the *' Next '* option, the software opens a window featuring a preview of CT. In addition, further important information becomes available by clicking on "DICOMtags", where you can find information about how the image was taken, image quality and general information.

After checking that the TC is the right one and correctly representing the object in the study, you can select the *' Convert '* option.

The software opens a new window that allows you to choose the correct TC orientation, for example: top or bottom, anterior or posterior and right or left right.

The main screen of the software shows 4 sub-windows displaying the TC from different planes, as shown in the figure 2.19.

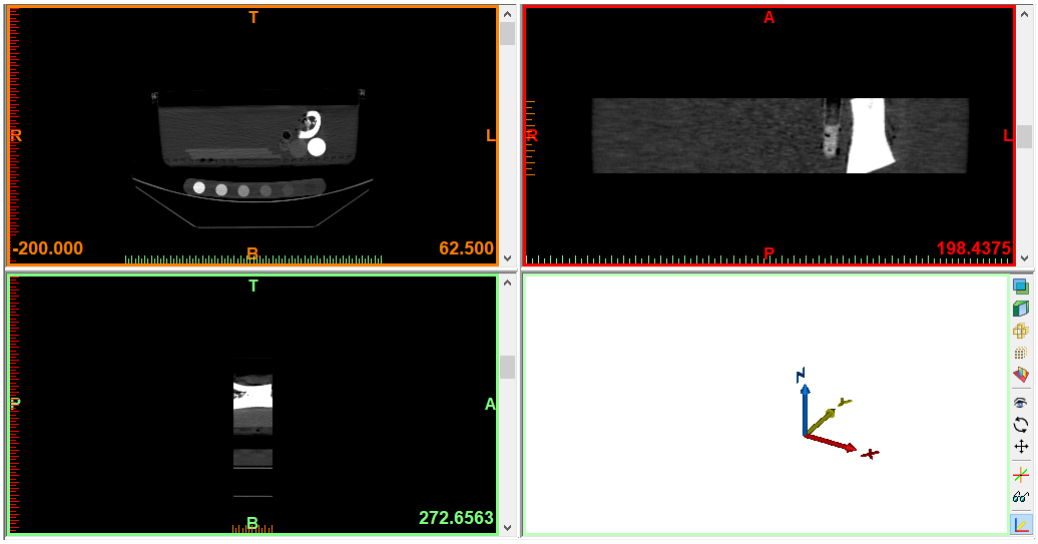

Figure 2.18 - CT scan imported in Mimics software

The 3D model, that can be rotated and moved using the right button and the mouse wheel, will be in the lower-right window will be.

it is necessary to define a mask in order to build a 3D object in Mimics Innovation Suite software. A mask is a group of pixels that will use the same colour to define different sections in the multiple slices.

It is necessary to select *'New mask'* to create a mask, the software then opens a window called *'Thresholding'*, where the values corresponding to the extremes of each range are set to ' Min ' and ' Max '. The mask defines a range of values that represents a particular tissue or object. In addition, the option *' fill holes '* has been selected for any inaccuracies within the mask to be standardized.

For cortical bone and cancellous bone, the default values of mimics for adult compact bone and adult cancellous bone have been retained.

To enter these values, you must open the *'predefined thresholds sets'* drop-down menu and select *"Adult compact Bone".* The adult compact bone range is between 662 HU and 1988 HU, while the adult spongious bone range is between 141 HU and 661 HU.

The Hounsfield Unit is a value attributed to a voxel corresponding to the average attenuation of corresponding tissue volume.

This choice of range is important because it allows a good tissue discrimination within the TC. In some cases, this range value is modified to hide the screws or is enlarged to obtain a better view of SmartBone®, which has a low density when implanted.

Fifteen masks corresponding to the various elements present in the test were created, in order to assess the correctness of the range of HU values obtained with Software ImageJ. On fourteen masks, the HU ranges defined with the software Image J correspond to the elements defined with such software have been set. a mask, however, was created to define the Phantom in order to improve the reconstruction of the 3D model.

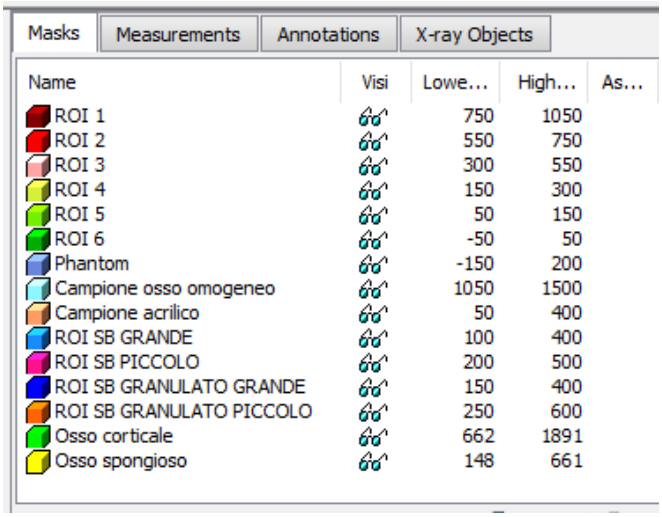

Figure 2.19 - Mask created in Mimics Innovation Suite software

Each mask was focused on the item of interest, to verify the correctness of each range.

Selecting *'Edit Mask',* Mimics Innovation Suite software allows to edit the selected mask and selecting the *'Clipping'* button, each mask can be cropped on the item in question.

Subsequently, it was verified that each element was well defined by the masks created and that there were no significant gaps.

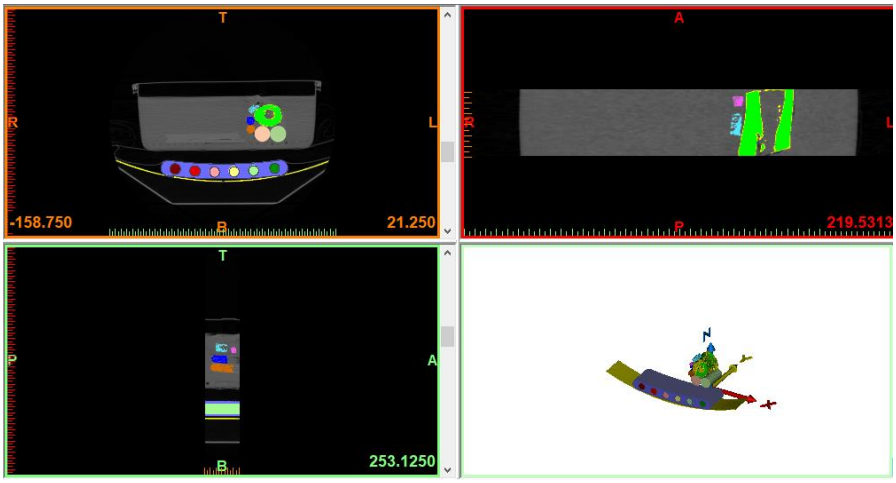

Figure 2.20 - Four view of Mimics software, after masks were focused on the elements

As a result, the HU ranges defined on Image J software are also corrected for the Mimics Innovation Suite software to segment and define accurately the various elements present in the test.

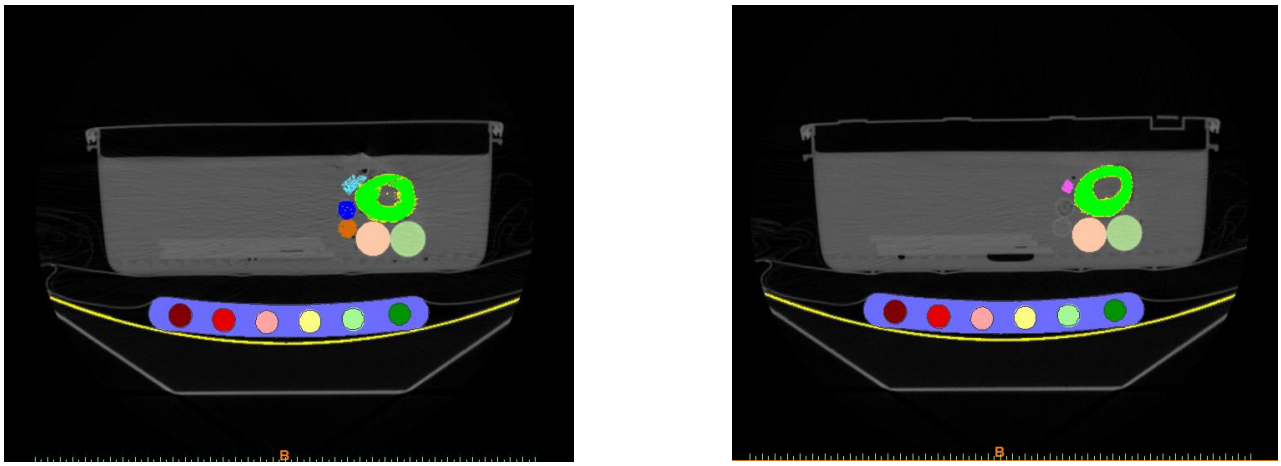

Figure 2.21 - Axial view in the Mimics software. In the image on the left is visible Samrtbone sample 1 (blue) in the image on the right is shown sample 2 (fuchsia)

Once all the masks have been created and after evaluating their correctness according to the Image J software; It was possible to convert them to a 3D object by clicking *"Calculate 3D".*

Mimics Innovation Suite allows to choose the quality of the 3D model. All fifteen masks have been selected and "optimal" quality has been selected, which is recommended by the software. Therefore, the software creates a new model that is shown in figure 2.22.

If the model presents some defects it can be edited manually through *'edit mask'*.

Once you have selected the mask that has imperfections there are two alternatives to modify the template.

One is editing once slice at a time by selecting *'edit mask'*. The other option is multiple slices editing, selecting *'multiple slice edit'*. The difference between these two options are the following: the first allows working on a single slice at a time, while the second allows drawing two slices and then interpolating the models from the two slices previously that drawn.

The 3D model that allows to identify the elements present in the test is as follows:

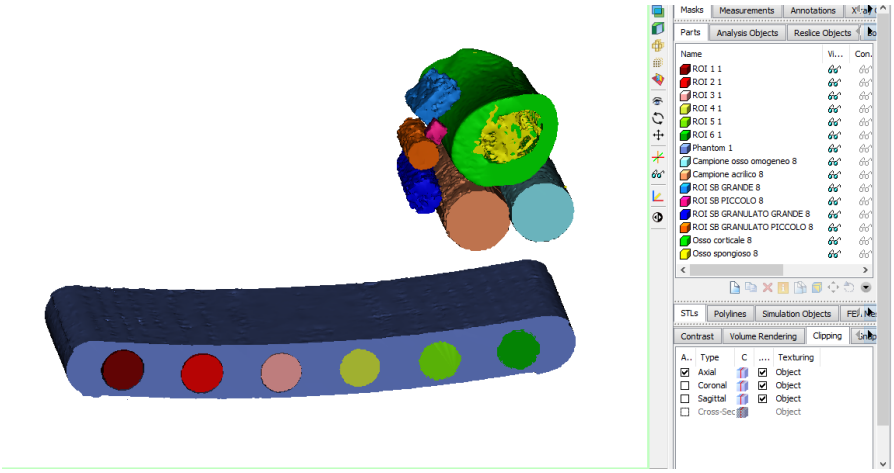

Figure 2.22 - 3D Model obtained with Mimics Innovation Suite software

The same procedure was also repeated for the acquisition at 140KV in STANDARD mode, with a FULL FOV and with the MAR; to assess the correctness of the HU range obtained with Image J software.

As previously noted with the Image J software, the calculated 3D model is correct and the intervals of HU for each element are the same one has both in the absence and in the presence of the MAR. This also allows to assess the correctness of the MAR algorithm in relation to the initial acquisition because it does not introduce any distortion of HU. The 3D model obtained with the acquisition in presence of the MAR that allows to identify the elements present in the test is shown in figure 2.23:

Figure 2.23 - 3D Model obtained for acquisition with MAR algorithm

2.8. RELATIONSHIP BETWEEN THE QUANTITY OF HYDROXYLAPATITE (HA) ON THE CALIBRATION PHANTOM AND THE AVERAGE HU VALUES

The Regions of interest (ROI) on the six inserts of the QRM-BDC/6 Calibration Phantom were taken into account; and the HU average values on each volume of the six inserts, showed in table 3.17 were considered.

The values considered are relative to 4 acquisitions:

- No metal,
- In the presence of metal: screw and plaque,
- In the presence of metal: close stem,
- In the presence of metal: far stem.

These HU average values were put in relation to the quantity of hydroxyapatite [mg HA/ cm3] present on the six inserts of the calibration phantom, the density values were supplied by the phantom manufacturer in the data-sheet.

The relations obtained were shown in the chapter 3.

2.9. MINERALIZATION

The HU average value on the volume of each SmartBone® sample were inserted into the model previously obtained, and in this way the corresponding value of Hydroxyapatite in mg HA/cm^3 was obtained.

Therefore, starting from the SmartBone® characterization HU, it is possible obtained the correspondent amount of HA in mg HA/cm^3 through obtained linear model.

That is, if you have a 'n' number of HU average value, you have a ' m' number of hydroxyapatite amount (HA) in mg HA/cm^3.

The HU average values on volume obtained from the reference zones of four SmartBone® samples and the HU average values obtained from the reference slices for each SmartBone® element were considered.

The reconstruction with 140 KV in STANDARD, with FULL FOV and with MAR was considered, instead the acquisitions in presence of metallic elements were not considered to exclude any artefacts.

2.10. CLINICAL CASES

The first part of the clinical case analysis was carried out in collaboration with the medicine Scholar Riccardo Garibaldi.

In the C.T.O Orthopaedics department, the clinical information of a series of patients has been collected.

Two clinical cases were chosen to carry out a quantitative assessment of bone regeneration and the efficiency of the SmartBone® substitutes. Thanks to the skills and help of the medicine scholar it was possible to better understand the clinical information of each Patient.

2.10.1. CLINICAL INFORMATION

Within the framework of a retrospective observational clinical study, approved by local Ethical Committee, following good clinical practice and adhering to the principles of the Helsinki declaration, anonymized data from patients who underwent reconstructive surgeries with SmartBone® were retrieved for this work. Informed consents were duly recorded too.

PATIENT 1

Patient ID: 9000926399

Date of birth: 13.05.1970- (Years 48)

Date of surgery: 28.03.2017

CT: TC left wrist/ left hand

TC PRE: 17.03.2017

TC POST (after n months): 05.12.2017 (after 9 months)

Pathology: fracture

Location: Left Distal radius

Pre-Operative: 16.03.2017

Left wrist X-ray: compound fracture of the distal epiphysis of the radio in plaster cast (pall-shower).

Figure 2.24 - X-ray patient 1 performed on 16.03.2017

Figure 2.25 - X-ray patient 1 performed on 16.03.2017

Post-Operative: 20.04.2017

Sequelae of reduction and synthesis with plaque and metal screws of fracture of distal radium and ulna, with outbreak of fracture in way of consolidation.

Figure 2.26 - X-ray patient 1 performed on 20.04.2017

Figure 2.27 - X-ray patient 1 performed on 20.04.2017

25.05.2017

Fracture of the distal epiphyses of radium and ulna in advanced consolidation in the presence of metallic means of synthesis (plaque and screws) in the seat.

Figure 2.28 - X-ray patient 1 performed on 25.05.2017

Figure 2.29 - X-ray patient 1 performed on 25.05.2017

29.08.2017

Rx control of wrist fracture in treatment by means of synthesis regularly contained by the bone tissue; Concomitant fracture of the ulnar styoid in treatment with synthetic screw

Figure 2.30 - X-ray patient 1 performed on 29.08.2017

CT SCAN 9.12.2017

Control of the articular fracture of the distal epiphyses of radium in advanced consolidation in treatment with on-site synthesis means; Concomitant fracture of the ulnar styoid consolidated in treatment with synthetic screw

Surgical Operation 28.03.2017

DIAGNOSIS DESCRIPTION: compound fracture distal radius and styloid ulnar, left wrist

SURGICAL PROCEDURE

KIND OF SURGERY: reduction and synthesis radius with volar plating Aptus FPL + synthetic bone graft SmartBone®; Reduction and synthesis styloid ulnar with screw aptus hand 2.3

DESCRIPTION: ischemic upper left limb (Laccio at 280 mm Hg per 120 ') in anaesthesia of plexus; Horizontal traction; volar Incision on the wrist; Access under the radial flexor of the carpus; After the square Pronator detachment is reached the outbreak of fracture that appears multifragmented and composed.

It was proceeded to reduce the fracture under control of brilliancy, synthetic bone grafting SmartBone® and volar positioning Aptus FPL with good stability of the synthesis. Control in Brilliancy. Washes, hemostasis, PQ suture, 1 Redon and skin suture.

At the end of the dynamic manoeuvres the distal ulnar radius appears unstable, it is therefore performed dorso-ulnar incision, opening of the Extensor retinacle at the 5 channel level: dorsal lesion is observed ulnar distal radio capsule, with integrity of the VI channel With Ulnar extensor of the carpus that appears well centered. Dorsal capsulorrafia in retension, but at the end persistence of instability. It is therefore accessible to the ulnar extensor of the carpus, isolation of the ulnar styloid that appears partially decomposed, reduction and synthesis with 1 2.3 mm aptus hand screw. At the end good recovery of distal ulnar radio stability, retinacle suture, 1 redon, cutaneous suture.

PATIENT 2

Patient ID: 2017303031

Date of birth: 08.02.1964 - (Years 54)

Date of surgery: 11.04.2017

CT: Right knee CT

TC PRE: 04.04.2017

TC POST (after n months): 05.12.2018 (after 17 months)

Pathology: compound fracture

Location: external tibial plate, peroneal malleolus

Clinical information:

Pre-Operative: 04.04.2017

Right knee CT: The CT scan of the right knee was carried out in a spiral technique and completed using multiplanar and 3D reconstructions. Multi-fragmentary displacement fracture with sinking of the external tibial plate. Compound fracture of the head of the peroneal malleolus

11.04.2017

Right leg X-ray: Disarranged and sunken fracture of the external tibial plate with involvement of the interspinous region, Compound fracture of the head of the peroneal malleolus.

Post-op 19.07.2017

Right leg X-ray: Fracture control of the proximal third of the tibia treated with metal synthesis means, restorative bone callus is observed.

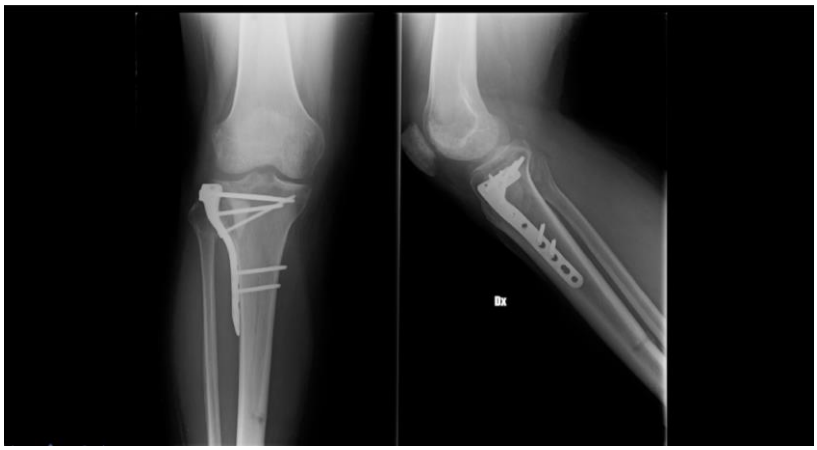

Figure 2.31 - X-ray patient 1 performed on 19.07.2017

01.12.2017

Right leg X-ray: A regular radiographic evolution of the fracture focus is observed in treatment with metal synthesis means.

Figure 2.32 - X-ray patient 1 performed on 01.12.2017

Surgical Operation: 11.04.2017

SURGICAL PROCEDURE

DESCRIPTION: Stabilization with prefix

epidural anaesthesia, sterile surgical field preparation, Scaffolding knee with PREFIX 2 screws + 2 screws. Control in brightness of reduction of Subluxation. CT exam is required for continuation therapy

2.10.2. DENSITOMETRIC ANALYSIS - BONE REGROWTHS ASSESSMENT

A method to evaluate bone regeneration after surgery is to perform a grayscale analysis on the post-operatory CT.

The optimum condition is that in which an immediately post-operatory CT and a post-operatory CT after n months are available, so that a densitometric analysis can be performed on both CT. In this way, comparing the grayscale between the two exams and also referring to the HU ranges determined previously the bone regeneration in time is possible to evaluate.

In this case for both clinical cases, a pre-operatory TC and a post-operatory TC, after n months, were available. So, a densitometric analysis on the post-operatory TC was performed, indeed the grayscale on bone graft region was compared with HU ranges determined previously, to identify cortical bone, cancellous bone and SmartBone®.

PATIENT 1

With the software Image J, the post-operative TC, after 9 months, was imported into the software, the reconstruction with the MAR was chosen in order to reduce the presence of metallic artifacts, caused by the metal prosthesis to avoid the alteration of the grayscale. This reconstruction consists of 68 images. Im 554-Im 621 – 68 Images

The slices, in which the presence of the regrown bone volume is clearly visible, are identified: Im 588, Im 589, IM590, Im 591.

Figure 2.33 - Reconstructed area with implant of SmartBone®

After identifying the bone volume of interest on all four images were traced of the regions of Interest (ROI) on the area in analysis.

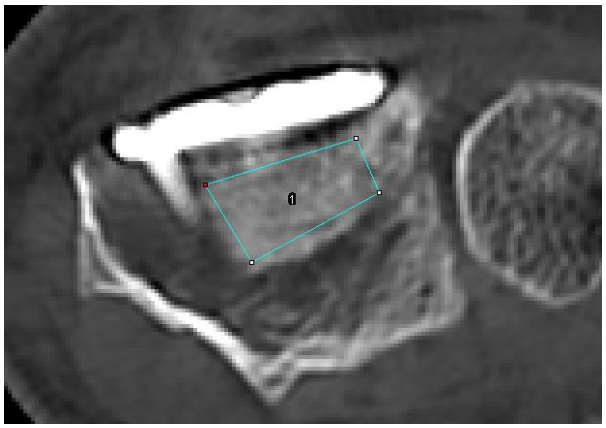

Figure 2.34 - Region of interest in Im 588

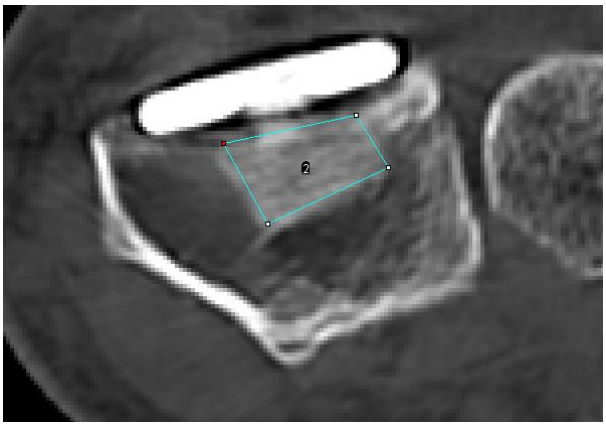

Figure 2.35 - Region of interest in Im 589

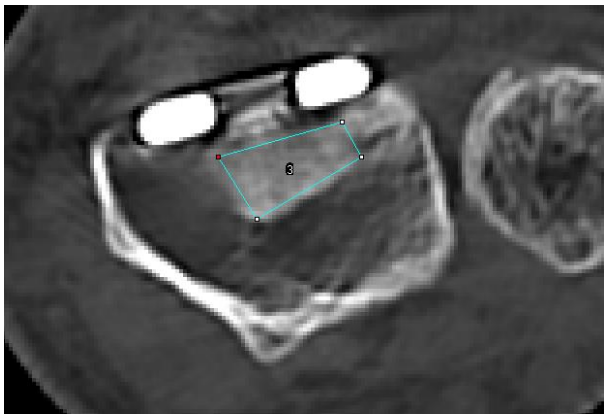

Figure 2.36 - Region of interest in Im 590

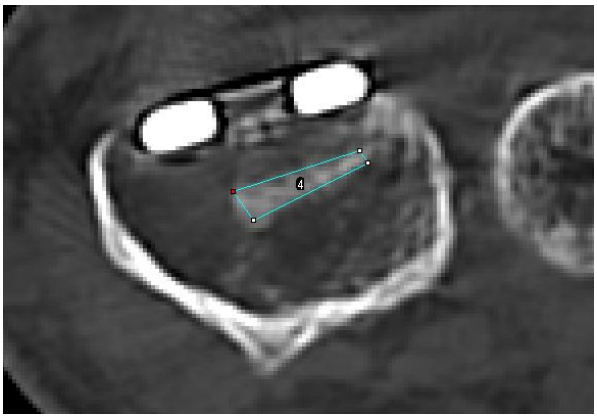

Figure 2.37 - Region of interest in Im 591

Measurements were made, for all four ROI, in relation to the grayscale analysis, carried out previously in the radiological study. The following parameters were obtained:

- Average HU value on 2D region,
- Standard Deviation (STD),
- Minimum HU value within 2D ROI,
- Maximum HU value within 2D ROI.

These values were mediated by number of slices in question (in this case 4 slices), to obtain the parameters of interest on the volume of re-grown bone.

PATIENT 2

The same procedure with Image J software was performed for this clinical case. Post-operatory CT, after 17 months, was used for densitometric analyse. The slices, in which the presence of the regrown bone volume is clearly visible, are identified: from Im 646, to Im 666,

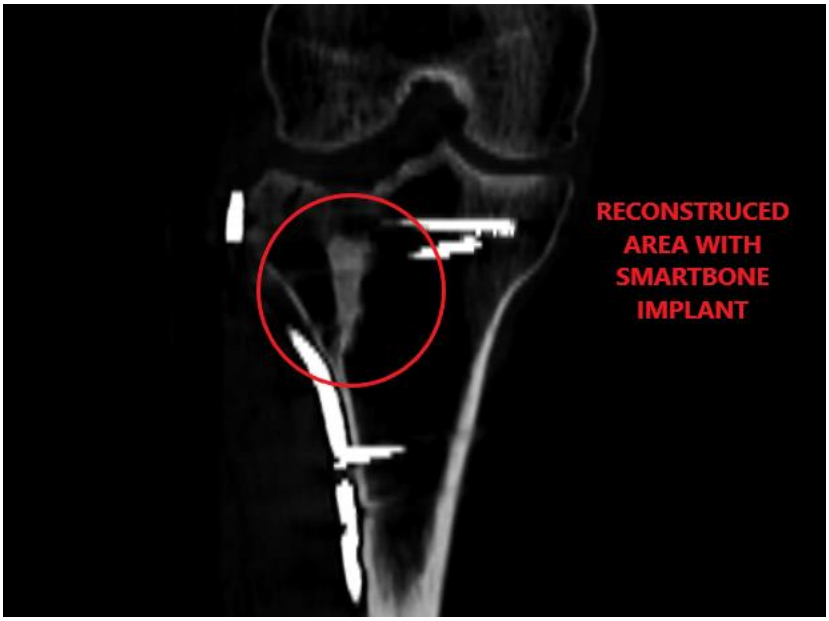

Figure 2.38 - Reconstructed area with implant of SmartBone®

The **Mimics** software has been used to identify these zones on the volume of re-grown bone. The acquisition with the MAR was imported into the software and then 3 masks were created:

- Cortical green-Bone: 662 – 1988 Hu,
- Cyan – 100 – 500 Hu,
- Fuchsia 501 – 661 Hu

The Fuchsia mask represents the difference between the upper limit of the Cancellous bone and the upper limit of the SmartBone® range (501-661 HU). This mask was created to identify those areas that do not belong to the SmartBone® nor to the Cortical bone but fall into the range of the Cancellous bone.

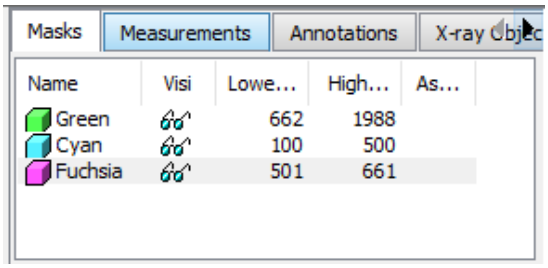

Figure 2.39 - Mimics Innovation Suite interface, where created masks are shown

The aim is to identify areas where the bone regrowth has occurred and SmartBone® has been replaced.

Moreover, through the Mimics Innovation Suite software, the percentage of area of the cortical bone, of the spongious bone and of the cyan colour has been assessed for each slice.

2.10.3. MINERALIZATION

The mineralization of the volume of regrown bone has been assessed.

The linear model, obtained previously, was resumed:

No metal: $\boldsymbol{y = 0,8986x + 15,257}$

The HU average value, of the volume of regrown bone, was replaced instead of the X within the linear model; in this way, the amount of hydroxyapatite (HA) in mg HA/cm^3, of regrown bone, was obtained. That is, the material mineralization in term of Hydroxyapatite (HA) in mg HA/cm^3 was obtained.

2.10.4. VOLUMETRIC METHOD

Since both the pre-operatory CT and the post-operatory CT were present as diagnostic tests, an overlap of 3D models was possible to perform in order to evaluate bone regeneration.

A method to evaluate the volumetric bone growth after the SmartBone® implant is the overlapping of volumes. Two volumetric models (two volumes) are needed to proceed with overlapping, the first built by through pre-operatory CT and the second one constructed through the post-operatory CT. CT-scan is the starting point from which different body district models for various patients can be reconstructed. The reconstruction of the areas of interest was carried out using the Mimics Innovation Suite software by Materialise, which reconstructs a 3D model as close as possible to the patient's anatomy. Indeed, in this case the goal is the reconstruction of a 3D bone model.

The accuracy of 3D models depends on how CT-scan was carried out. Moreover, some "slices" were modified manually to make them more consistent with the patient's anatomy.

The first step is to import the patient's TC to create the model.

PATIENT 1: The pre-operatory CT performed on 17/03/2017 and the post-operatory CT performed on 05/12/2017, after 9 months of operation, were imported into the software.

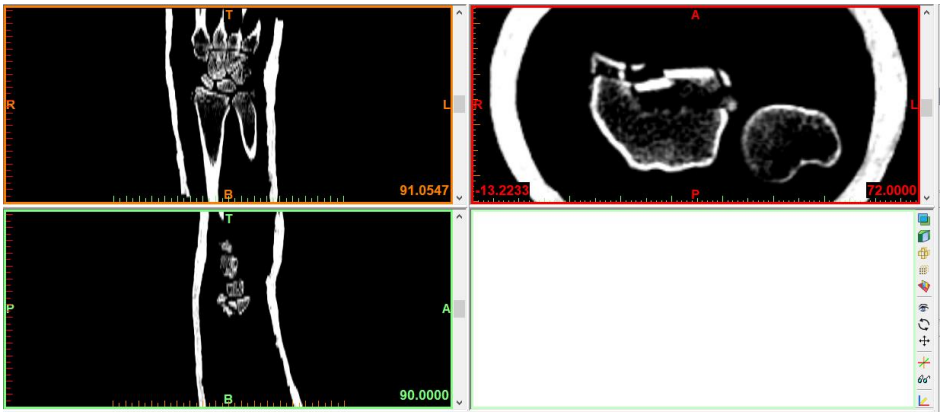

Figure 2.40 – pre-operatory CT performed on 17/03/2017 was imported into Mimics Innovation Suite software

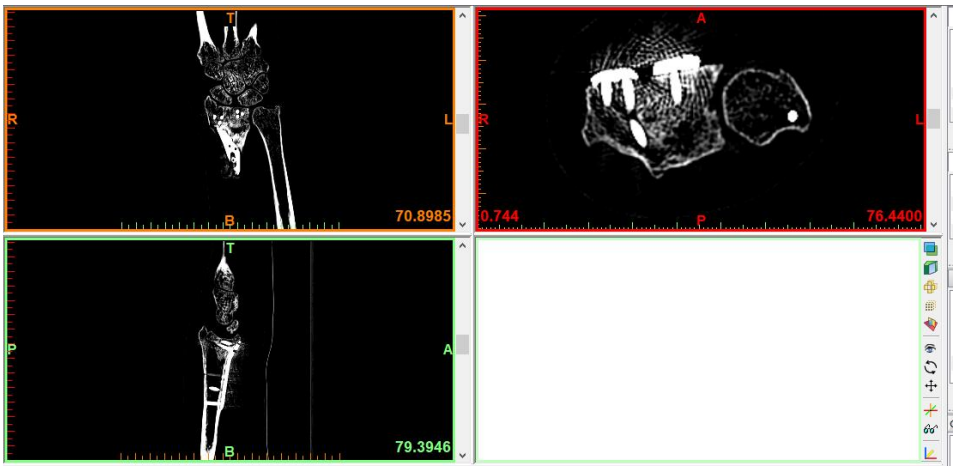

Figure 2.41 – post-operatory CT performed on 05/12/2017 was imported into Mimics Innovation Suite software

A mask called ' bone ' was created for both TC-Scans, which has allowed to identify this tissue in the TC images. The default values of Mimics software for bone have been kept. The bone range is between 148 HU to 2999 HU.

Once the mask was created it was possible to convert it into a 3D object by clicking on *'calculate 3D'*.

In this case, an ' optimal ' quality was chosen and later, the 3D model was calculated.

The 3D model can be rotated and moved using the right button and the wheel of the mouse.

The segmentations performed for the Pre-operative TC and for the Post-operative TC are shown below.

TC Pre-Op - Date: 17/03/2017 - 100KV, 200mA

Project Information

Mimics Project Info

Patient Information | Study Information | Slices

Description	Value	Unit
ID	47466	
Date	20170317	
Scanner	GE_MEDICAL_SYSTEMS/BrightSpeed	
X-ray Tube Current	200	mA
KVP	100	kV
Institute	Osp CTO Radiologia Torino	
Physician	UNKNOWN UNKNOWN	

Table 2.11 - Study Information

=== Slices Information ===		
Description	**Value**	**Unit**
Width	512	px
Height	512	px
Pixel Size	0.351562	mm
Algorithm	BONE	
Field of View	180.00	mm
Gantry Tilt	0.000	degree
Number of Slices	76	

Table 2.12 - Slices Information

3D MODEL OF TOTAL RADIUS AND ULNA - TOTAL RADIUS - PART OF RADIUS - FRACTURE AREA IN THE RADIUS

Figure 2.42 - 3D model of TOTAL RADIUS AND ULNA

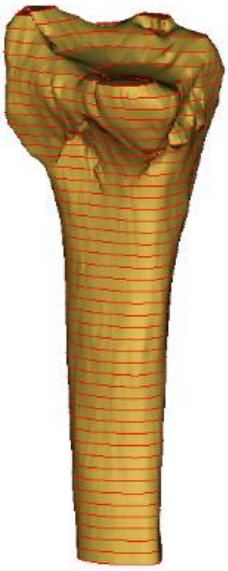

Figure 2.43 - 3D model of TOTAL RADIUS

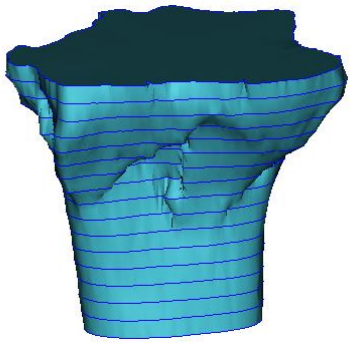

Figure 2.44 - 3D model of PART OF RADIUS

Figure 2.45 - 3D model of FRACTURE AREA

In the follow 2D image of axial section has the compact bone been segmented (blue) using the predefined range: 662 – 1988 HU and is visible the zone of the fracture and the overlapped zones.

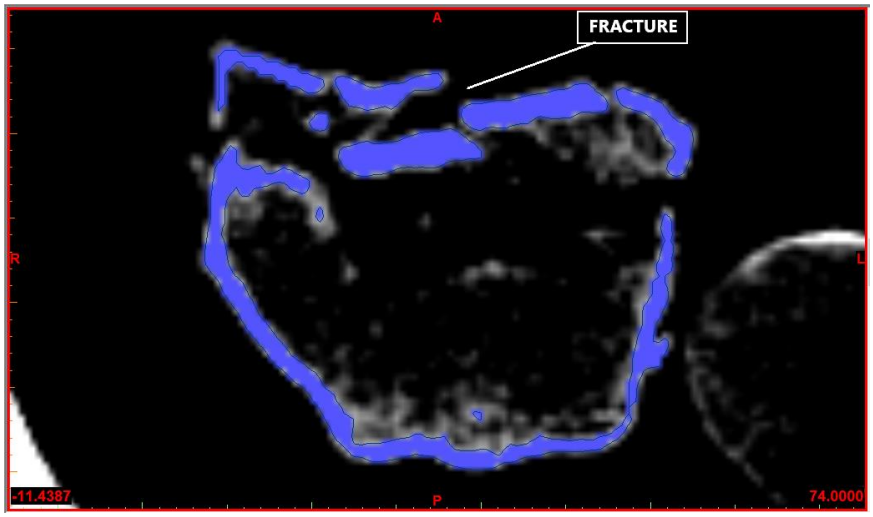

Figure 2.46 - Thresholding of fracture area

TC POST-OP - DATE 05/12/2017 - 100KV, 200 mA

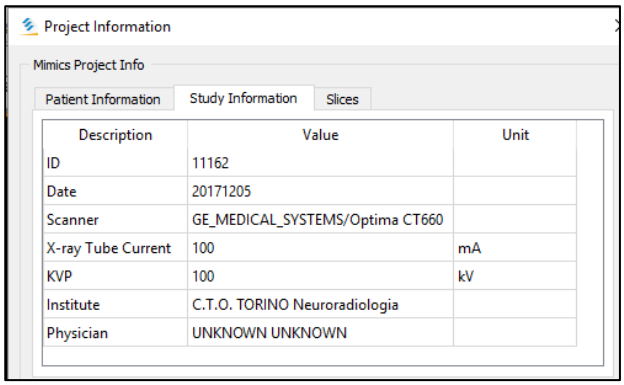

=== Slices Information ===		
Description	**Value**	**Unit**
Width	512	px
Height	512	px
Pixel Size	0.292969	mm
Algorithm	BONEPLUS	
Field of View	150.00	mm
Gantry Tilt	0.000	degree
Number of Slices	484	

Table 2.13 - Study Information
Table 2.14 - Slices Information

MODEL OF TOTAL RADIUS AND ULNA - TOTAL RADIUS - PART OF RADIUS - FRACTURE AREA IN THE RADIUS

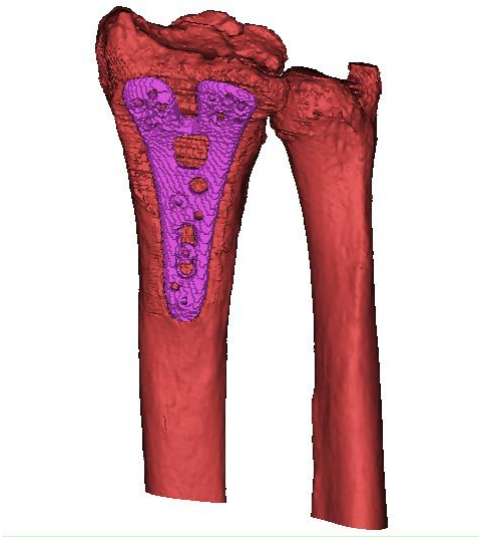

Figure 2.47 - 3D model of TOTAL RADIUS AND ULNA

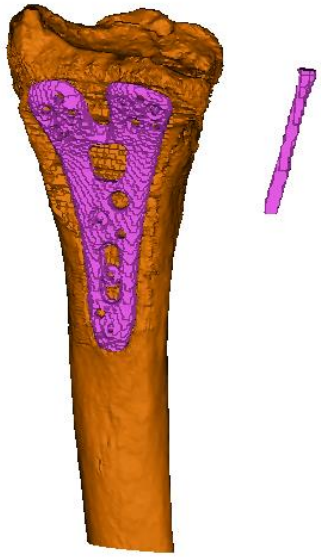

Figure 2.48 - 3D model of TOTAL RADIUS

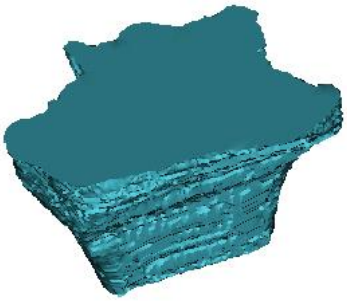

Figure 2.49 - 3D model of PART OF RADIUS

Figure 2.50 - 3D model of FRACTURE AREA

PATIENT 2: the same procedure was carry out for Patient 2. The Pre-operative TC was performed on 04/04/2017 and the Post-operative TC was performed on 21/09/2018, after 17 months from surgery.

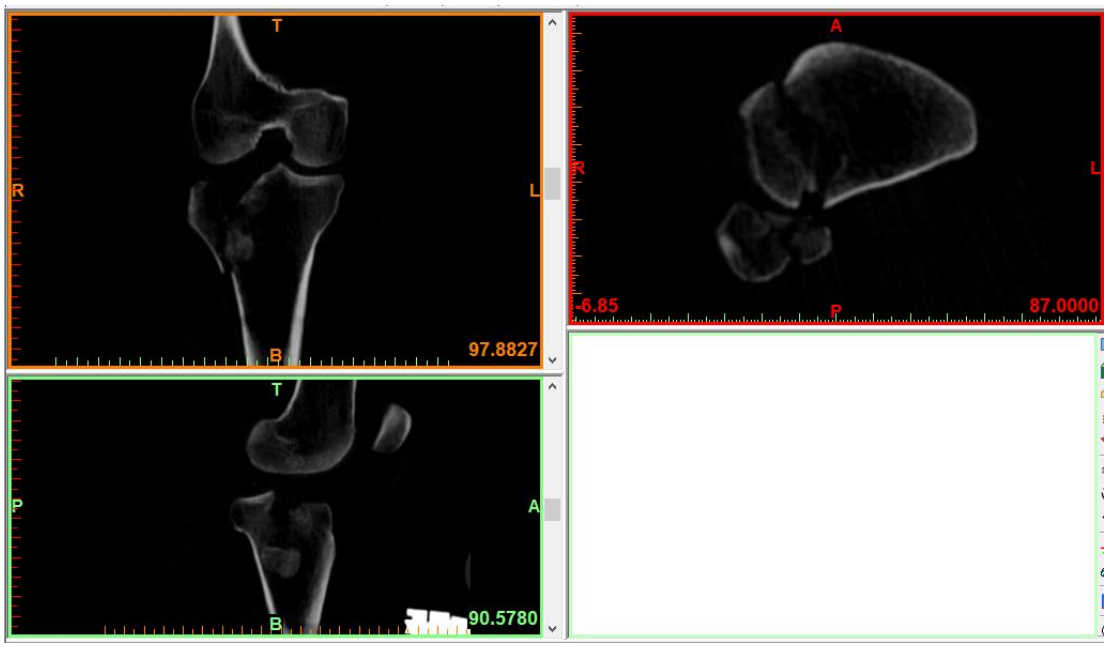

Figure 2.51 - pre-operatory CT performed on 04/04/2017 was imported into Mimics Innovation Suite software

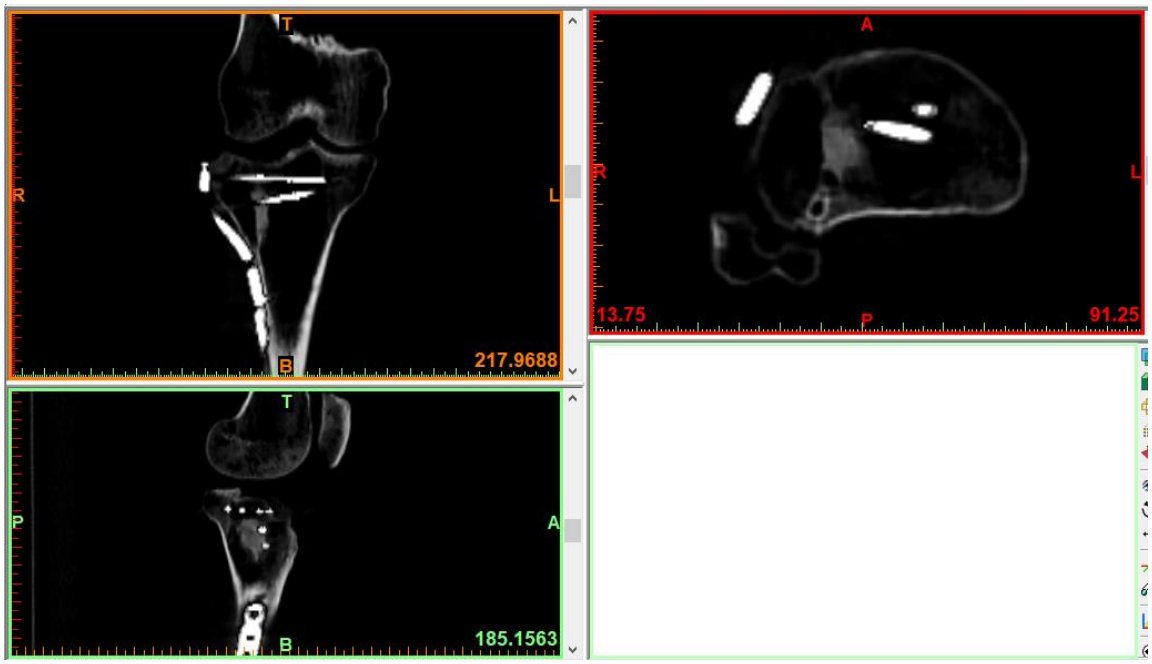

Figure 2.52 - post-operatory CT performed on 21/09/2018 was imported into Mimics Innovation Suite software

TC Pre-Op - Data: 04/04/2017 - 100KV, 150mA

Project Information

Mimics Project Info

Patient Information | Study Information | Slices

Description	Value	Unit
ID	47678	
Date	20170404	
Scanner	GE_MEDICAL_SYSTEMS/BrightSpeed	
X-ray Tube Cur...	150	mA
KVP	100	kV
Institute	Osp CTO Radiologia Torino	
Physician	UNKNOWN UNKNOWN	

Table 2.15 - Study Information

=== Slices Information ===		
Description	**Value**	**Unit**
Gantry Tilt	0.000	degree
Pixel Size	0.365234	mm
Slice Increment	0.600	mm
Slice Thickness	1.250	mm
Field of View	187.00	mm
Number Slices	327	
Width	512	px
Height	512	px
Algorithm	STANDARD	

Table 2.16 - Slices Information

MODEL OF TOTAL RIGHT KNEE - TOTAL TIBIA AND FIBULA - TOTAL TIBIA

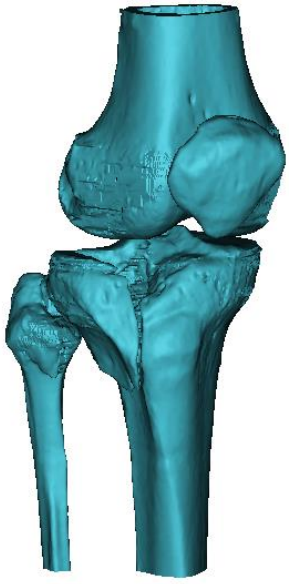

Figure 2.53 - 3D model of RIGHT KNEE

Figure 2.54 - 3D model of TOTAL TIBIA AND FIBULA

Figure 2.55 - 3D model of TOTAL TIBIA

TC POST-OP - DATE 21/09/2010 - 140KV, 30 mA

Project Information

Mimics Project Info

Patient Information | Study Information | Slices

Description	Value	Unit
ID	17193	
Date	20180921	
Scanner	GE_MEDICAL_SYSTEMS/Optima CT660	
X-ray Tube Cur...	30	mA
KVP	140	kV
Institute	C.T.O. TORINO Neuroradiologia	
Physician		

=== Slices Information ===		
Description	**Value**	**Unit**
Gantry Tilt	**0.000**	**degre**
Pixel Size	**0.78125**	**mm**
Slice Increment	**1.250**	**mm**
Slice Thickness	**1.250**	**mm**
Field of View	**400.00**	**mm**
Number of Slices	**144**	
Width	**512**	**px**
Height	**512**	**px**
Algorithm	**STANDARD**	

Table 2.17 - Study Information
Table 2.18 - Slices Information

MODEL OF TOTAL RIGHT KNEE - TOTAL TIBIA AND FIBULA - TOTAL TIBIA

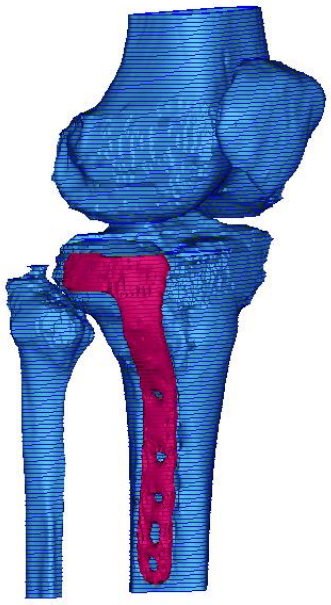

Figure 2.56 - 3D model of RIGHT KNEE

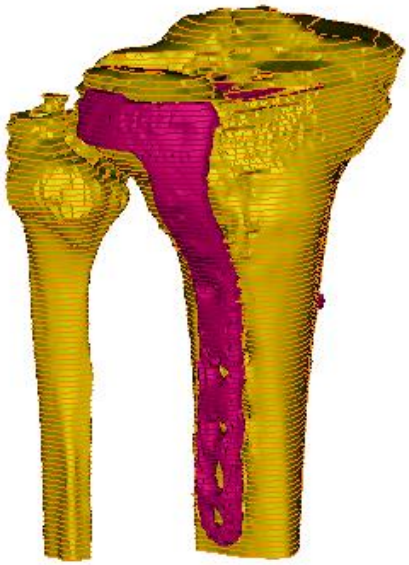

Figure 2.57 - 3D model of TOTAL TIBIA AND FIBULA

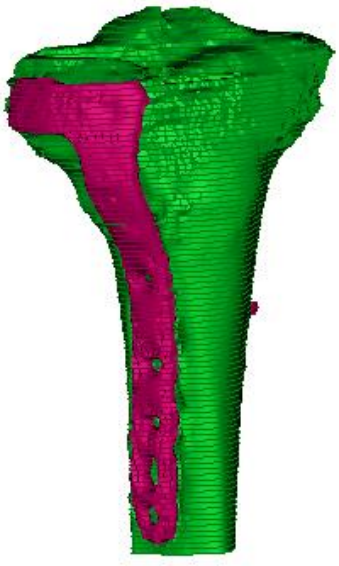

Figure 2.58 - 3D model of TOTAL TIBIA

Once the models have been created, they have been imported into the Mimics Innovation Suite Software of Materialise to perform the following steps.

METHOD OF CALCULATING VOLUMES

For the construction of the two volumetric models, Mimics Innovation Suite Software of Materialise was used, which is commonly used for 3D drawings or for modifying mesh and CAD bodies.

The procedure performed for Patient 1 is shown below.

With this software, two. stl files were imported with the Mimics software, one corresponding to the initial preoperative ' part ', ' Bone – Fracture – Pre-op ' and the other corresponding to the postoperative ' part ', ' Bone – Fracture – Post op '.

When both files are loaded, the situation is as shown in the figure.

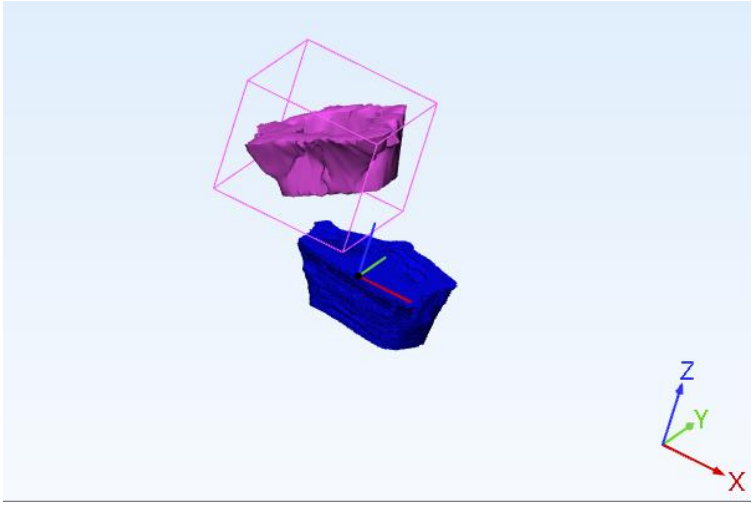

Figure 2.59 - Software view after models opening

Before creating the volumetric mesh, surface improvement changes were made, and the subsequent creation of the surface mesh was carried out.

Surface changes

The commands of *Smooth, Reduce and Fix Wizard* were used to improve the surface of models imported from Mimics Innovation Suite.

- Smooth operation was performed by selecting *Fix – smooth.*

  Smooth: This operation allows to decrease “noise” in the mesh (f.e. introduced during the scanning process) and to make it smoother. It gives the best results if triangles in the mesh have more or less a uniform size. [62]

- ' Reduce ' command was run by clicking on *Fix – Reduce.*

  Reduce: This function reduces the number of triangles in chosen entità

- The Fix Wizard function is performed by selecting *Fix-Fix Wizard*.

  The *Fix Wizard* offers you a user interface where all the fixing functions are grouped logically according to the problem to solve. It also offers extensive analysis functions, highly automated fixing tools and 3-matic Research will advise you, based on this information, a fixing step. The diagnostics page is the key-step in the Fixing Wizard. In this step you can always determine what is wrong with the STL-file. Based on the diagnosis, the fixing wizard will advise you an action. You can use this advice as a guideline through the fixing process.

After the execution of these commands the models are visibly improved at surface level, as can be seen in the figure 2.60.

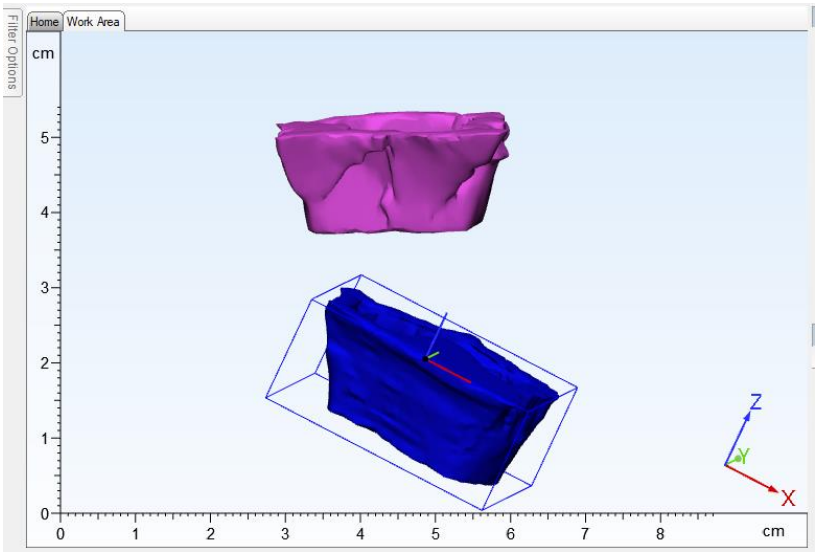

Figure 2.60 - this image shows the Surface improvements of models

MESH CREATION

SURFACE MESH

Then the surface meshes were created by going to select the following commands:

Remesh – Adaptative Remesh: this command Optimize and locally refine the mesh while preserving detailed features. [63]

Remesh – Uniform Remesh: this operation provides a uniform and high quality surface mesh.[63]

The Target triangle edge length is 1,000 mm

Surface Mesh Quality Analysis

After creating surface meshes, the quality analysis was carried out by selecting *Remesh – Analyze mesh quality,* to check the quality of the mesh. It is important to verify that the built-in surface meshes are correct. This command allows to check that the mesh created exceeds all the set criteria. In this case all the criteria have been respected.

VOLUME MESH

After evaluating the correctness of the surface meshes, it has proceeded to construct the volumetric models by going to create the volume meshes. To do this, it was selected the command: *Remesh – Create Volume Mesh*.

The 4-node tetrahedron(TET4) are geometric element, which were chosen to the construction of the 3D domain. In addition, the value to set on ' Maximum edge length ' must be at least twice the ' Triangle edge length ' set for the surface mesh, to have a uniform mesh inside the model. In This case the value of 2.000 mm has chosen. [63]

After creating the volume mesh, it was important to evaluate the quality.

There are different measures for measuring the quality of a volume mesh. For a volume mesh with tetrahedral elements, the quality of the entire mesh depends on the quality of its tetrahedral elements. [62]

Analyze Volume Mesh Quality

With the command *Remesh – Analyze mesh quality* it was checked that the volume mesh created respect all the set criteria.

ALIGNMENT PROCEDURE

The two-volume alignment and overlap procedure has been performed, after the two volumetric models have been created: one relative to the pre-operative TC and the other for the post-operative TC.

The manual mode was chosen as an alignment procedure, which for orthopaedic cases produces better results. [27]

This procedure was performed with the Mimics Innovation Suite software using commands that allow the translation and rotation of a model on the other. The commands selected are: *Align – interactive Translate* and *align – interactive Rotate.*

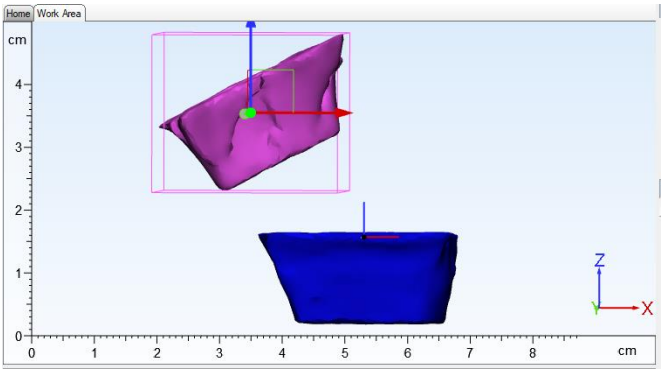

Figure 2.61 - interactive Translate

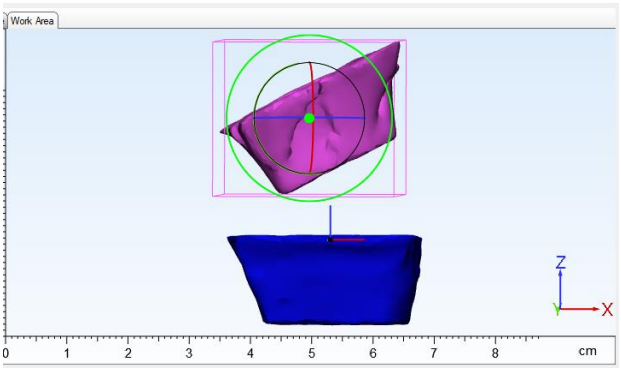

Figure 2.62 - interactive Rotate

Overlapping models

The overlap of volumes is important to evaluate the volumetric bone growth that occurs after the SmartBone® implant. The two volumetric models aligned, and overlapping are visible in the following figure, it is also observed how the anatomy of the patient has been respected.

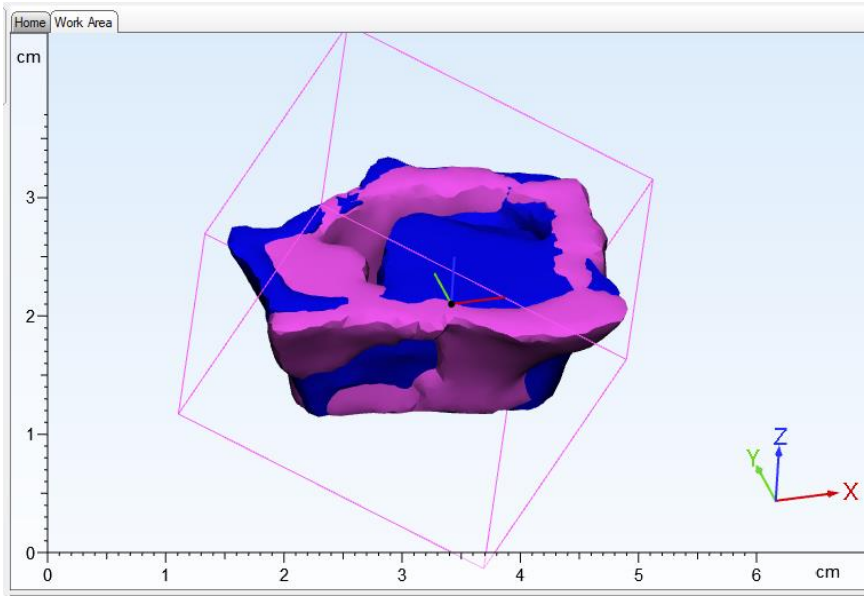

Figure 2.63 - overlapping models of patient 1

The two volumetric models aligned and overlapping for Patient 2 are shown in the following figure:

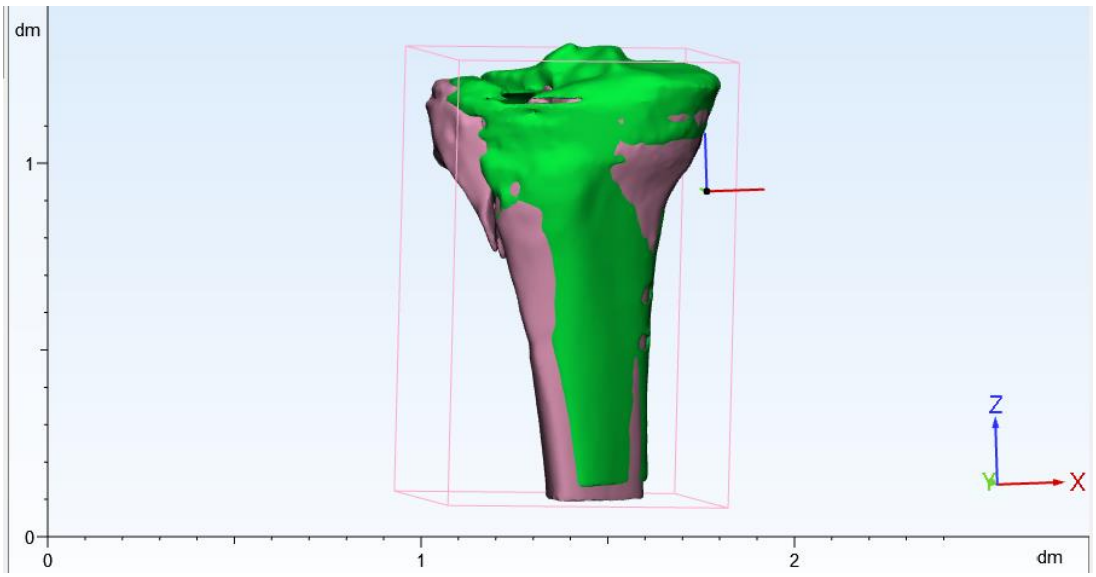

Figure 2.64 - overlapping models of patient 2

Subtraction of volumes

The subtraction of volumes was performed to establish how much volume has increased after the surgical operation, so that it is possible to understand how much bone has been regenerated. The subtraction was performed with materialise's "3-Matic Research 12.0" software.

After verifying that the overlapping is correct, the subtraction of volumes was carried out. This was done by subtracting the post-operative model volume from the pre-operative model volume. In 3 Matic this step is performed using Boolean subtraction, an operation carried out on two solids, the two models in the studio in this case.

On the main screen, the ' *design* ' option has been selected and the software opened a drop-down menu where it has selected the ' *Boolean Subtraction* ' option. At this point, a window opens in the lower-right part of the main screen, where the volumes to be subtracted (figure) must be inserted. After selecting the two volumes, it has been selected select '*Apply*'. *Design – Boolean Subtraction* and then the software showed the remaining volume, which is the regenerated bone after the surgical operation.

Subsequently, the volume obtained was imported in the Mimics Innovation Suite software and the numerical value of the volume was calculated by the software.

3. RESULTS

3.1. RESULTS OF PATIENT CENTERING

Below, the results obtained by varying the patient centring, as explained in Chapter 2.4., are shown.

3.1.1. RESULTS OF SMARTBONE®CENTERING

The follow graphs show the behaviour of the SmartBone® samples as a function of centering. These graphs represent the HU trend as a function of centering. The blue curve represents the HU trend in the absence of metal, while the other two curves show the HU trend in the acquisitions in which the Centering is changed: red curve centering of + 5cm, green curve centering of -5cm.

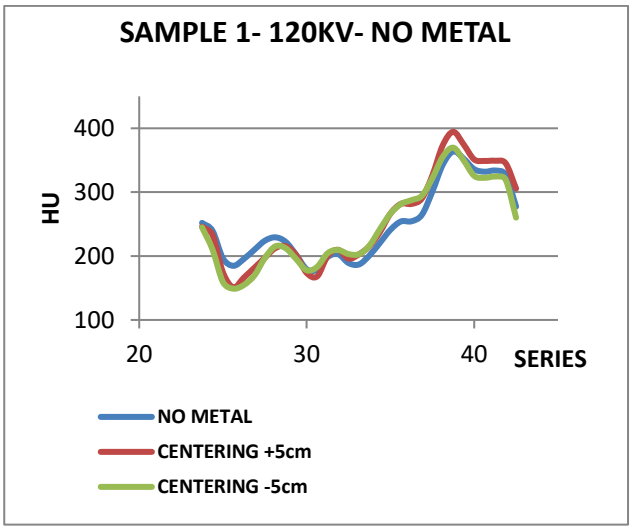

Figure 3.1 - HU trend as a function of centering for sample 1 in the acquisition with 120 kV

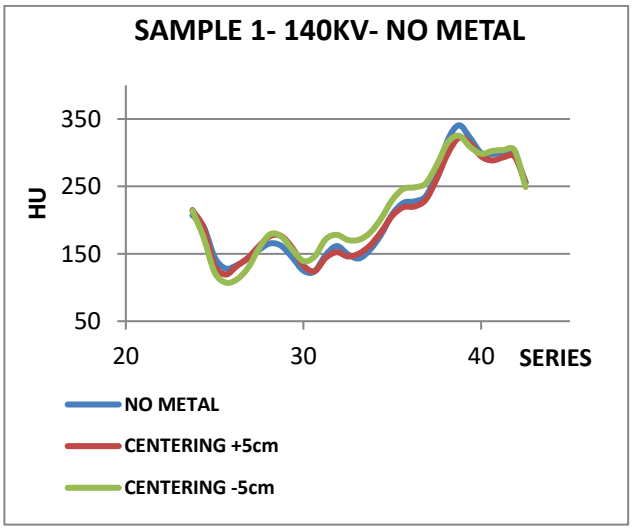

Figure 3.2 – HU trend as a function of centering for sample 1 in the acquisition with 140 kV

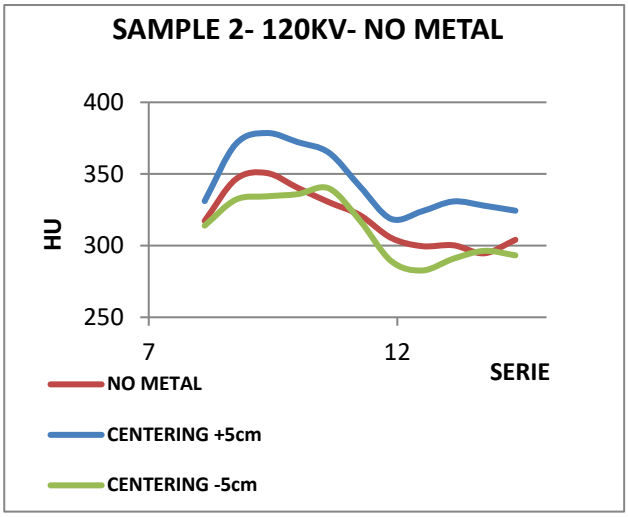

Figure 3.3 - HU trend as a function of centering for Sample 2 in the acquisition with 120 kV

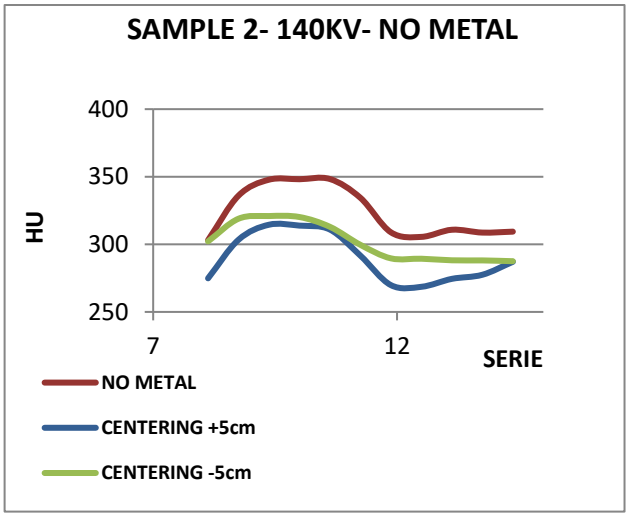

Figure 3.4 - HU trend as a function of centering for Sample 2 in the acquisition with 140 kV

For all four **samples of SmartBone®,** a reference slice was considered.

Four tables each corresponding to a SmartBone® sample are shown below. The three main columns represent the three acquisitions considered. In the ' average ' row, the average HU value within the ROI of the reference slice considered is reported; And the ' STD ' line shows the corresponding standard deviation. The blue ' difference ' line shows the calculated difference. In fact, this line shows the difference between the average HU value of the ROI obtained from the metalless acquisition without changes in centering and the average HU value of the same ROI obtained from the acquisition in which the variate centering.

	SAMPLE 1 - REFERENCE SLICE : 38,75											
	NO METAL				CENTERING +5cm				CENTERING -5cm			
	STADARD		STANDARD MAR		STADARD		STANDARD MAR		STADARD		STANDARD MAR	
	120KV	140KV	120 KV	140KV	120KV	140KV	120 KV	140KV	120KV	140KV	120 KV	140KV
	IM61	IM163	IM61	IM163	IM61	IM163	IM61	IM163	IM61	IM163	IM61	IM163
AVERAGE	363,8	340,7	363,8	340,7	394,4	322,2	394,5	322,2	369,6	325,2	369,6	325,2
STD	87,1	84,3	87,1	84,3	97,3	72,8	97,2	72,8	74,7	76,5	74,7	74,5
DIFFERENCE					**30,6**	**18,5**	**30,6**	**18,5**	**5,8**	**15,5**	**5,8**	**15,5**

Table 3.1 - the table shows the values calculated for reference slice of sample 1. The HU average and Standard deviation values are shown for acquisition without changes in centering, with +5cm centering e -5cm centering. The blue line shows the difference calculated between the HU average values without changes in centering and those with variate centering.

	SAMPLE 2 - REFERENCE SLICE : 11,25											
	NO METAL				CENTERING +5cm				CENTERING -5cm			
	STADARD		STANDARD MAR		STADARD		STANDARD MAR		STADARD		STANDARD MAR	
	120KV	140KV	120 KV	140KV	120KV	140KV	120 KV	140KV	120KV	140KV	120 KV	140KV
	IM12	IM119	IM12	IM119	IM12	IM119	IM12	IM119	IM12	IM119	IM12	IM119
AVERAGE	321,2	334,4	321,2	334,4	341,2	291,6	341,2	291,6	317,4	299,6	317,5	299,6
STD	77,4	79,4	77,4	79,3	81,0	67,7	81,0	67,7	80,0	71,7	80,1	71,7
DIFFERENCE					**20,0**	**42,8**	**20,0**	**42,8**	**3,8**	**34,8**	**3,8**	**34,8**

Table 3.2 - the table shows the values calculated for reference slice of sample 2. The HU average and Standard deviation values are shown for acquisition without changes in centering, with +5cm centering e -5cm centering. The blue line shows the difference calculated between the HU average values without changes in centering and those with variate centering.

	SAMPLE 3 - REFERENCE SLICE : 32,5											
	NO METAL				CENTERING +5cm				CENTERING -5cm			
	STD		STD MAR		STD		STD MAR		STD		STD MAR	
	120KV	140KV	120 KV	140KV	120KV	140KV	120 KV	140KV	120KV	140KV	120 KV	140KV
	IM50	IM153	IM50	IM153	IM50	IM153	IM50	IM153	IM50	IM153	IM50	IM153
AVERAGE	318,8	278,5	318,8	278,5	308,1	282,6	308,2	285,6	304,9	272,4	304,9	272,3
STD	81,9	82,2	86,1	82,2	93,4	87,7	93,3	87,7	101,4	89,8	101,4	89,8
DIFFERENCE					**10,6**	**4,1**	**10,6**	**7,2**	**13,9**	**6,1**	**13,9**	**6,1**

Table 3.3 - the table shows the values calculated for reference slice of sample 3. The HU average and Standard deviation values are shown for acquisition without changes in centering, with +5cm centering e -5cm centering. The blue line shows the difference calculated between the HU average values without changes in centering and those with variate centering.

	SAMPLE 4 - REFERENCE SLICE : 38,12											
	NO METAL				CENTERING +5cm				CENTERING -5cm			
	STD		STD MAR		STD		STD MAR		STD		STD MAR	
	120KV	140KV	120 KV	140KV	120KV	140KV	120 KV	140KV	120KV	140KV	120 KV	140KV
	IM60	IM162	IM60	IM162	IM60	IM162	IM60	IM162	IM60	IM162	IM60	IM162
AVERAGE	544,7	481,9	544,7	481,9	535,4	479,9	535,4	479,9	545,8	490,7	545,8	490,7
STD	82,5	69,4	82,4	69,5	97,1	92,3	97,2	92,2	133,6	105,9	133,6	106,0
DIFFERENCE					**9,3**	**2,0**	**9,3**	**2,1**	**1,1**	**8,8**	**1,1**	**8,8**

Table 3.4 - the table shows the values calculated for reference slice of sample 4. The HU average and Standard deviation values are shown for acquisition without changes in centering, with +5cm centering e -5cm centering. The blue line shows the difference calculated between the HU average values without changes in centering and those with variate centering.

3.1.2. RESULTS OF THE CENTERING ON THE PHANTOM AND THE CYLINDRICAL SAMPLES

The follow graphs show the behaviour of the Calibration Phantom and of two cylindrical samples with homogeneous density as a function of centering.

These graphs represent the HU trend as a function of centering. The blue curve represents the HU trend in the absence of metal, while the other two curves show the HU trend in the acquisitions in which the Centering is changed: red curve centering of -5cm, green curve centering of +5cm.

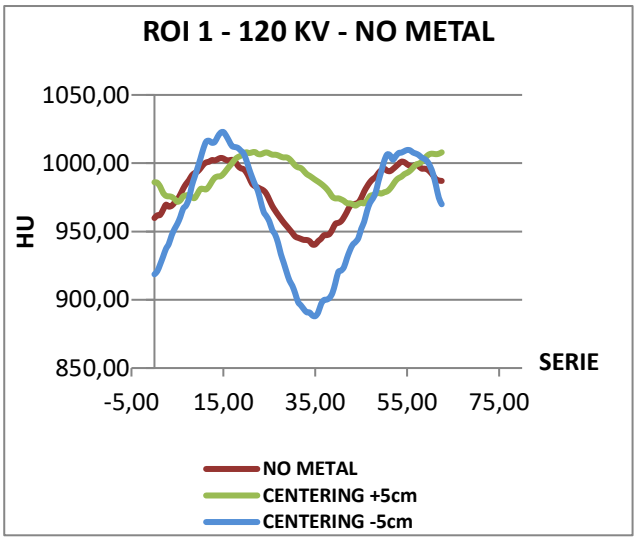

Figure 3.5 - HU trend as a function of centering for ROI1 in the acquisition with 120 kV

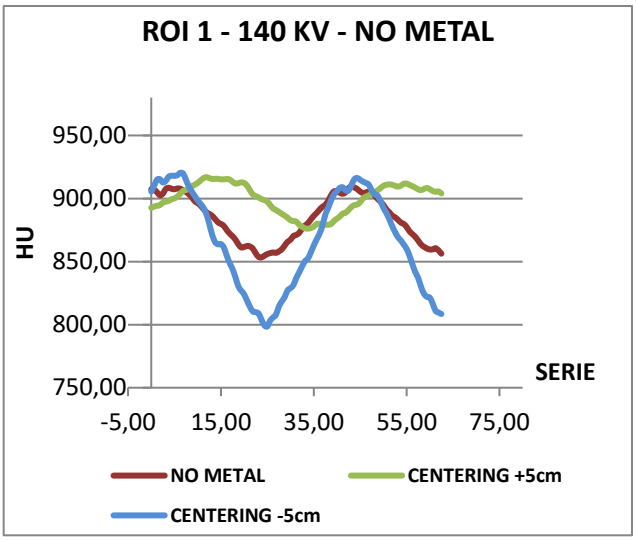

Figure 3.6 - HU trend as a function of centering for ROI1 in the acquisition with 140 kV

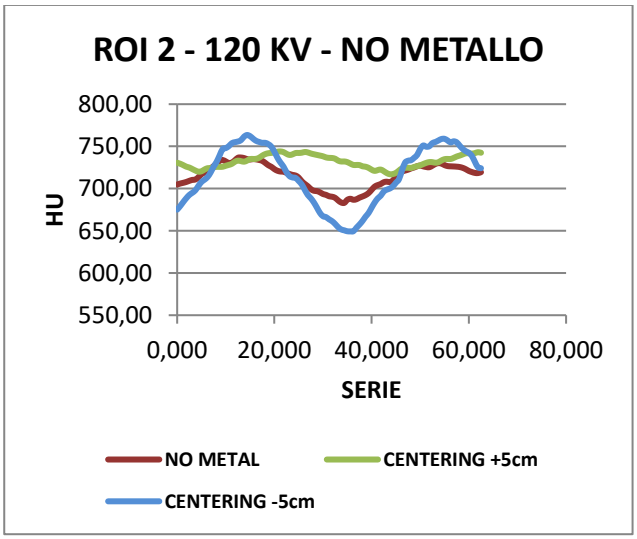

Figure 3.7 - HU trend as a function of centering for ROI2 in the acquisition with 120 kV

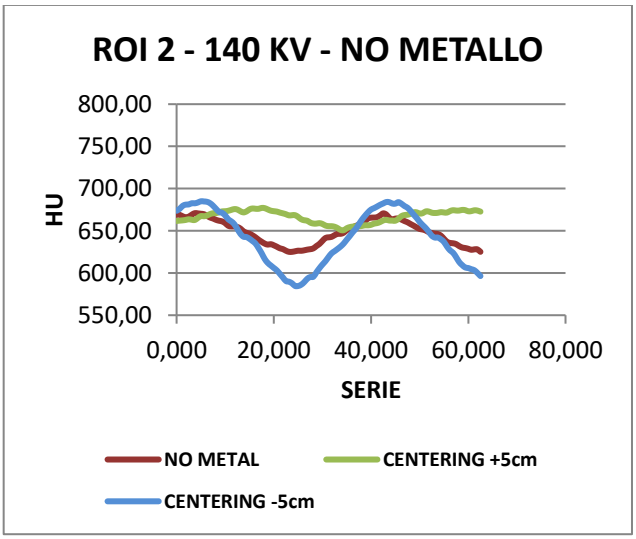

Figure 3.8 - HU trend as a function of centering for ROI2 in the acquisition with 140 kV

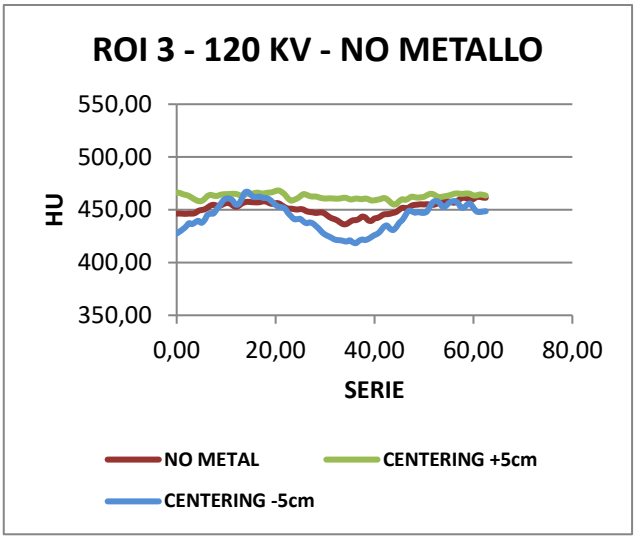

Figure 3.9 - HU trend as a function of centering for ROI3 in the acquisition with 120 kV

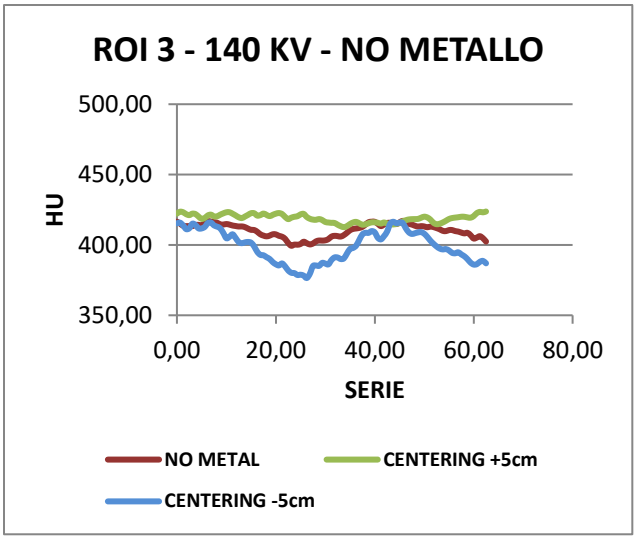

Figure 3.10 - HU trend as a function of centering for ROI3 in the acquisition with 140 kV

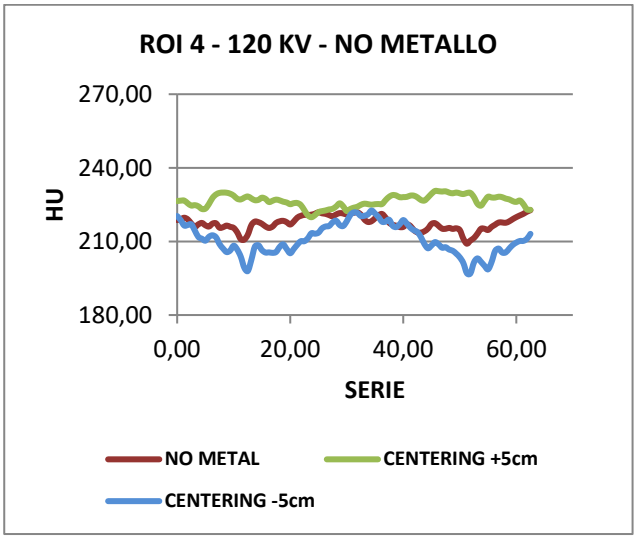

Figure 3.11 - HU trend as a function of centering for ROI4 in the acquisition with 120 kV

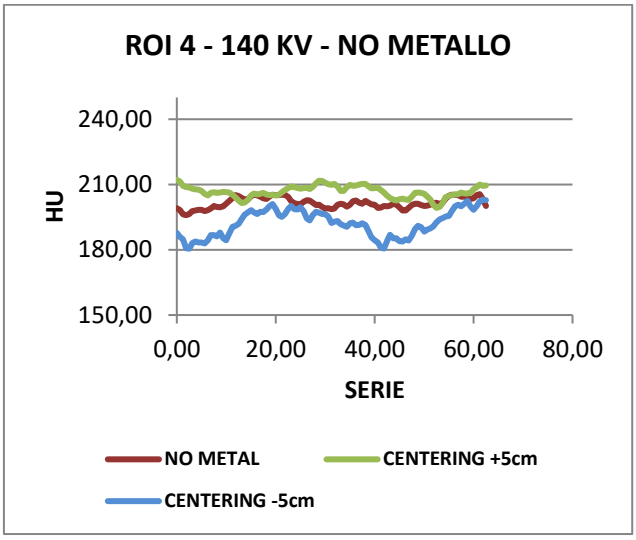

Figure 3.12 - HU trend as a function of centering for ROI4 in the acquisition with 140 kV

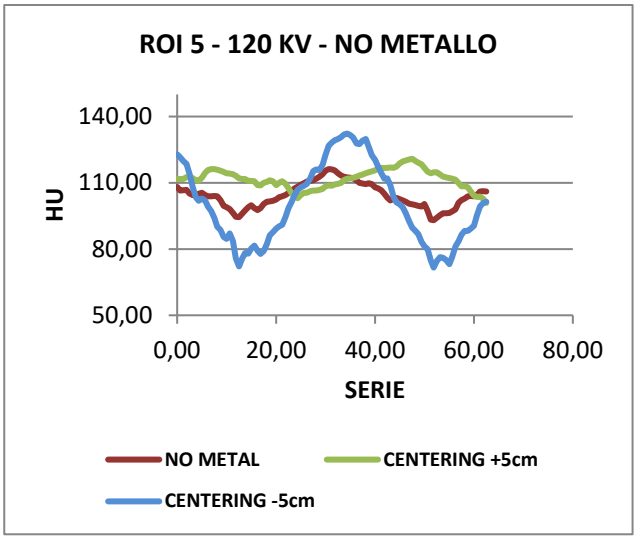

Figure 3.13 - HU trend as a function of centering for ROI5 in the acquisition with 120 kV

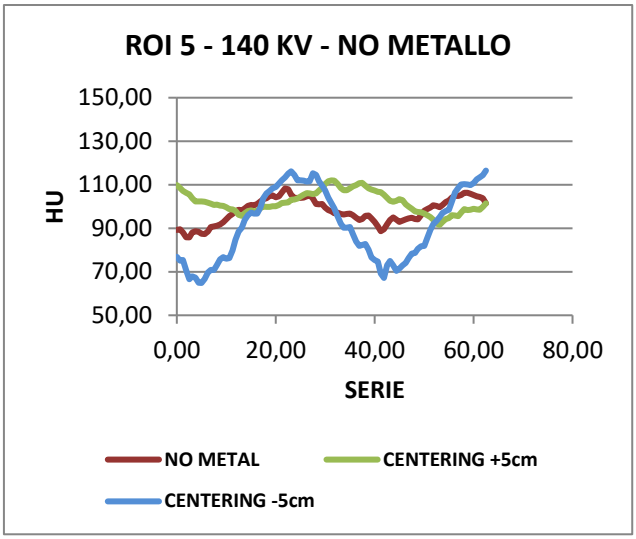

Figure 3.14 - HU trend as a function of centering for ROI5 in the acquisition with 140 kV

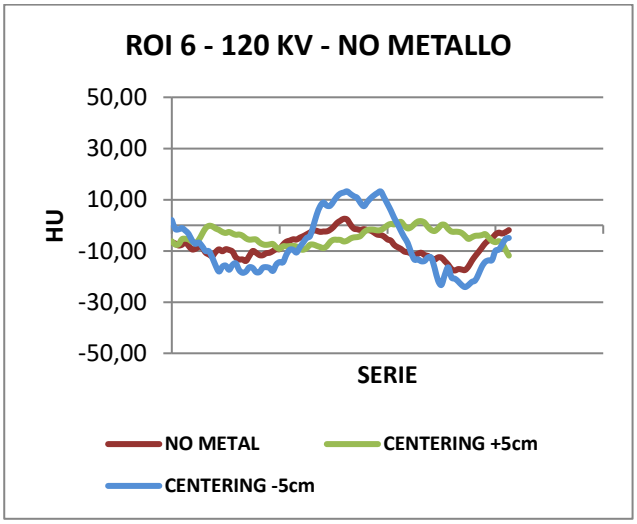

Figure 3.15 - HU trend as a function of centering for ROI6 in the acquisition with 120 kV

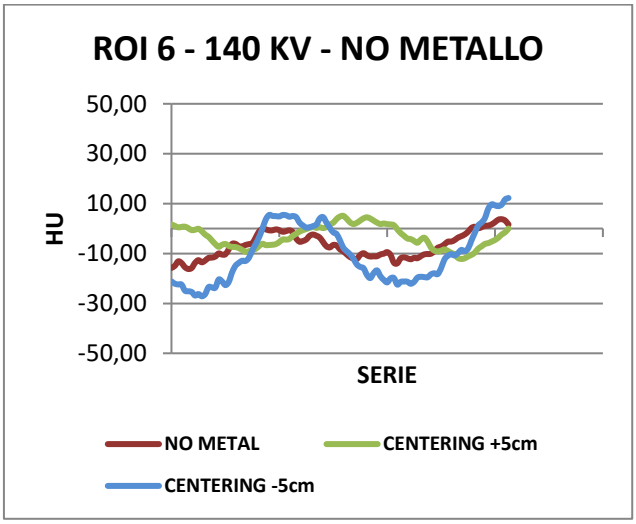

Figure 3.16 - HU trend as a function of centering for ROI6 in the acquisition with 140 kV

The following graphs show the HU trend as a function of centering of the two cylindrical samples.

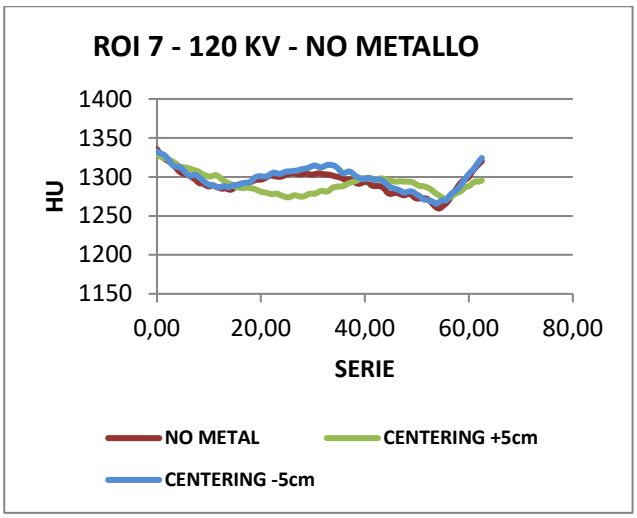

Figure 3.17 - HU trend as a function of centering for ROI7 in the acquisition with 120 kV

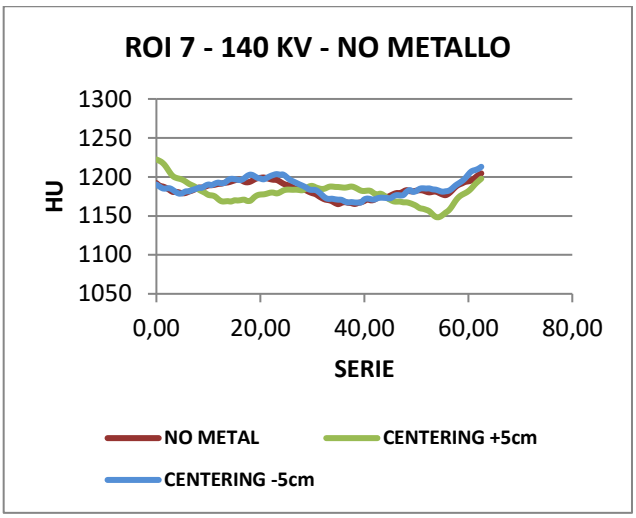

Figure 3.18 - HU trend as a function of centering for ROI7 in the acquisition with 140 kV

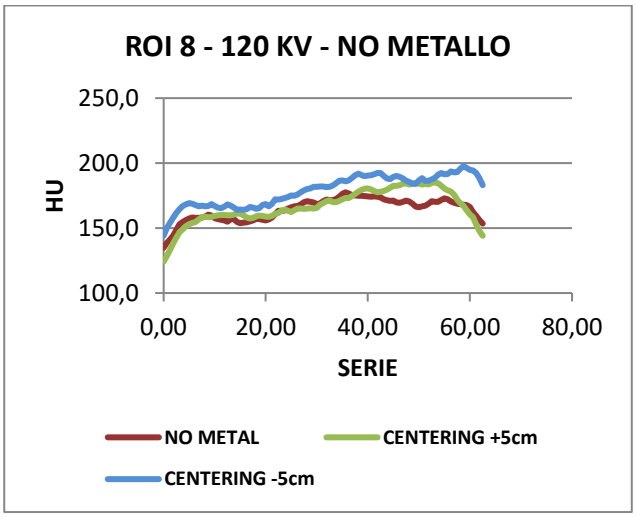

Figure 3.19 - HU trend as a function of centering for ROI8 in the acquisition with 120 kV

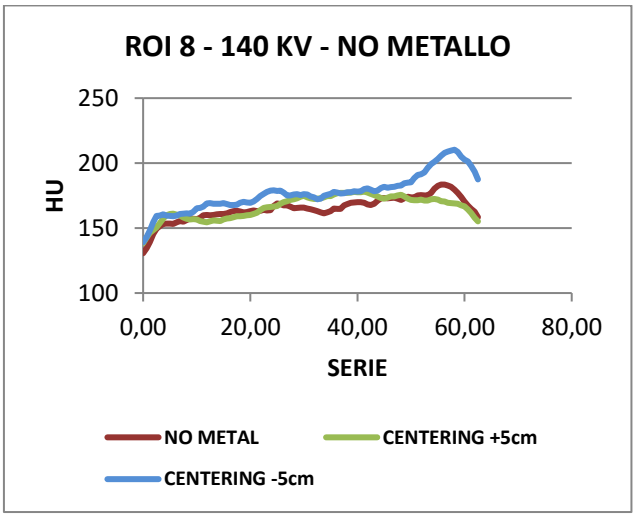

Figure 3.20 - HU trend as a function of centering for ROI8 in the acquisition with 140 kV

3.2. VOLTAGE AND MAR PRESENCE RESULTS

Below, the results obtained by varying the voltage between 120kV or 140kV and with the activation or not of MAR algorithm, in presence of metal elements, as explained in Chapter 2.5., are shown.

3.2.1. RESULTS OF THE VOLTAGE AND PRESENCE OF THE MAR FOR THE SMARTBONE®

The tables corresponding to a SmartBone® sample are listed below. The four main columns represent the four acquisitions considered. In the ' average ' row, the average HU value within the ROIs considered is reported; and the ' STD ' line shows the corresponding standard deviation.
The blue ' difference ' line shows the difference calculated. In fact, this line shows the difference between the average HU value of the ROIs obtained from the metalless acquisition and the average HU value of the same ROIs obtained from the acquisition in presence of metallic elements.

Sample 1 - SmartBone® sample of dimensions 20x10x10 mm: the sample 1 is present from the slice 23.75 to the slice 42.5.

	ROI SMARTBONE SAMPLE 1 - DIM 10x 20x20 mm - from slice 23.75 to the slice 42.5															
	NO METAL				CLOSE STEM				SCREW AND PLAQUE				FAR STEM			
	STANDARD		STANDARD MAR		STANDARD		STANDARD MAR		STANDARD		STANDARD MAR		STANDARD		STANDARD MAR	
	120KV	140KV	120 KV	140KV	120KV	140KV	120 KV	140KV	120KV	140KV	120 KV	140KV	120KV	140KV	120 KV	140KV
AVERAGE	248,2	205,2	248,2	205,2	378,4	294,8	266,2	223,1	242,4	207,4	243,7	215,4	285,3	244,1	243,1	223,8
DIFFERENCE					**130,2**	**89,6**	**18,0**	**17,9**	5,8	2,2	4,5	10,2	37,1	39,0	5,1	18,7

Table 3.5 - the table shows the values calculated for sample 1 volume. The HU average and Standard deviation values are shown for acquisition without metal element, with close stem, with screw and plaque and far stem. The blue line shows the difference calculated between the HU average values without metal and those with metal elements.

Sample 2 - SmartBone® sample of dimensions 10x10x10 mm: the sample 2 is present from the slice 8.125 to 14.375.

ROI SMARTBONE SAMPLE 2 - DIM 10x 10x10 mm - from slice 8.125 to slice 14.375																
	NO METAL				CLOSE STEM				SCREW AND PLAQUE				FAR STEM			
	STANDARD		STAND. MAR		STANDARD		STAND. MAR		STANDARD		STAND. MAR		STANDARD		STAND. MAR	
	120KV	140KV	120 KV	140KV	120KV	140KV	120 KV	140KV	120KV	140KV	120 KV	140KV	120KV	140KV	120 KV	140KV
AVERAGE	319,1	323,7	319,1	323,7	508,1	393,8	388,5	334,1	334,2	283,1	337,9	286,8	411,8	365,5	352,5	325,1
DIFFERENCE					**189,0**	**70,0**	**69,4**	**10,4**	15,1	-40,7	18,9	-36,9	92,7	41,8	33,4	1,3

Table 3.6 - the table shows the values calculated for sample 2 volume. The HU average and Standard deviation values are shown for acquisition without metal element, with close stem, with screw and plaque and far stem. The blue line shows the difference calculated between the HU average values without metal and those with metal elements.

Sample 3 - Sample of granulated SmartBone® – granulometry 2-4mm:

for this sample the slices from 17.5 to 47.5 were taken into consideration

ROI GRANULATED SMARTBONE SAMPLE 3 - GRANULOMETRY 2-4mm - from slice 17.5 to 47.5																
	NO METAL				CLOSE STEM				SCREW AND PLAQUE				FAR STEM			
	STANDARD		STAND. MAR		STANDARD		STAND. MAR		STANDARD		STAND. MAR		STANDARD		STAND. MAR	
	120KV	140KV	120 KV	140KV	120KV	140KV	120 KV	140KV	120KV	140KV	120 KV	140KV	120KV	140KV	120 KV	140KV
AVERAGE	321,9	288,5	324,9	288,5	391,4	341,9	305,1	290,3	329,1	297,2	323,7	293,3	109,5	155,5	281,3	263,2
DIFFERENCE					**69,5**	**53,4**	**19,9**	**1,8**	62,3	44,8	18,6	2,9	212,4	133,0	43,7	25,3

Table 3.7 - the table shows the values calculated for sample 3 volume. The HU average and Standard deviation values are shown for acquisition without metal element, with close stem, with screw and plaque and far stem. The blue line shows the difference calculated between the HU average values without metal and those with metal elements.

Sample 4 - Sample of granulated SmartBone® – granulometry 0.25mm:

This sample is visible from slice 23.125 to 47.5.

ROI GRANULATED SMARTBONE SAMPLE 4 - GRANULOMETRY 0,25 mm - 23.125 to 47.5.																
	NO METAL				CLOSE STEM				FAR STEM				SCREW AND PLAQUE			
	STANDARD		STAND. MAR		STANDARD		STAND. MAR		STANDARD		STAND. MAR		STANDARD		STAND. MAR	
	120KV	140KV	120 KV	140KV	120KV	140KV	120 KV	140KV	120KV	140KV	120 KV	140KV	120KV	140KV	120 KV	140KV
AVERAGE	542,8	478,1	542,8	478,1	261,8	306,4	448,3	418,9	376,6	399,2	505,0	478,0	537,5	485,0	527,8	484,5
DIFFERENCE					**281,0**	**171,7**	**94,6**	**59,3**	166,2	79,0	37,8	0,1	5,3	6,9	15,0	6,4

Table 3.8 - the table shows the values calculated for 3 sample volume. The HU average and Standard deviation values are shown for acquisition without metal element, with close stem, with screw and plaque and far stem. The blue line shows the difference calculated between the HU average values without metal and those with metal elements.

For all four **samples of SmartBone®,** a reference slice was considered:

Sample 1 - SmartBone® sample of dimensions 20x10x10 mm: reference slice is 38,75

SAMPLE 1 (SMARTBONE® 20x10x10 mm) - REFERENCE SLICE: 38,75								
	NO METAL				CLOSE STEM			
	STANDARD		STAND. MAR		STANDARD		STAND. MAR	
	120KV	140KV	120 KV	140KV	120KV	140KV	120 KV	140KV
AVERAGE	363,8	340,7	363,8	340,7	526,3	435,1	416,4	366,6
STD	87,1	84,3	87,1	84,3	126,0	103,1	114,3	102,6
DIFFERENCE					**162,4**	**94,4**	**52,6**	**25,9**

Table 3.9 - the table shows the values calculated for reference slice of sample 1. The HU average and Standard deviation values are shown for acquisition without metal element, with close stem, with screw and plaque and far stem. The blue line shows the difference

SAMPLE 1 (SMARTBONE® 20x10x10 mm) - REFERENCE SLICE: 38,75								
	FAR STEM				SCREW AND PLAQUE			
	STANDARD		STAND. MAR		STANDARD		STAND. MAR	
	120KV	140KV	120 KV	140KV	120KV	140KV	120 KV	140KV
AVERAGE	436,0	371,1	388,2	347,9	394,7	323,4	389,7	330,1
STD	100,4	95,3	97,2	92,0	79,8	73,8	72,3	69,5
DIFFERENCE	72,1	30,4	24,4	7,2	30,9	17,3	25,9	10,6

Table 3.10 - the table shows the values calculated for reference slice of sample 1 . The HU average and Standard deviation values are shown for acquisition without metal element, with close stem, with screw and plaque and far stem. The blue line shows the difference calculated between the HU average values without metal and those with metal elements.

Sample 2 - SmartBone® sample of dimensions 10x10x10 mm: reference slice is 11,25

SAMPLE 2 (SMARTBONE® 10x10x10 mm) - REFERENCE SLICE: 11,25								
	NO METAL				CLOSE STEM			
	STANDARD		STAND. MAR		STANDARD		STAND. MAR	
	120KV	140KV	120 KV	140KV	120KV	140KV	120 KV	140KV
AVERAGE	321,2	334,4	321,2	334,4	525,4	410,1	397,2	349,2
STD	77,4	79,4	77,4	79,3	117,3	108,7	65,6	86,9
DIFFERENCE					**204,1**	**75,8**	**76,0**	**14,8**

Table 3.11 - the table shows the values calculated for reference slice of sample 2. The HU average and Standard deviation values are shown for acquisition without metal element, with close stem, with screw and plaque and far stem. The blue line shows the difference calculated between the HU average values without metal and those with metal elements.

SAMPLE 2 (SMARTBONE® 10x10x10 mm) - REFERENCE SLICE: 11,25								
	FAR STEM				SCREW AND PLAQUE			
	STANDARD		STAND. MAR		STANDARD		STAND. MAR	
	120KV	140KV	120 KV	140KV	120KV	140KV	120 KV	140KV
AVERAGE	428,0	386,7	370,7	344,8	340,0	284,9	341,4	288,2
STD	76,7	61,1	61,7	64,1	82,2	87,7	81,6	86,1
DIFFERENCE	106,8	52,3	49,5	10,4	18,8	49,4	20,1	46,2

Table 3.12 - the table shows the values calculated for reference slice of sample 2. The HU average and Standard deviation values are shown for acquisition without metal element, with close stem, with screw and plaque and far stem. The blue line shows the difference calculated between the HU average values without metal and those with metal elements.

Sample 3 - Sample of granulated SmartBone® – granulometry 2-4mm: reference slice is 32,5.

SAMPLE 3 (GRANULATED SB, GRANULOMETRY 2-4mm - REFERENCE SLICE: 32,5								
	NO METAL				CLOSE STEM			
	STADARD		STANDARD MAR		STADARD		STANDARD MAR	
	120KV	140KV	120 KV	140KV	120KV	140KV	120 KV	140KV
AVERAGE	318,8	278,5	318,8	278,5	385,1	349,9	284,2	283,7
STD	81,9	82,2	86,1	82,2	104,8	104,6	96,4	91,9
DIFFERENCE					**66,3**	**71,4**	**34,6**	**5,3**

Table 3.13 - the table shows the values calculated for reference slice of sample 3. The HU average and Standard deviation values are shown for acquisition without metal element, with close stem, with screw and plaque and far stem. The blue line shows the difference calculated between the HU average values without metal and those with metal elements.

SAMPLE 3 (GRANULATED SB, GRANULOMETRY 2-4mm - REFERENCE SLICE: 32,5								
	FAR STEM				SCREW AND PLAQUE			
	STADARD		STANDARD MAR		STADARD		STANDARD MAR	
	120KV	140KV	120 KV	140KV	120KV	140KV	120 KV	140KV
AVERAGE	110,4	160,7	285,5	257,0	317,2	297,3	307,7	288,4
STD	154,7	128,0	108,0	108,8	86,5	83,4	88,6	83,6
DIFFERENCE	208,4	117,7	33,2	21,4	1,6	18,8	11,0	9,9

Table 3.14 - the table shows the values calculated for reference slice of sample 3. The HU average and Standard deviation values are shown for acquisition without metal element, with close stem, with screw and plaque and far stem. The blue line shows the difference calculated between the HU average values without metal and those with metal elements.

Sample 4 - Sample of granulated SmartBone® – granulometry 0.25mm: the reference slice is 38,12

SAMPLE 4 (GRANULATED SB, GRANULOMETRY 0,25 mm - REFERENCE SLICE: 38,12								
	NO METAL				CLOSE STEM			
	STADARD		STANDARD MAR		STADARD		STANDARD MAR	
	120KV	140KV	120 KV	140KV	120KV	140KV	120 KV	140KV
AVERAGE	544,7	481,9	544,7	481,9	280,3	318,8	453,7	425,1
STD	82,5	69,4	82,4	69,5	393,3	304,4	120,1	93,3
DIFFERENCE					**264,5**	**163,2**	**91,0**	**56,8**

Table 3.15 - the table shows the values calculated for reference slice of sample 4. The HU average and Standard deviation values are shown for acquisition without metal element, with close stem, with screw and plaque and far stem. The blue line shows the difference calculated between the HU average values without metal and those with metal elements.

SAMPLE 4 (GRANULATED SB, GRANULOMETRY 0,25 mm - REFERENCE SLICE: 38,12								
	FAR STEM				SCREW AND PLAQUE			
	STADARD		STANDARD MAR		STADARD		STANDARD MAR	
	120KV	140KV	120 KV	140KV	120KV	140KV	120 KV	140KV
AVERAGE	386,9	409,6	517,9	492,9	538,1	494,3	531,9	491,5
STD	99,2	122,7	69,8	86,7	99,3	81,4	94,1	74,6
DIFFERENCE	157,8	72,4	26,9	11,0	6,7	12,3	12,9	9,5

Table 3.16 - the table shows the values calculated for reference slice of sample 4. The HU average and Standard deviation values are shown for acquisition without metal element, with close stem, with screw and plaque and far stem. The blue line shows the difference calculated between the HU average values without metal and those with metal elements.

3.2.2. VOLTAGE AND MAR PRESENCE RESULTS FOR CALIBRATION PHANTOM AND CYLINDRICAL SAMPLES

The follow table 3.17 contains the results relative to six homogeneous inserts of calibration phantom.

The four main columns represent the four acquisitions considered. There are six main rows corresponding to the six ROIs plotted on the six inserts of phantom. In the ' ROI ' row, the average HU value within the volume of insert considered is reported; the blue ' difference ' line shows the calculated difference. In fact, this line shows the difference between the average HU value of the ROIs obtained from the acquisition without metal elements and the average HU value of the same ROIs obtained from the acquisition in presence of metallic elements.

AVERAGE	NO METAL				CLOSE STEM				SCREW AND PLAQUE				FAR STEM			
	STANDARD		STAND. MAR		STANDARD		STAND. MAR		STANDARD		STAND. MAR		STANDARD		STAND. MAR	
	120KV	140KV	120 KV	140KV	120KV	140KV	120 KV	140KV	120KV	140KV	120 KV	140KV	120KV	140KV	120 KV	140KV
ROI 1	979	884	979	884	964	880	969	885	963	876	963	876	964	879	972	885
DIFFERENCE					**15**	**4**	**9**	**1**	**16**	**8**	**15**	**8**	**15**	**5**	**6**	**1**
ROI 2	715	648	715	648	718	647	718	647	709	647	709	647	708	644	710	645
DIFFERENCE					**3**	**1**	**3**	**1**	**6**	**2**	**6**	**1**	**7**	**4**	**5**	**3**
ROI 3	451	410	451	410	448	405	449	408	447	408	447	407	445	406	446	407
DIFFERENCE					**3**	**5**	**2**	**2**	**4**	**3**	**5**	**3**	**6**	**4**	**5**	**4**
ROI 4	217	202	217	202	219	201	216	201	218	199	218	200	219	202	217	199
DIFFERENCE					**2**	**0**	**2**	**1**	**0**	**2**	**1**	**2**	**2**	**0**	**0**	**2**
ROI 5	104	98	104	98	108	101	104	98	105	96	105	96	107	99	102	96
DIFFERENCE					**4**	**3**	**0**	**0**	**1**	**2**	**1**	**2**	**3**	**1**	**2**	**2**
ROI 6	-8	-7	-8	-7	-5	-4	-8	-6	-8	-7	-7	-7	-4	-5	-8	-7
DIFFERENCE					**3**	**3**	**0**	**1**	**0**	**0**	**0**	**0**	**4**	**2**	**0**	**0**

Table 3.17 - the table shows the values calculated for all ROIs of calibration phantom. The HU average and Standard deviation values are shown for acquisition without metal element, with close stem, with screw and plaque and far stem. The blue line shows the difference calculated between the HU average values without metal and those with metal elements.

The following table 3.18 has the same structure as the previous one, but it shows the results for the two cylindric samples of known density.

AVERAGE	NO METAL				CLOSE STEM				SCREW AND PLAQUE				FAR STEM			
	STANDARD		STAND. MAR		STANDARD		STAND. MAR		STANDARD		STAND. MAR		STANDARD		STAND. MAR	
	120KV	140KV	120 KV	140KV	120KV	140KV	120 KV	140KV	120KV	140KV	120 KV	140KV	120KV	140KV	120 KV	140KV
ROI 7	1294	1184	1294	1184	1286	1186	1294	1185	1290	1180	1296	1182	1160	1261	1287	1178
DIFFERENCE					**7**	**2**	**0**	**1**	**4**	**4**	**2**	**1**	**133**	**77**	**6**	**5**
ROI 8	164	165	164	165	198	186	165	165	158	161	159	163	138	117	158	163
DIFFERENCE					**34**	**21**	**1**	**0**	**6**	**4**	**5**	**2**	**26**	**48**	**7**	**2**

Table 3.18 - the table shows the values calculated for the ROIs of two cylindrical samples. The HU average and Standard deviation values are shown for acquisition without metal element, with close stem, with screw and plaque and far stem. The blue line shows the difference calculated between the HU average values without metal and those with metal elements.

3.3. DOSE EVALUATION

The CTDI vol values provided by the scanner for all acquisitions have been reported in the following Graph. The blue bars refer to the acquisitions with 120 kV while the sky blue ones to the acquisitions at 140 Kv.

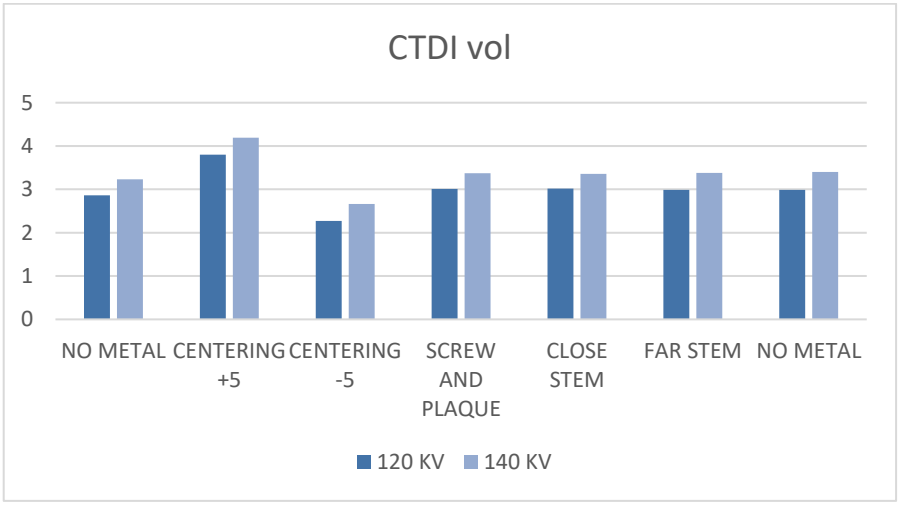

Figure 3.21 - This graph shows the CTDIvol values for each acquisition both to 120 kV and 140 kV

3.3. VALIDATION OF IMAGE SOFTWARE: HU RANGES FOR ALL ELEMENTS IN THE TEST

The HU ranges for all elements present in the test were calculated during validation procedure of two software, Image j and Mimics Innovation Suite. The values obtained are shown below:

SAMPLES OF SMARTBONE	**RANGE DI HU**
SAMPLE 1: Smartbone 10x20x20 mm	100-400
SAMPLE 2: Smartbone 10x10x10 mm	200-500
SAMPLE 3: Smartbone granulated 2-4mm	100-400
SAMPLE 4: Granulated Smartbone 0, 25mm	250 - 600
CYLINDRICAL SAMPLES	
Homogeneous Bone Sample -ROI 7	1050-1400
Homogeneous Acrylic sample -ROI 8	50-400
ROI PHANTOM	
ROI 1	750-1050
ROI 2	550-750
ROI 3	300-550
ROI 4	150-300
ROI 5	50-150
ROI 6	(-50) - +50

Table 3.19 – this table shows HU ranges for all elements presented in the test

3.4. RELATIONSHIP BETWEEN THE QUANTITY OF HYDROXYLAPATITE ON THE CALIBRATION PHANTOM AND THE AVERAGE HU VALUES

The following table shows the average HU values on the volumes of the six inserts of Calibration Phantom calculated for all acquisitions and the corresponding hydroxyapatite values (mg HA/ cm^3).

120 KV				140KV			
NO METAL				NO METAL			
	NO MAR	MAR	mg HA / cm3		NO MAR	MAR	mg HA / cm3
ROI 1	979	979	800	ROI 1	884	884	800
ROI 2	715	715	600	ROI 2	648	648	600
ROI 3	451	451	400	ROI 3	410	410	400
ROI 4	217	217	200	ROI 4	202	202	200
ROI 5	104	104	100	ROI 5	98	98	100
ROI 6	-8	-8	0	ROI 6	-7	-7	0
SCREW AND PLAQUE				SCREW AND PLAQUE			
	NO MAR	MAR	mg HA / cm3		NO MAR	MAR	mg HA / cm3
ROI 1	963	963	800	ROI 1	876	876	800
ROI 2	709	709	600	ROI 2	647	647	600
ROI 3	447	447	400	ROI 3	408	407	400
ROI 4	218	218	200	ROI 4	199	200	200
ROI 5	105	105	100	ROI 5	96	96	100
ROI 6	-8	-7	0	ROI 6	-7	-7	0
CLOSE STEM				CLOSE STEM			
	NO MAR	MAR	mg HA / cm3		NO MAR	MAR	mg HA / cm3
ROI 1	964	969	800	ROI 1	865	869	800
ROI 2	713	711	600	ROI 2	639	638	600
ROI 3	449	450	400	ROI 3	404	405	400
ROI 4	219	216	200	ROI 4	201	197	200
ROI 5	108	104	100	ROI 5	101	98	100
ROI 6	-5	-8	0	ROI 6	-4	-5	0
STELO LONTANO				FAR STEM			
	NO MAR	MAR	mg HA / cm3		NO MAR	MAR	mg HA / cm3
ROI 1	964	972	800	ROI 1	879	885	800
ROI 2	707	706	600	ROI 2	646	644	600
ROI 3	445	446	400	ROI 3	406	407	400
ROI 4	219	217	200	ROI 4	202	199	200
ROI 5	107	102	100	ROI 5	99	95	100
ROI 6	-4	-8	0	ROI 6	-5	-7	0

Table 3.20 – this table shows: the hu average values for acquisition without MAR are in sky blue column, the hu average values for acquisition with mar are in green column and the amount of hydroxyapatite for each insert of calibration phantom in pink column.

The attention was focused on the acquisitions carried out with a voltage of 140 KV

The values of HU expressed as a function of the amount of HA (mg ha/cm3) were represented in the following graphs.

The Blue line represents the interpolation between the HU values, in the x-axis, and the corresponding HA (mg ha/cm^3) values on the y-axis, and it was possible to observe that the relation tends to be linear. The trendline was plotted and the equation of the line that connect the HU average values and the amount of hydroxyapatite was obtained.

NO METAL

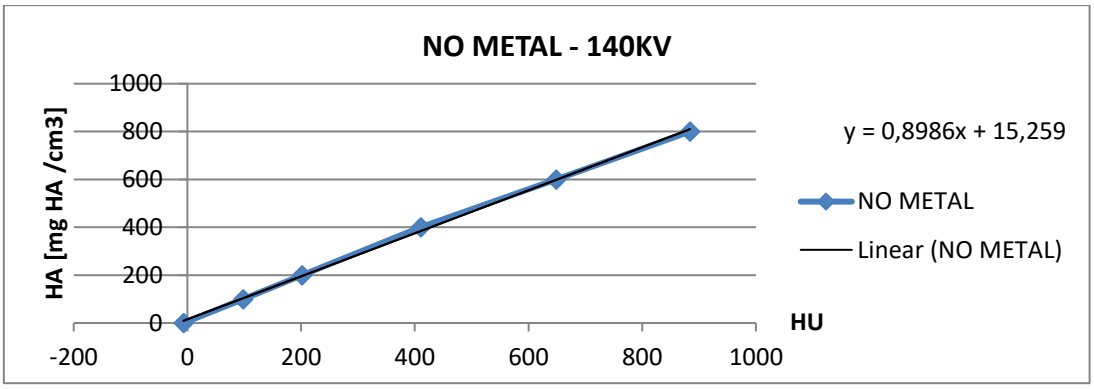

Figure 3.22 - blue line represents the interpolation between the HU average values, for acquisition without metal, and the corresponding HA values, the black straight line is the trend line relative to blue line

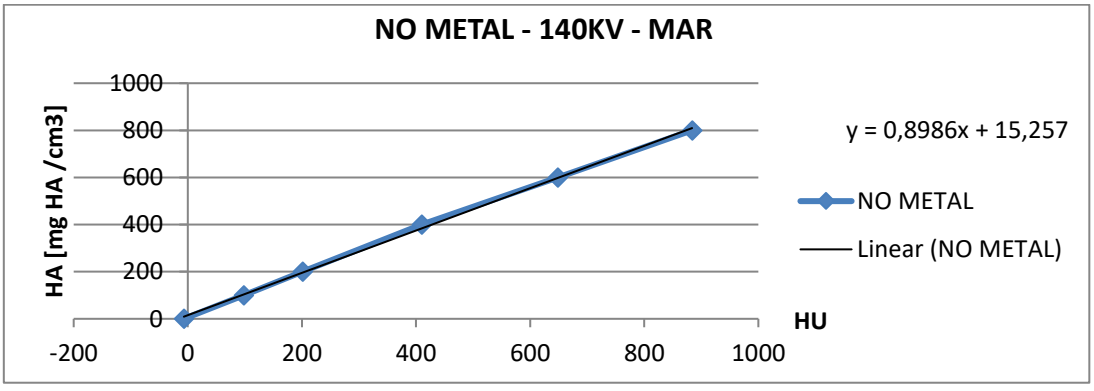

Figure 3.23 - blue line represents the interpolation between the HU average values, for acquisition without metal and with MAR, and the corresponding HA values, the black straight line is the trend line relative to blue line

METAL: CLOSE STEM

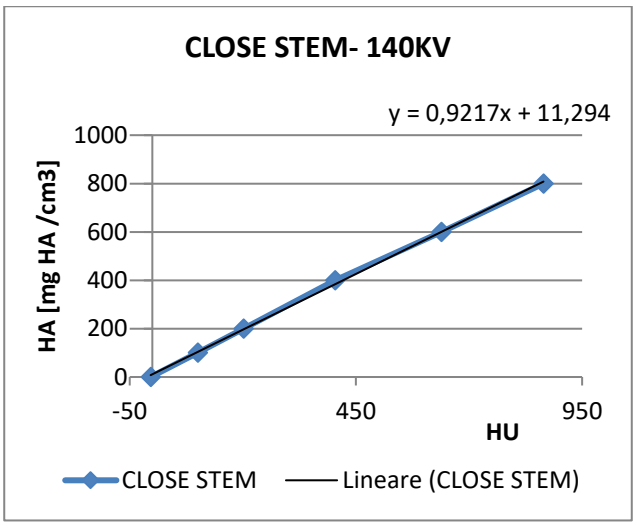

Figure 3.24 - blue line represents the interpolation between the HU average values, for acquisition with close stem and the corresponding HA values; the black straight line is the trend line relative to blue line.

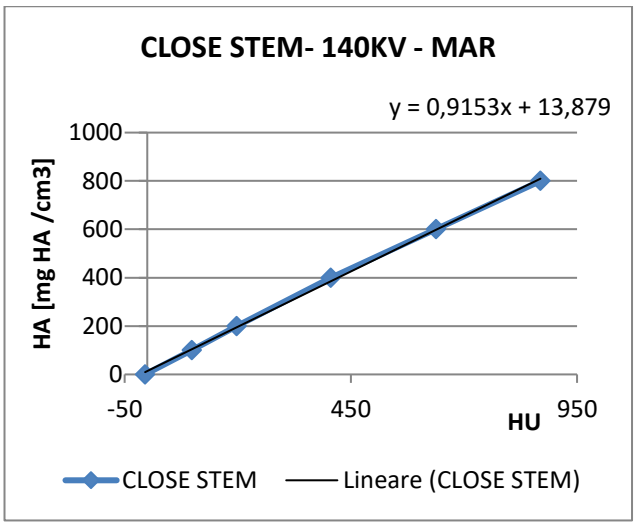

Figure 3.25 - blue line represents the interpolation between the HU average values, for acquisition with close stem and with MAR; the black straight line is the trend line relative to blue line.

METAL: FAR STEM

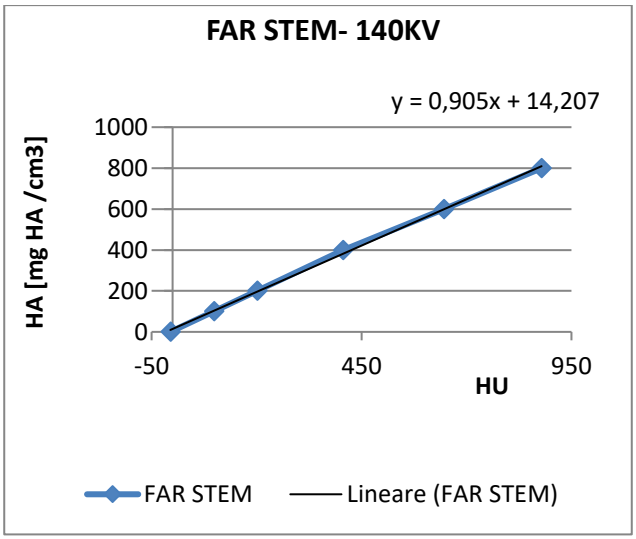

Figure 3.26 - blue line represents the interpolation between the HU average values, for acquisition with far stem and the corresponding HA values; the black straight line is the trend line relative to blue line.

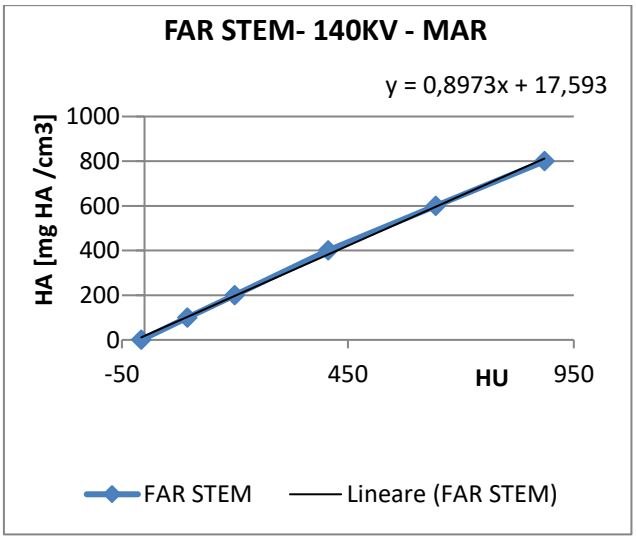

Figure 3.27 - blue line represents the interpolation between the HU average values, for acquisition with far stem and with MAR; the black straight line is the trend line relative to blue line.

METAL: SCREW AND PLAQUE

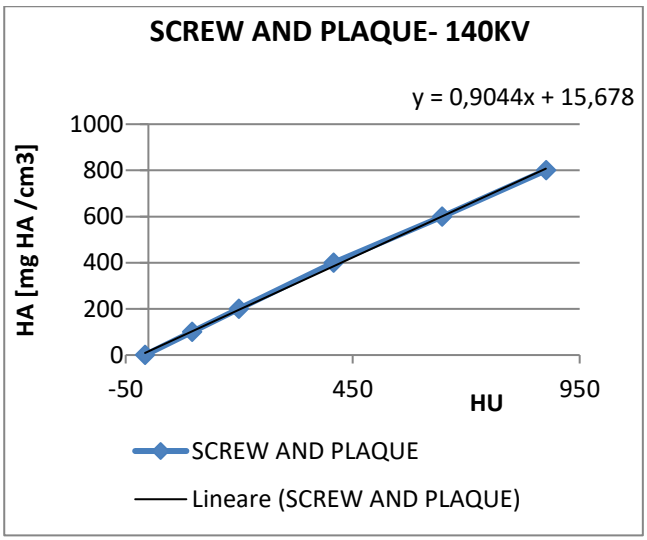

Figure 3.28 - blue line represents the interpolation between the HU average values, for acquisition with screw and plaque and the corresponding HA values; the black straight line is the trend line relative to blue line.

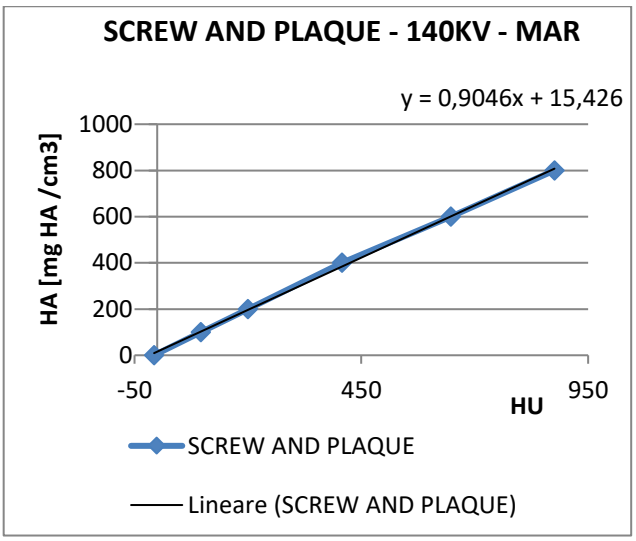

Figure 3.29 - blue line represents the interpolation between the HU average values, for acquisition with screw and plaque and with MAR; the black straight line is the trend line relative to blue line.

.

3.5. MINERALIZATION

The following results are obtained performing the procedure explained in chapter 2.8.

The linear model used is the following:

Acquisition without metal and with MAR – **y = 0,8986x + 15,257**

The table 3.21 shows the values obtained on volume of SmartBone® samples, while the table 3.22 refers to a reference slices of SmartBone® samples.

In both tables, the four main columns are related to SmartBone® Samples. The blue line shows the HU average values relative to each sample. These values were inserted into linear model to obtain the hydroxyapatite values corresponding. So the red line shows the corresponding values in mgHA/cm^3 obtained from the linear model.

REFERENCE REGION

	ZONE REFERENCE - AVERAGE HU VALUE -NO METAL-RIC 140 KV-STANDARD MAR-FULL FOV			
	SMARTBONE SAMPLES			
	1 : SMARTBONE 10x20x20mm	2 : SMARTBONE 10x10x10mm	3 : GRANULATED SMARTBONE 2-4 mm	4 : GRANULATED SMARTBONE 0,25mm
HU	205	324	288	478
y [mg HA/cm3]	**200**	**306**	**275**	**445**

Table 3.21 - The HU average values calculated on volume for each SmartBone® sample are shown in the blue line. The amount of hydroxyapatite obtained from the linear model and corresponding of each SmartBone® sample is shown in red line.

REFERENCE SLICE

	REFERENCE SLICE - AVERAGE HU VALUE -NO METAL-RIC 140 KV-STANDARD MAR-FULL FOV			
	SMARTBONE SAMPLES			
	1 : SMARTBONE 10x20x20mm	2 : SMARTBONE 10x10x10mm	3 : GRANULATED SMARTBONE 2-4 mm	4 : GRANULATED SMARTBONE 0,25mm
HU	341	334	278	482
y [mg HA/cm3]	**321**	**316**	**265**	**448**

Table 3.22 - The HU average values calculated on reference slice for each SmartBone® sample are shown in the blue line. The amount of hydroxyapatite obtained from the linear model and corresponding of each SmartBone® sample is shown in red line.

3.6. CLINICAL CASES

3.6.1. DENSITOMETRIC ANALYSIS: BONE REGROWTHS ASSESMENT

PATIENT 1

The table 3.23 shows the measurements obtained for all four ROI; in particular:

- Average HU value on 2D region,
- Standard Deviation (STD),
- Minimum HU value within 2D ROI,
- Maximum HU value within 2D ROI.

The Blue row shows the HU average values on the volume of interest.

Label	Area	Mean	StdDev	Min	Max	Perim.	Slice	MinThr	MaxThr
MAR:ROI IM 588:MP000588	68,23	463,10	95,68	166,00	777,00	35,32	35,00	-32768,00	32767,00
MAR:ROI IM 589:MP000589	56,46	500,85	112,66	180,00	939,00	31,69	36,00	-32768,00	32767,00
MAR:ROI IM 590:MP000590	42,23	478,84	114,13	177,00	842,00	28,33	37,00	-32768,00	32767,00
MAR:ROI IM 591:MP000591	17,24	429,12	122,36	116,00	733,00	22,98	38,00	-32768,00	32767,00
VALOR MEDIO		467,98	111,20	159,75	822,75				

Table 3.23 - the average values related of regenerated bone volume in study are shown in blue line

The following images show the areas of the regrown bone: in green the areas of cortical bone (662 – 1988 HU), in fuchsia the areas related to the Cancellous bone (501 – 661 HU) and in Cyan the areas related to SmartBone® or Cancellous bone (100 – 500 HU).

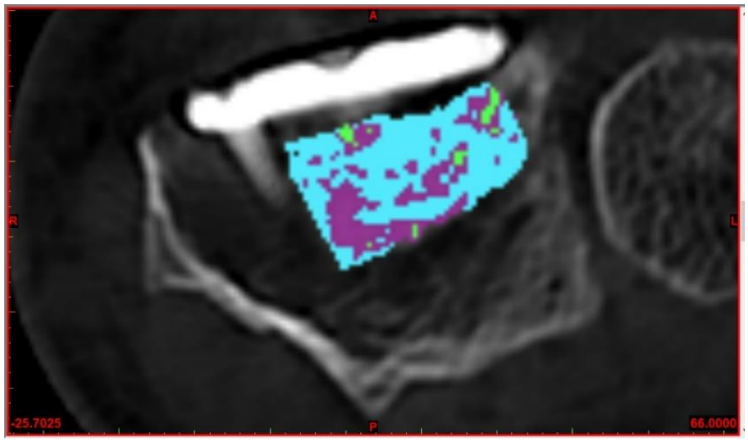

Figure 3.30 – this image shows the region of regrown bone in the Im66. Green area is cortical bone, fuchsia area is cancellous bone and cyan area is related to Smartbone® or cancellous bone

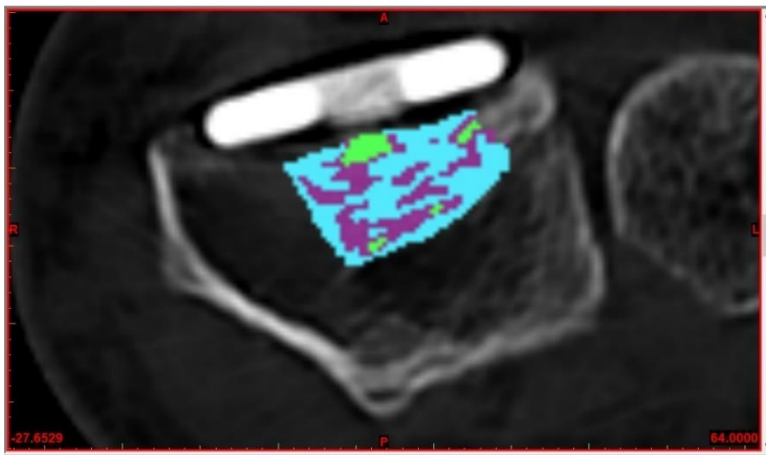

Figure 3.31 - this image shows the region of regrown bone in the Im64. Green area is cortical bone, fuchsia area is cancellous bone and cyan area is related to Smartbone® or cancellous bone

The area percentage of cortical bone, of cancellous bone and of unidentifiable one, represented by cyan colour, has been assessed for each slice.

slice number	area (mm^2)			
	Green	Fuchsia	Cyan	Area tot.
60	0,82	4,29	23,90	29,01
62	4,74	17,06	43,78	65,58
64	6,29	28,28	51,17	85,74
66	3,65	36,12	72,97	112,74

Table 3.24 - the amount of each region (green, fuchsia and cyan) on total area was calculated for each slice and it is shown in this table.

slice number	area (%)			
	Green %	Fuchsia %	Cyan %	TOT. %
60	3	15	82	100
62	7	26	67	100
64	7	33	60	100
66	3	32	65	100

Table 3.25 - the percentage of each region (green, fuchsia and cyan) on total area was calculated for each slice and it is shown in this table

As reference slices were considered the 64 and the 66.

In Slice 64 It is noted that: 7% is relative to the cortical bone, while the 33% is equal to the cancellous bone.

In Slice 66, it is observed that: 3% is relative to the cortical bone and the 32% to the cancellous bone.

Instead, the 60% in slice 64 and 65% in slice 66 cannot be identified because it falls within both the SmartBone® range and the cancellous bone range.

PATIENT 2

The same measurements were obtained for the patient 2. In the following table are shown the mean values obtained for all ROI from the 22 slices

	Mean	StdDev	Min	Max
AVERAGE	488,43	145,84	184,76	788,90

Table 3.26 - the average values related of regenerated bone volume in study are shown in blue line

The following images show the areas of the regrown bone: in green the areas of cortical bone (662 – 1988 HU), in fuchsia the areas related to the Cancellous bone (501 – 661 HU) and in Cyan the areas related to SmartBone® or Cancellous bone (100 – 500 HU).

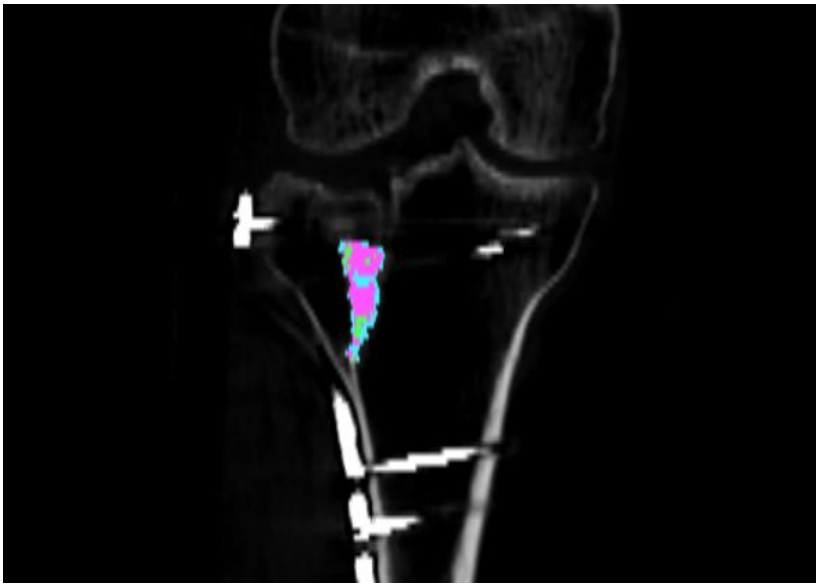

Figure 3.32 - this image shows the volume of regrown bone in the Im66. Green area is cortical bone, fuchsia area is cancellous bone and cyan area is related to Smartbone® or cancellous bone

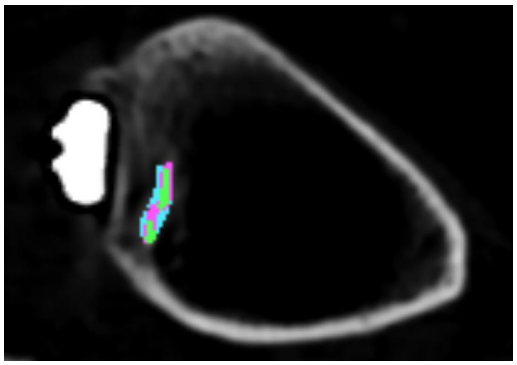

Figure 3.33 - this image shows the region of regrown bone in the Im 71.25. Green area is cortical bone, fuchsia area is cancellous bone and cyan area is related to Smartbone® or cancellous bone.

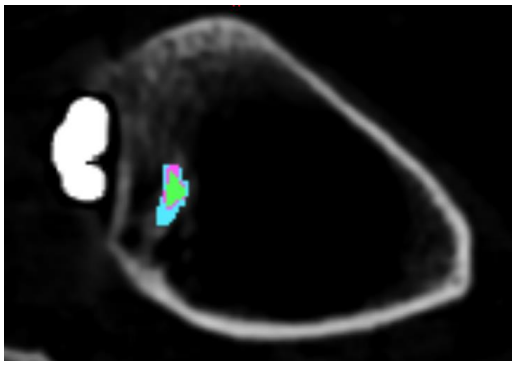

Figure 3.34 - this image shows the region of regrown bone in the Im 72.50. Green area is cortical bone, fuchsia area is cancellous bone and cyan area is related to Smartbone® or cancellous bone.

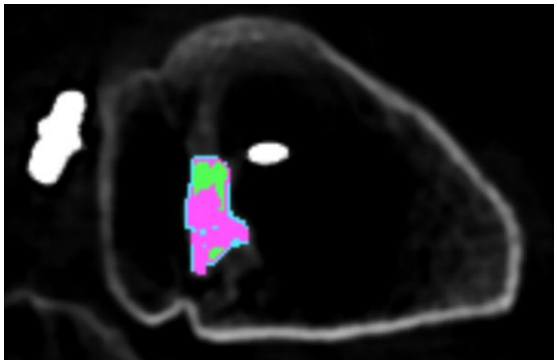

Figure 3.35 - this image shows the region of regrown bone in the Im 83.75. Green area is cortical bone, fuchsia area is cancellous bone and cyan area is related to Smartbone® or cancellous bone.

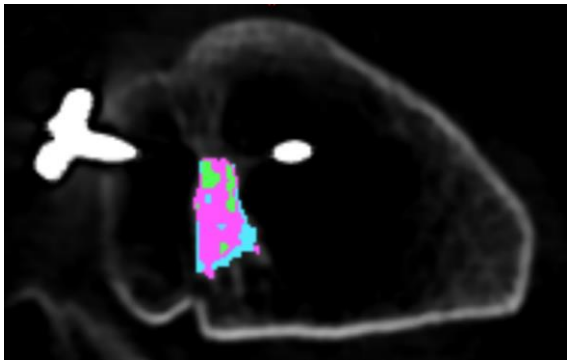

Figure 3.36 - this image shows the region of regrown bone in the Im 85.00. Green area is cortical bone, fuchsia area is cancellous bone and cyan area is related to Smartbone® or cancellous bone.

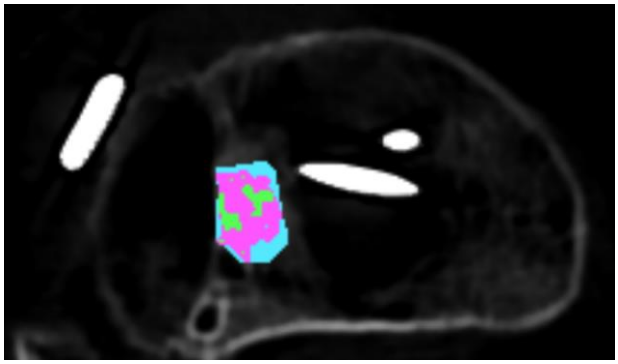

Figure 3.37 - this image shows the region of regrown bone in the Im 91.25. Green area is cortical bone, fuchsia area is cancellous bone and cyan area is related to Smartbone® or cancellous bone.

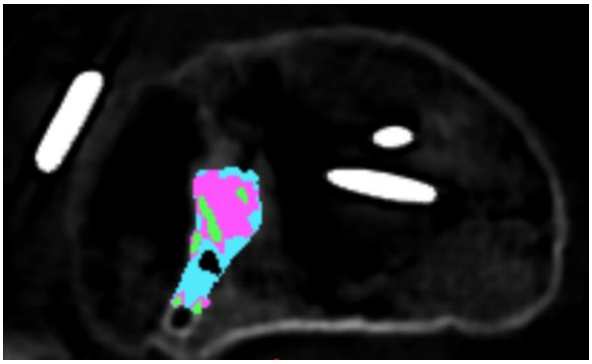

Figure 3.38 - this image shows the region of regrown bone in the Im 92.50. Green area is cortical bone, fuchsia area is cancellous bone and cyan area is related to Smartbone® or cancellous bone.

The mean percentage of cortical bone, of spongious bone and of unidentifiable one, represented by cyan colour, has been assessed for each slice.

slice number	area (mm2)			
	Green	Fuchsia	Cyan	Tot. Area
AVERAGE	11,35	34,81	32,25	78,42

Figure 3.39 - the average value of each region (green, fuchsia and cyan) on total area was calculated for each slice and it is shown in this table.

slice number	area (mm2)			
	Green(%)	Fuchsia(%)	Cyan(%)	Tot. Area(%)
AVERAGE %	16	44	40	100

Figure 3.40 – the mean percentage of each region (green, fuchsia and cyan) on total area was calculated for each slice and it is shown in this table

In the volume considered, it is noted that: 16% is relative to the cortical bone, while the 44% is equal to the cancellous bone.

Instead, the 40% cannot be identified because it falls within both the SmartBone® range and the cancellous bone range.

3.6.2. MINERALIZATION OF THE REGROWN BONE VOLUME

The average HU value for the regrown bone volume obtained:

PATIENT 1: in the table 3.23 is equal to: **x=467,98 HU**

As a result, a hydroxyapatite mineralization of the material in mg HA/cm^3 is obtained:

$$y = 0,8986 \times 467,98 + 15,257 \longrightarrow y = 435,8\ mg\ HA/cm^3$$

PATIENT 2: In the table is equal to: **x=488,43 HU**

As a result, a hydroxyapatite mineralization of the material in mg HA/cm^3 is obtained:

$$y = 0,8986 \times 488,43 + 15,257 \longrightarrow y = 454,12\ mg\ HA/cm^3$$

3.6.3. VOLUMETRIC METHOD: MEASURE THE REGROWN BONE VOLUME

The remaining volume obtained by overlapping of models with Mimics Innovation Suite software is showed in figure 3.41 and 3.42. This is the regenerated bone of the Patient 1 after 9 months from the surgery and the implant of bone substitute.

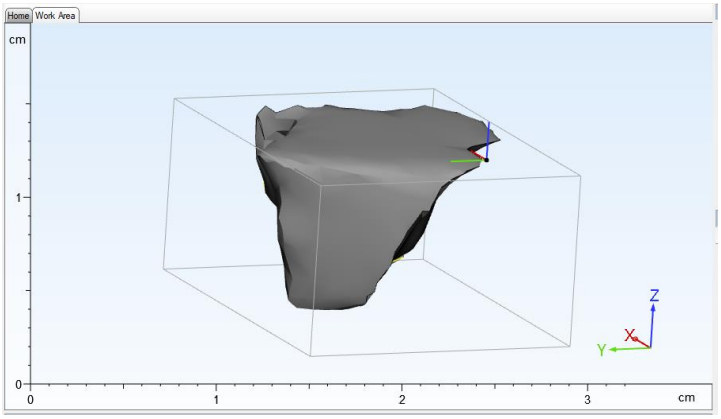

Figure 3.41 – the volume obtained by overlapping of volumes

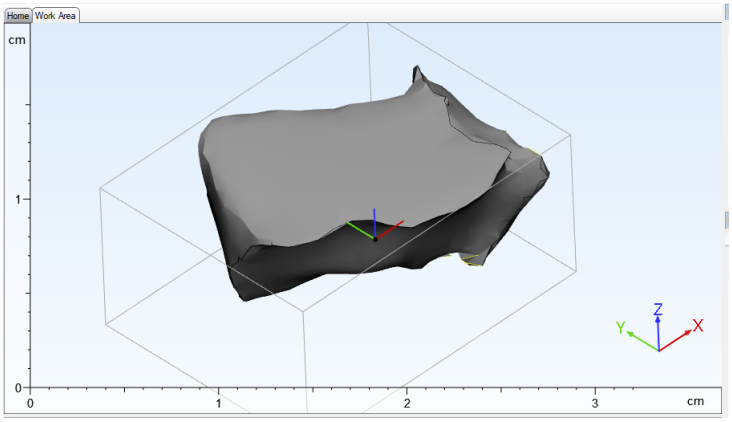

Figure 3.42 - the volume obtained by overlapping of volumes

The measure of surface and of the volume obtained was calculated with the Mimics Innovation Suite software and it is showed below.

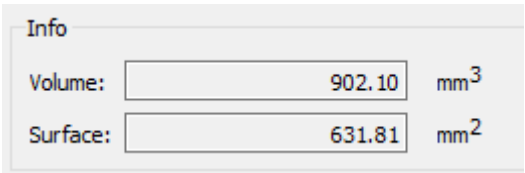

Figure 3.43 – Volume and surface of regenerated bone calculated with Mimics Innovation suite software

The regenerated bone of the Patient 2 after the surgery with the implant of bone substitute is shown below.

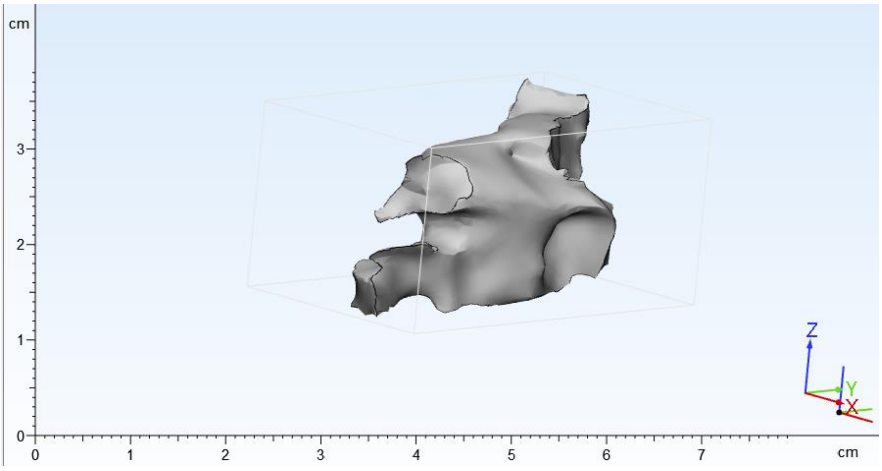

Figure 3.44 - the volume obtained by overlapping of volumes

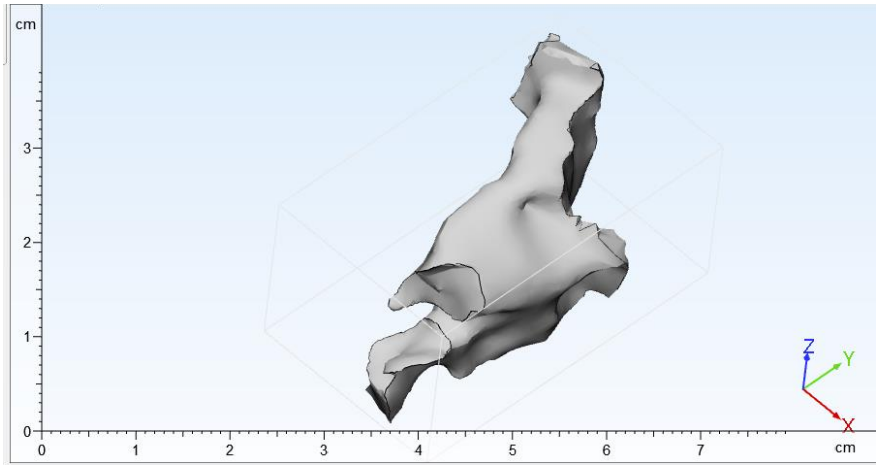

Figure 3.45 - the volume obtained by overlapping of volumes

The measure of surface and of the volume obtained it was calculated with the Mimics software and it is showed below.

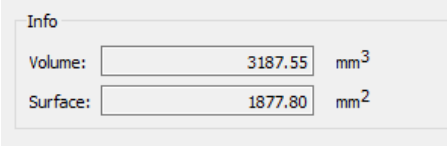

Figure 3.46 - Volume and surface of regenerated bone calculated with Mimics Innovation suite software

4. DISCUSSIONS

4.1. CENTERING EVALUATION

The centering effect on acquisition of SmartBone® samples, calibration phantom and cylindrical samples was evaluated to define the possible results, which could be present, with the variation of the patient's position.

The behaviour of the SmartBone® samples as a function of centering was shown in chapter 3.1.1.
The graphs 3.1, 3.2, 3.3 and 3.4 represent the Hounsfield unit (HU) trend as a function of patient centering for SmartBone® compact samples (sample#1 and sample#2) and for both acquisition with 120 kV and 140 kV.
In graphs, the blue curve represents the HU trend in acquisition in absence of metal and without changes in centring, while the other two curves show the HU trend in acquisitions with varied centering: red curve centering of + 5cm, green curve centering of -5cm.
The three curves tend to have the same trend and the red and green curves do not have significant deviations from the blue curve, therefore there are no significant variations with the variation of centering.

A reference slice was also considered for all four SmartBone® samples.
The HU average value of region of interest (ROI) relative to SmartBone® samples was calculated for each reference slice.
The difference between the HU average value of ROIs obtained from acquisition in absence of metal and without changes in centring and the HU average value of the same ROIs obtained from acquisition with varied centering was evaluated.
The difference calculated were shown in the tables 3.1, 3.2, 3.3 and 3.4.; it was observed that the ‘difference’ is not significant, because the two terms, which have been subtracted, are the same order of magnitude. Therefore, significant variations depending on centring are not present, so the SmartBone® acquisition is not influenced significantly.

The influence of the Centering (raising or lowering the TC table by 5 cm) in the acquisition of calibration phantom QRM-BDC/6 and of two cylindrical samples was shown in chapter 3.1.2.
The graphs from 3.5 to 3.16 represent the Hounsfield unit (HU) trend as a function of patient centering for all six phantom's inserts and for both acquisition with 120 kV and 140 kV.
Red curve represents the HU trend in acquisition in absence of metal and without changes in centring, while the other two curves show the HU trend in acquisitions with varied centering: green curve centering of + 5cm, blue curve centering of -5cm.

The HU trends of two inserts (ROI 3 and ROI 4) are shown in the graphs 3.9, 3.10, 3.11 and 3.12 and they are constant along the longitudinal direction of acquisition.
Instead, the HU trend within the ROI 1, ROI 2, ROI 5 and ROI 6, shown in the graphs 3.5, 3.6, 3.7, 3.8, 3.13, 3.14, 3.15 and 3.16, tends to be cyclical and has significant deviations from the curve in the absence of metal acquisition and without changes in centering.
This is most evident in the case of centering at -5cm (blue curve).

These inserts are placed in a marginal position of FOV, where X-ray radiogenic beam have not to pass through large thicknesses, but in this case X-ray beam found phantom inserts that have significant size and density; so, this situation can cause the sinusoidal trend.

Moreover, the GE TC 64 slices has a modulation of the dose (mAs) according to the scout and the centering, that can cause this trend.
Modulation is carried out based on the last scout made. For the TC 64 slices of GE the second scout is the lateral scout view (LL) and when this scout is made, the mAs that will be used during the acquisition are modulated.
If the LL scout view is of low quality because the centering is too low, then the TC reads the wrong densities and then delivers a different dose. Therefore, if the phantom is so low in the LL projection the TC reads wrong values and the modulation of the dose is strange and not linear.
Centering influences the scanogram acquisition and the volume of data, with variations of anodic current; which are between 75% and 141% of the value obtained for positioning at the isocentre if centering changes from -5 cm to +5 cm by the isocentre. [64]
In addition, the operation of the spiral reconstruction algorithm causes cyclical trend.
Therefore, centering is essential for a correct evaluation of calibration phantom.

As regards the two cylindrical samples of known density, from graphs 3.17 ,3.18, 3.19, 3.20 is observed that the centering would seem not to affect their evaluation. The curves, in fact, have a little oscillating trend, quite homogeneous and with irrelevant deviations between them.

In conclusion, patient centering is important to carry out a correct analyse.
The calibration phantom presence, under patient position, will be recommended into CT scan protocol, which will be define at the end of this study.
If the centering is complicated, it is suggested not to center the patient too low, rather it is better to center it upwards; so that the trend of the HU is the least fluctuating possible and the deviations from the reference curve are lower.

4.2. VOLTAGE AND MAR PRESENCE EVALUATION

SmartBone® implant is usually associated with orthopaedics metallic elements to give a more stability. Metal elements cause artifacts into CT acquisition, therefore the better voltage and the efficiency of MAR algorithm were evaluated to reduce these artifacts as much as possible.

Voltage and MAR presence results for SmartBone® samples were shown in chapter 3.2.1.
The difference between the HU average values for acquisition without metal and the HU average values for acquisition with metal elements (close stem, screw and plate and far stem) was calculated for each SmartBone® sample volume.
These results are shown in the tables: 3.5, 3.6, 3.7 and 3.8.
This bone substitute is not homogeneous, and it has an intrinsic porosity, that is a characteristic of the material cannot be excluded. These Porosities are included on evaluation of SmartBone® volumes and they decrease the HU values. So, a reference slice was also considered to do an evaluation more homogeneous.

The same difference was calculated for each SmartBone® samples reference slice and the results are shown in the table: 3.9, 3.10, 3.11, 3.12, 3.13, 3.14, 3.15 and 3.16
The acquisition with close stem was considered the 'worst condition' because stem has larger size than screw and plate and is closer to elements in the test, so close stem influences more the acquisition.
Therefore, the attention was paid to acquisition without metal elements and to the acquisition with close stem, to do reliable considerations.
The difference calculated in acquisition with close stem with a voltage of 120 kV and without MAR algorithm may be up 200HU. This value decreases with a voltage of 140kV, but it is observed that the difference never exceeds 100 HU with MAR algorithm applied to both voltage.
The better result is obtained with a voltage of 140 kV and in the presence of the MAR algorithm, because the maximum difference is about 50 HU.
Therefore, the difference between the acquisition without metal and the acquisition with metal elements decreases with a voltage of 140 kV and in the presence of the MAR algorithm, so with these parameters the HU values in acquisition with metal elements are more similar to HU values

of acquisition without metal. In other words, the results are better with the combination of these parameters because the artifacts are reduced.
The same results are obtained both for SmartBone® samples volume and for SmartBone® samples reference slice.

The behaviour of calibration phantom is not influenced by presence of metallic elements; indeed, it is not possible to make special observations on the performance of HU values. The difference between the HU average valued of six inserts of acquisition without metal and the HU average values of acquisition with metal elements was calculated and the results are shown in the table 3.17.
The difference values calculated are very small and the maximum difference is about 15 HU.
This is probably due to calibration phantom position, which compared to the other elements is more distant from the metal elements and it is less influenced by noticeable artefacts.

Moreover, the behaviour of two homogeneous cylindrical samples were assessed, paying more attention to cylindric acrylic sample (ROI 8) which is closer to the metal elements and the HU values are most affected.
The difference HU values relative to cylindrical insert are shown in the table 3.18.
In also this case more attention was paid for acquisition with close stem. The difference for ROI 8 is about 34 HU in the acquisition with 120 kV and without MAR, instead it is 21 HU in the acquisition with 140 kV and without MAR. it is noted that using a voltage of 140 KV is better than 120KV.
The difference values obtained with a voltage of 120 kV with MAR and a voltage of 140 kV with MAR are very similar but slightly lower values is obtained with a voltage of 140 kV; this could be given by the fact that the efficiency of the MAR is more present at high voltage.
These difference values are lesser than values of acquisition without MAR algorithm.

So, the better acquisition of the cylindrical samples and also of the Calibration Phantom was obtained with a voltage of 140KV and in the presence of the MAR algorithm and this supports the considerations previously made for the SmartBone®.

In conclusion, it was observed for all samples present in the test that the best voltage is 140 kV to reduce metal artifacts.

Besides, MAR algorithm permits to reduce much the problem of metallic artefact, but it does not allow to compensate for this difference of HU in a total way.

The HU values obtained with a voltage of 140 kV with MAR in presence of metal elements are more similar to real values.

Therefore, the best setting of parameters especially in the case of metal elements is: Acquire at 140kV in the presence of MAR.

4.3. DOSE EVALUATION

The choice of voltage to construct the CT scan protocol should be made taking into account the patient dose.

CTDIvol is a Dose Index and from graph 3.21 it is noted that, when switching from a voltage of 120kV to a voltage of 140 kV there is an increase of the CTDIvol. However, this increase is less than a 15% increase and therefore the voltage of 140 kV is also considered acceptable.

4.4. HU RANGES FOR ALL ELEMENTS IN THE TEST

The HU ranges for all elements present in the test were determined and they are shown in the table 3.19.

The compact SmartBone® samples and the large granulated sample (granulometry 2-4mm) have a HU range of: 100-500 HU, while the granulated sample with a granulometry of 0.25 mm has a range of: 200-600 HU. The granulated powder-like sample has higher HU values because it is more compact.

Compact SmartBone® samples and granulated sample (granulometry 2-4mm) have a HU range comparable with that of the cancellous bone.

These HU values are due to an intrinsic porosity of the material, which being less compact has lower HU values. As mentioned above the concept of porosity is important for bone density and is represented by lacunae of different sizes present in cancellous and compact bone.

The cancellous bone has a more relevant porosity due to open spaces or pores that are related to the canaliculi, osteocyte lacunae and osteonal canals. [65]

So, the HU values of SmartBone® are similar to the cancellous bone and therefore this bone substitute has an intrinsic porosity that is an important feature for bone tissue engineering.

Indeed, Porosity and pore size of biomaterials are relevant in osteointegration and new bone formation; relatively larger pores favour direct osteogenesis, as they allow vascularisation and high oxygenation, while smaller ones result in osteochondral ossification. [35]

4.5. RELATIONSHIP BETWEEN THE QUANTITY OF HYDROXYLAPATITE ON THE CALIBRATION PHANTOM AND THE AVERAGE HU VALUES

The amount of hydroxyapatite on each insert of calibration phantom has been declared on data-sheet. These values were put in relation with HU average values calculated on six inserts.
A linear relationship was obtained between HU average values of the six inserts of calibration phantom and the amount of hydroxyapatite declared by the firm. This analyse was carried out for acquisition with 140 kV.
The trend lines, obtained for acquisitions without metal element both in absence of MAR and with MAR, are shown in figures 3.22 and 3.23.
These trend line have the same angular coefficient while the intercept varies by 0.002. This supports the results obtained earlier because the presence of the MAR is irrelevant in the absence of metal and not negatively affects the acquisition.
ACQUISITION NO METAL – 140 kV - $y = 0,8986x + 15,259$
ACQUISITION NO METAL – 140 kV – MAR - $y = 0,8986x + 15,257$

The same procedure was performed for acquisitions with metal elements.
A linear relation between HU average calculated and the amount of hydroxyapatite were obtained both in the absence and in the presence of the MAR.
In this case, trend lines vary if the MAR algorithm is used or not.
In the acquisition with close stem the angular coefficient is 0,9217 without MAR and 0,9153 with use of MAR. The intercept is 11,294 in the first case and 13,879 in the second one.
ACQUISITION CLOSE STEM – 140 kV - $y = 0,9217x + 11,294$
ACQUISITION CLOSE STEM – 140 kV – MAR - $y = 0,9153x + 13,879$

Consequently, the trend line obtained in the presence of the MAR algorithm is considered to be more correct, indeed considering the previous results these acquisitions were carried out in the presence of metallic elements and the use of MAR algorithm is suggested

4.6. MINERALIZATION

The linear relation of acquisition without metal elements and with140 kV in presence of MAR algorithm was considered.

$y = 0,8986x + 15,257$

This linear model relates HU values (x) and amount of hydroxyapatite [mg HA/cm^3] (y).

The HU average value of each SmartBone® sample was substitute for x into the straight-line equation and the corresponding amount of hydroxyapatite was obtained.

These results were shown in the tables: 3.21 and 3.22. This means that the mineralization of material is expressed as Hydroxyapatite in mg HA/cm^3.

TABLE 3.21 - REFERENCE REGION

The table 3.21 views the values calculated on each SmartBone® sample volume.

The mineralization of the sample 1 (SB large, size 10x 20x20 mm) was compared with that of the sample 2 (SB small, size 10x10x10 mm).

The value of HA (mg HA/cm^3) of sample 1 are of an order of magnitude lower than that of sample 2. The SmartBone® Sample 1 has HU average value lesser and as a result Hydroxyapatite value lesser too, because, as mentioned above in chapter 2.3.3, in this sample there are quite some black spots due to the presence of air.

This sample of SmartBone® has a very high porosity for two reasons: first the porosity is an important intrinsic feature of this material and it cannot be excluded; second this sample has a defect on the corner of block that decrease the HU values.

The mineralization of the sample 3 (granulated, with particle size of 2-4mm) was compared with that of the sample 4 (granulated, with particle size of 0, 25mm).

The value of HA (mg HA/cm^3) of sample 3 is about 200 mg HA/cm^3 lower than that of sample 4.

Besides, the powder granulated (sample 4 of particle size 0, 25mm) has the HU average value greater and as a result Hydroxyapatite value greater too, because it is made of finer grains and hence it is more compact and less porous. Instead, larger granulated (sample 3 of particle size 2-4mm) has the HU average value lesser and as a result Hydroxyapatite value lesser too, because the particle size is greater and hence the porosity is greater.

TABLE 3.22 - REFERENCE SLICE

The table 3.22 views the values calculated on each SmartBone® sample reference slice

The mineralization of the sample 1 (SB large, of dimensions 10x20x20 mm) was compared with that of the sample 2 (SB small, size 10x10x10 mm).

The value of HA (mg HA/cm^3) are of the same order of magnitude for both samples.

This result is different from the one obtained in table 3.21 because in this case e reference slice was considered. The reference slice chosen for sample 1 excludes the big black spots due to of defect on the corner of block.

Therefore, two samples have HU values very close, the same degree of mineralization and a similar porosity.

The mineralization of the sample 3 (granulated, with particle size of 2-4mm) was compared with that of the sample 4 (granulated, with particle size of 0, 25mm).

The value of HA (mg HA/cm^3) of sample 3 is about 200 mg HA/cm^3 lower than that of sample 4, as shown in the table above 3.21. This supports what was previously demonstrated for the granulates in the event of reference areas being considered.

This shows that the SmartBone® small granulated (sample 4 with 0,25 mm particle size), being finer and more compact, has less air presence and less porosity and therefore tends to higher HU values and a higher degree of mineralization. While in the larger granulated (sample 3 of Granulometry 2-4mm), the porosity is greater, and it has lower HU values and so a lower mineralization degree.

4.7. CLINICAL CASES

4.7.1. DENSITOMETRIC ANALYSIS

The densitometric evaluation of regrown bone volume is based on a grayscale analysis. The parameters calculated on volume for both clinical cases are: HU average HU value, standard deviation (STD), HU average minimum value, HU average maximum.

The average HU values of regrown bone volume, presented in the blue row of the tables 3.23 and 3.26 below the 'mean' column, are about:

- 468HU for the Patient 1,
- 488 HU for the Patient 2.

This value is included in the HU range defined previously for block SmartBone® samples equal to: 100-500 HU.

The HU average maximum values are:

- 822 HU for the Patient 1,
- 789 HU for the Patient 2.

It was noted that average maximum value of HU on the volume in analysis exceeds the range defined for SmartBone® and falls within the cortical bone range of 662-1981 HU; this shows that the process of osseointegration has begun.

The HU range of the cancellous bone is 148 – 661 HU; it is noted that SmartBone® and cancellous bone have about the same range of HU which differs more in the upper limit of about 100 HU.

it is possible to observe, from the figures 3.31 and 3.32 for Patient 1 and from the figures 3.32-3.38 for the Patient 2, that in the volume where the bone substitute has been implanted, there are areas in which cortical bone (green zones) and cancellous bone (fuchsia zones) are regrown.

The table 3.25 shows that for patient 1 the 3% is related to cortical bone, 32% to the cancellous bone and 60% belongs to Cyan. The table 3.40 shows that for patient 2 the 16% is cortical bone, 44% cancellous bone and 40% is Cyan.

It is observed, both from the images and from the obtained values, that for the patient 2 the areas occupied by cortical bone and cancellous bone are greater than those of the patient 1.

This could be due to the fact that in patient 2 the bone regeneration process is in a more advanced stage, in fact post-operatory TC of patient 2 was performed 17 months after the surgical operation compared to that of patient 1 which was performed 9 months after the surgery.
Regarding areas in Cyan it is not possible to say for sure whether they belong to the SmartBone® or the cancellous bone. They could be SmartBone® but also bone regrowth of spongious already reshaped and already completely new bone. This, however, cannot be seen from the radiographic analysis but only through histological examinations.

4.7.2. MINERALIZATION CLINICAL CASES

The mineralization in terms of mg HA/cm^3 of the portion of regrown bone is:
435,8 mg HA/cm^3 for the patient 1 and 454,12 mg HA/cm^3 for the patient 2.
It is noted that the values are of the same order of magnitude and the value for patient 2 is slightly higher than the other. Therefore, the bone portion relative to patient 2 has a slightly higher mineralization degree and therefore the structure is a little more compact.
Also, both values are higher than the values calculated for the SmartBone® samples and shown in the tables 3.21 and 3.22. In addition, both values are higher than the values calculated for SmartBone® and shown in the tables, but they are similar to the values found for the Smartbone sample 4 (granulated sample with granulometry 0.25mm).
So, the area of regrown bone for both cases has a greater mineralization than that of the smartbone and a higher density.

4.7.3. VOLUMETRIC METHOD CLINICAL CASES

The volume of regenerated bone obtained from overlapping of models was shown in the chapter 3.6.3. For the patient 1 the volume is about 902mm^3 instead for the patient 2 it is about 3188mm^3. Patient 2 volume is bigger than patient 1 volume. This could be due to the fact that the evaluation of patient 2 was performed after 17 months unlike that of the patient 1 that was carried out after 9 months; so, the bone regeneration for patient 2 is a more advanced stage.
Another reason could be that the body district of interest relative to patient 2 is bigger than anatomical area of patient 1. So also, the size of the intervention area and the graft implanted could be larger.

5. CONCLUSION

5.1. ACQUISITION PROTOCOL

The results analysis allowed the construction of a CT scan protocol suitable for the densitometric evaluation of the SmartBone® bone substitute.

The acquisition should be performed in the following way.
A voltage of 140 KV is recommended, based on the results obtained previously.
The level of the ASiR ™ (Adaptive Statistical Iterative Reconstruction) algorithm should be set at 30%, as it is proven to be efficient.
The acquisition should be performed with a STANDARD reconstruction kernel.
Current (mA) modulation is not required if SmartBone® material is inserted into small joints like: wrist, knee, elbow, ankle and shoulder. The current value of 30 mA is suggested for small joints; indeed, this value allows to obtain a good SNR for all patients because these anatomical districts have a limited variability between different patients.
Current (mA) modulation system is suggested if SmartBone® material is implanted into axial skeleton and the current value may vary between 30 mA to 300 mA.
The use of calibration phantom is recommended, and the position is defined under the anatomical district to scan.
From the evaluations performed previously on centring, precise centering and without variations is recommend, but if this is difficult a higher centering to a maximum of 5cm is recommend.
Five reconstructions should be associated with the acquisition:

- STANDARD - FULL FOV 40 cm - MAR
- BONE – FULL FOV 40 cm
- STANDARD – FOV 20 cm
- BONE – FOV 20 cm
- STANDARD – FOV 20 cm – MAR

The reconstruction with full FOV allows to visualize the entire anatomical district under examination. The presence of the MAR is more efficient if metallic elements are present, as previously demonstrated.
The reconstructions with a FOV 20 cm allow to better focus the details. For a quantitative study of the regrown bone and the SmartBone® material, it is advisable to use the reconstruction with a full FOV, with the STANDARD algorithm and with MAR.

5.2. MINERALIZATION

The mineralization of the SmartBone® is not a predictable range because it derives from bovine material. Therefore, it is permissible that mineralization values of this material are not identical, but they are slightly different.
In spite of this, the material behaviour without metal and in the presence of close stem (worst condition) is the same. Indeed, the CT scan protocol for smartbone acquisition is univocal for any conditions.
The HU values of smartbone samples, evaluated with conditions defined into protocol, are of the same order of magnitude.

A linear relationship between HU average values of the six inserts of calibration phantom and the amount of hydroxyapatite declared by the firm was obtained previously.
The HU average value of each SmartBone® sample was substitute into linear model and the corresponding amount of hydroxyapatite was obtained.
This means that the mineralization of material is expressed as Hydroxyapatite in mg HA/cm^3.
The amount of hydroxyapatite was evaluated for each smartbone sample.
Comparing reference slice of sample 1 (block size 10x20x20) and reference slice of sample 2 (small block of size 10x10x10), it was observed that they have the same orders of magnitude and they are affected in the same way by radiologic parameters.
the HU average value of powder granulated sample (sample 4 of particle size 0, 25mm) is greater than HU average value of larger granulated (sample 3 of particle size 2-4mm), because the first one is more compact while the second one is more porous.

The sample 4 (particle size 0, 25mm) has grains of smaller size so it is a more compact granulated, there is less air and less porosity, and therefore it has higher HU values and an higher mineralization degree.

5.3. CLINICAL CASES

After bone substitute's implant, bone remodelling has to be evaluated. In this thesis work two methods for assessing bone growth have been applied. These methods are: volumetric and densitometric analysis.

TC is an imaging diagnostic technique and it is the starting point to conduct the bone regeneration analysis.

The volumetric analysis method permits to assess quantitatively a bone substitute. This method can be performed if a pre-operatory TC and a post-operatory TC, after n months (with $9 \leq n \leq 24$) are available.

Two 3D volumetric models by CT exams have to be created and then these models are overlapped, and they are subtracted to obtain the volume of new generation bone.

A methodology based on densitometric analysis was proposed, which permits to assess qualitatively and quantitatively a bone substitute.

This method can be carried out if a post-operatory TC, after n months (with $9 \leq n \leq 24$), is available.

This methodology is based on grayscale analyse, indeed it compares the HU values of regenerate bone region with the HU ranges defined with use of two software. The goal of this method is to identify if the HU values are of cortical bone, cancellous bone or bone substitute.

The limitation is that if the HU values are included in the HU range between 100HU to 500 HU, it is not possible define if these HU values are smartbone or cancellous bone.

This limitation could be overcome through histological examinations or if a immediately post-operatory TC and a post-operatory TC, after n months, are available; it could be possible carry out a comparison of HU values between two TC scan and hence evaluate HU values in time.

For clinical validation of developed methodology, two clinical cases have been used.
a pre-operatory TC and a post-operatory TC, after 9 months for patient 1 and after 17 months for patient 2, were available.
Densitometric analysis was hence performed on post-operative TC with evaluation of mineralization too.
So, regeneration bone in time was evaluated: for patient 1 the 3% is related to cortical bone and 32% to the cancellous bone instead for patient 2 the 16% is cortical bone and 44% is cancellous bone.
It was observed that in patient 2 the bone regeneration process is in a more advanced stage, in fact post-operatory TC of patient 2 was performed 17 months after the surgical operation compared to that of patient 1 which was performed 9 months after the surgery.

Moreover, it was possible to execute a volumetric evaluation, because a pre-operatory TC and a post-operatory TC were available for both clinical cases, basing on overlapping of 3D models to calculate the volume of bone regeneration.

In addition, post-operatory TC of the patient 2 was performed according to CT scan protocol defined and it was observed that the application of densitometric methodology was been simple and effective.

6. BIBLIOGRAPHY

[1] S. C. Cowin and S. B. Doty, *Tissue Mechanics*. 2007.

[2] A. M. Weatherholt, R. K. Fuchs, and S. J. Warden, "Specialized connective tissue: Bone, the structural framework of the upper extremity," *J. Hand Ther.*, vol. 25, no. 2, pp. 123–132, 2012.

[3] J. Rho, "Mechanical properties and the hierarchical structure of bone," vol. 20, pp. 92–102, 1998.

[4] J. P. Iannotti and R. D. Parker, *NETTER Atlante di anatomia fisiopatologica e clinica: Apparato locomotore 3*, Seconda ed. 2013.

[5] H. Lodish and J. Darnell, *Molecular Cell Biology*. New York: Scientific American Books, 1995.

[6] E. Bam, "Noncollagenous matrix proteins and their role in mineralization," vol. 6, pp. 111–123, 1989.

[7] J. Bilezikian, L. Raisz, and G. Rodan, *Principles of Bone Biology*. San Diego, USA, 1996.

[8] "Structure of Bones." [Online]. Available: https://courses.lumenlearning.com/wm-biology2/chapter/structure-of-bones/.

[9] Nobile Collegio Chimico Farmaceutico Universitas Aromatariorum Urbis, *Il farmacista 2011: la cura del paziente*. 2011.

[10] A. Speciani and L. Speciani, *Osteoporosi*. 2008.

[11] E. C. Marinoni, *Osteoporosi: le nuove prospettive in ortopedia e traumatologia*. 2007.

[12] P. Cabitza, *Ortopedia*. Società editrice Esculapio.

[13] N. M. Hancock, "Biology of bone," *Univ. Press*, 1972.

[14] G. Marotti, "The structure of bone tissues and the cellular control of their deposition."

[15] R. Pietrabissa, *Biomateriali per protesi e organi artificiali*. 1996.

[16] "INTRODUCTION TO BONE BIOLOGY: ALL ABOUT OUR BONES." [Online]. Available: https://www.iofbonehealth.org/introduction-bone-biology-all-about-our-bones.

[17] "Bone Basics and Bone Anatomy." [Online]. Available: https://askabiologist.asu.edu/bone-anatomy.

[18] A. C. Guyton and J. E. Hall, *Textbook of Medical Physiology*. Philadelphia, 1996.

[19] C. Di Bello, *Biomateriali. Introduzione allo studio dei materiali per uso biomedico*. 2009.

[20] A. Teti and A. Zambonin Zallone, "Basi cellulari del rimodellamento osseo."

[21] E. F. Morgan, G. L. Barnes, and T. A. Einhorn, *The Bone Organ System : Form and Function*, Fourth Edition. Elsevier, 2013.

[22] R. B. Salter, *Textbook of Disorders and Injuries of the Musculoskeletal System*, 1st ed. 1970.

[23] M. Navarro *et al.*, “Biomaterials in orthopaedics Biomaterials in orthopaedics,” pp. 1137–1158, 2008.

[24] V. Campana *et al.*, “Bone substitutes in orthopaedic surgery : from basic science to clinical practice,” pp. 2445–2461, 2014.

[25] W. Wang and K. W. K. Yeung, “Bioactive Materials Bone grafts and biomaterials substitutes for bone defect repair : A review,” *Bioact. Mater.*, 2017.

[26] A. Bignon *et al.*, “Effect of micro- and macroporosity of bone substitutes on their mechanical properties and cellular response,” vol. 4, pp. 1089–1097, 2003.

[27] L. Pilone, G. Ciardelli, G. Perale, and R. Ferracini, “Evaluation methods of bone graft integration in reconstructive surgeries and consequent data analysis,” POLITECNICO DI TORINO - Facoltà di Ingegneria - Corso di Laurea Magistrale in Ingegneria Biomedica, 2017.

[28] F. Tamimi and M. H. Alkhraisat, “Bone Substitutes,” no. January 2017, 2011.

[29] D. S. Oh *et al.*, “Distinctive Capillary Action by Micro-channels in Bone-like Templates can Enhance Recruitment of Cells for Restoration of Large Bony Defect,” no. September, pp. 1–9, 2015.

[30] A. Ashton Acton, *Advances in Bioartificial Materials and Tissue Engineering Research and Application*, Scholarly. .

[31] F. Valentini, G. Longoni, D. Tonelli, and E. Landi, “SVILUPPO DI IMPIANTI CERAMICI BIOMIMETICI A POROSITA ’ CONTROLLATA PER LA RIGENERAZIONE DEL TESSUTO OSSEO,” ALMA MATER STUDIORUM UNIVERSITÀ DI BOLOGNA, 2010.

[32] A. Acocella, “Capitolo 3 : Materiali da innesto,” pp. 49–71.

[33] R. Bedini, R. Pecci, P. Ioppolo, and S. Università, “Proposta di valutazione microtomografica di alcuni sostituti ossei,” no. c. ISTITUTO SUPERIORE DI SANITÀ - Rapporti ISTISAN, 2009.

[34] F. PARONUZZI TICCO, T. VILLA, and G. PERALE, “VALUTAZIONE SPERIMENTALE DELLA COMPATIBILITÀ BIOMECCANICA DI UN SOSTITUTO OSSEO PER L’OSTEOTOMIA TIBIALE,” 2015.

[35] G. Pertici, F. Rossi, T. Casalini, and G. Perale, “Composite polymer-coated mineral grafts for bone regeneration : material characterisation and model study,” pp. 1–7, 2014.

[36] G. PERTICI *et al.*, “COMPOSITE POLYMER-COATED MINERAL SCAFFOLDS FOR BONE REGENERATION : FROM MATERIAL CHARACTERIZATION TO HUMAN STUDIES,” *J. Biol. Regul. Homeost. AGENTS*, vol. 29, no. 3, pp. 136–148, 2015.

[37] S. Cigni *et al.*, “L ’ utilizzo di matrice ossea demineralizzata in chirurgia ortopedica - Demineralized bone matrix in orthopedic surgery,” pp. 54–61, 2006.

[38] M. Hallman, L. Sennerby, and S. Lundgren, “A clinical and histologic evaluation of implant integration in the posterior maxilla after sinus floor augmentation with autogenous bone , bovine hydroxyapatite , or a 20 : 80 mixture . Bone augmentation procedures in localized defects in the alveolar ridge : clinical results with different bone grafts and bone-substitute materials .,” vol. 17, no. 5, 2002.

[39] F. Grecchi, G. Perale, V. Candotto, A. Busato, M. Pascali, and F. Carinci, “RECONSTRUCTION OF THE ZYGOMATIC BONE WITH SMARTBONE ® : CASE REPORT,” vol. 29, no. 3, pp. 42–47, 2015.

[40] D. D. Alessandro *et al.*, “scaffold (SmartBone 1) for maxillary sinus augmentation : A histologic study on bone regeneration,” *Int. J. Pharm.*, pp. 1–11, 2016.

[41] L. D. Dalle Carbonare and S. Giannini, “Diagnostica istologica delle malattie metaboliche dello scheletro: istomorfometria ossea,” vol. 56, no. 1, pp. 15–23, 2004.

[42] L. D. Dalle Carbonare *et al.*, “Bone microarchitecture evaluated by histomorphometry,” vol. 36, pp. 609–616, 2005.

[43] R. Bedini *et al.*, *Analisi microtomografica del tessuto osseo trabecolare: influenza della soglia di binarizzazione sul calcolo dei parametri istomorfometrici*. ISTITUTO SUPERIORE DI SANITA.

[44] M. G. Baldoni, N. Filice, and F. Carini, “VALUTAZIONE CLINICA E RADIOGRAFICA DEL RIMODELLAMENTO VOLUMETRICO DEGLI INNESTI OSSEI AUTOLOGHI NELLE RICOSTRUZIONI MAXILLO-FACCIALI DELLE CRESTE ATROFICHE A FINI IMPLANTARI ED ANALISI A CLUSTER DEI GENI COINVOLTI NEI PROCESSI DI RIMODELLAMENTO OSSEO,” UNIVERSITÀ DEGLI STUDI MILANO-BICOCCA - Facoltà di Medicina e Chirurgia, 2011.

[45] W. Rosenbrook, N. E. Gary, and R. A. Morse, “Measurement of Bone Mineral in vivo: An Improved Method,” vol. 142, no. 1958, 1963.

[46] K. Genant, E. Block, and T. Harris, “Musculoskeletal Appropriate Use of Bone Densitometry ’,” pp. 817–822.

[47] C. E. Cann and H. Genant, “Precise Measurement of Vertebral Mineral Content Using Computed Tomography.” 1980.

[48] K. L. Troy and W. B. Edwards, “Practical considerations for obtaining high quality quantitative computed tomography data of the skeletal system,” *Bone*, vol. 110, pp. 58–65, 2018.

[49] L. Faggioni, F. Paolicchi, and E. Neri, *Elementi di tomografia computerizzata*. 2010.

[50] I. Oransky, “Sir Godfrey N Hounsfield,” vol. 364, p. 2004, 2004.

[51] G. Guglielmi and M. Cammisa, “TOMOGRAFIA COMPUTERIZZATA QUANTITATIVA ASSIALE E PERFERICA,” pp. 1–9.

[52] H. K. Genant, G. Guglielmi, and M. Jergas, *Bone Densitometry and Osteoporosis*. 1998.

[53] G. Guglielmi, M. Nasuto, L. Y. Avery, and X. Cheng, “Bone densitometry : current status and future trends,” pp. 97–103, 2016.

[54] P. Ruegsegger, U. Elsasser, M. Anllker, H. Gnehm, H. Kind, and A. Prader, “Quantification of Bone MineraUzation Using Computed Tomography 1,” no. March, pp. 93–97, 1976.

[55] “Installazione del sistema ASiR™ - DoseTeam4you.” [Online]. Available: http://doseteam4you.com/2016/04/28/installazione-del-sistema-asir/.

[56] A. Brunatti and O. Rampado, “Dose reduction and metal artifact correction systems effectiveness in shoulder,” UNIVERSITA’ DEGLI STUDI DI TORINO SCUOLA DI MEDICINA.

[57] C. Guilfoile, P. Rampant, and M. House, “The impact of smart metal artefact reduction algorithm for use in radiotherapy treatment planning,” *Australas. Phys. Eng. Sci. Med.*, vol. 0, no. 0, p. 0, 2017.

[58] “Optima CT660 SE - Gamma Optima_ - Tomografia computerizzata - Categorie Prodotti GE Healthcare.” [Online]. Available: http://www3.gehealthcare.it/it-it/prodotti/categorie/computed_tomography/optima_family/optima_ct660_se.

[59] “Optima™CT660 Manuale dell’operatore, italiano 5448280-1IT Revisione: 1 ©2012GeneralElectricCompany Tutti i diritti riservati.” .

[60] “GE Lightspeed VCT _ GE VCT 64.” [Online]. Available: https://bctechnical.com/systems/vct-64/.

[61] “Bone Density Calibration Phantom (6 rods) - QRM-BDC/6.” Quality Assurance in Radiology and Medicine, p. 91096.

[62] R. Guide and M. N. V All, “Version 12.0 – Reference guide,” no. June, 2017.

[63] “Version 12.0 - Tutorial,” pp. 0–107.

[64] P. S. Florencio-silva, R.; Sasso, G.; Sasso-cerri, E.; Simões, M. J. & Cerri, “Biology of Bone Tissue: Structure, Function, and Factors That Influence Bone Cells,” *Biomed Res. Int.*, vol. 2015, pp. 1–17, 2015.

[65] P. Zioupos, R. B. Cook, and J. R. Hutchinson, “Some basic relationships between density values in cancellous and cortical bone,” vol. 41, pp. 1961–1968, 2008.

CT SCAN PROTOCOL

BONE SUBSTITUTE – SMARTBONE

Aim and Summary

The goal of this CT protocol is to achieve detailed data concerning the 3-dimensional property of the bone and the bone substitute - Smartbone. The resulting scans will be used to evaluate the bone regrown with Densitometric analysis. Moreover, the obtained scans will be applied to prepare a virtual 3D model. This virtual 3D model can be used on the Volumetric Quantitative analysis to evaluate the volume of bone regrowth. The following instructions are important. Please read them carefully before scanning

General Scan Requirements

- Take off any non-fixed metal prosthesis, jewellery, zippers or other metal objects that might tamper with the region to be scanned.
- Talk about the procedure with the patient. The patient must not move any part during the scanning sequence.
- Position the patient to maximize comfort and minimize motion.

SCAN PARAMETERS

Imaging modality	**CT**
Scanner type	**A common CT machine can be used. Please make sure that images fulfill the minimum requirements stated below.**
Patient Centering	**Set the table height so that the area to be scanned is centered in the field of view. [0 - +5 cm]**
Field of View (FOV)	**FULL FOV (FOV 40) - Scan all slices with the same FOV, reconstruction center and table height (coordinate system)**
ASIR	**ASIR 30%**
Algorthm	**A STANDARD algorithm**
	A BONE algorithm
	For scans where metal implants are present: A metal Artefact Reduction Method
kVp	**140 kV**
mAs	**30 mA for small joint**
	[30mA - 300 mA] As given by the automatic system for axial skeleton - modulation current system
Reconstructions	**• STANDARD - FULL FOV 40 cm - MAR • BONE – FULL FOV 40 cm • STANDARD – FOV 20 cm • BONE – FOV 20 cm • STANDARD – FOV 20 cm – MAR**

File Format

Provide the image data in standard DICOM format (axial).

Scan data

ONLY send the following images:

- The requested CT images at the given parameters
- The accompanying scout view
- An accompanying 3D reconstruction (if available) - Recent diagnostic X-ray images of the hip (if available